### Design of Securing Mechanism for Power Converter in Navy Integrated Power and Energy Corridor

by

#### Chris Tomlinson

B.S. Mechanical Engineering University of Nebraska - Lincoln (2013)

Submitted to the Department of Mechanical Engineering in partial fulfillment of the requirements for the degrees of Masters of Science in Naval Architecture and Marine Engineering

and

Master of Science in Mechanical Engineering at the

# MASSACHUSETTS INSTITUTE OF TECHNOLOGY May 2022

© Massachusetts Institute of Technology 2022. All rights reserved.

Author	
	Department of Mechanical Engineering
	May 6, 2022
Certified by	
v	Julie Chalfant
	Research Scientist
	Thesis Supervisor
Certified by	
v	Chryssostomos Chryssostomidis
	Professor of Mechanical and Ocean Engineering
	Thesis Supervisor
Accepted by	
•	Nicolas Hadjiconstantinou
	Professor of Mechanical Engineering
	Chair, ME Committee on Graduate Studies

# Design of Securing Mechanism for Power Converter in Navy Integrated Power and Energy Corridor

by

#### Chris Tomlinson

Submitted to the Department of Mechanical Engineering on May 6, 2022, in partial fulfillment of the requirements for the degrees of Masters of Science in Naval Architecture and Marine Engineering and Master of Science in Mechanical Engineering

#### Abstract

Future US Navy ships will need an updated electrical distribution system to solve two impending challenges. The first challenge is the increase in electrical generation and demand. The second challenge is that the loads will be more dynamic with more complex load profiles (e.g., pulses for energy weapons). A next-generation electrical system, Power Electronic Power Distribution System (PEPDS), is being developed to solve these challenges. It is a power/energy management and distribution system operating in the Medium Voltage AC/DC range that can convert power from AC and DC sources as required by the load using a power conversion module. The power conversion module for this system is known as the integrated Power Electronic Building Block (iPEBB). However, with this new electrical distribution system designed to be put on a ship, the components must be adequately secured. Currently, there is no established way to anchor the novel iPEBB. This thesis modeled a securing mechanism using a hinge design to provide the securing force. It was evaluated based on the structural integrity, bending, and shear stresses. Additionally, the material encompassing the iPEBB is investigated to determine the properties integral to its design. The model produced shows a practical path to secure the iPEBB without additional involvement from other support systems. While this design is functional, it may not be optimal. This thesis lays the foundation for additional study for more advantageous securing mechanism designs for the iPEBB.

Thesis Supervisor: Julie Chalfant

Title: Research Scientist

Thesis Supervisor: Chryssostomos Chryssostomidis Title: Professor of Mechanical and Ocean Engineering

#### Acknowledgments

I would like to show my gratitude to my thesis supervisors, Dr. Julie Chalfant and Professor Chryssostomos Chryssostomidis. Their candid feedback and wealth of knowledge kept this project on track and guided it away from many missteps. I am incredibly thankful for their patience and encouragement throughout this process.

I would like to thank Kelly Cooper and L.J. Petersen from the U.S. Office of Naval Research (ONR). This material is based upon research supported by, or in part by, the ONR under award numbers ONR N00014-16-1-2945 Incorporating Distributed Systems in Early-Stage Set-Based Design of Navy Ships and ONR N00014-16-1-2956 Electric Ship Research and Development Consortium.

I am grateful to the Engineering Duty Officer community and 2N leadership for providing this opportunity.

Thank you to the 2N students who have fostered a supportive environment empowering personal and professional development. A special thank you to LT Camilo Duque, LT Eric Young, and LT Ivan Reyes, whose welcomed wit and jovial demeanor animated many dark days.

Finally, I would like to thank my parents for their love and encouragement throughout my studies at MIT. Their staunch support of my studies means more to me than they will ever know.

### Contents

1	Intr	roduct	ion	17
	1.1	Backg	round	17
		1.1.1	Integrated Power and Energy System	19
		1.1.2	Power Electronic Power Distribution System	21
		1.1.3	Power Corridor	21
		1.1.4	Power Electronic Building Block	23
	1.2	Securi	ing Mechanism for iPEBB	24
		1.2.1	Reasons for Needing Anchoring Mechanism	25
		1.2.2	Mechanical Constraints	25
		1.2.3	Thermal and Electrical Constraints	25
	1.3	Focus	of Thesis	27
2	iPE	BB A	nalysis	29
	2.1	Physic	cal Characteristics of the iPEBB	29
	2.2	Scena	rios for Analysing Stress on iPEBB Key	30
	2.3	Analy	rsis of iPEBB Key	34
		2.3.1	iPEBB Key - Deflection	39
		2.3.2	iPEBB's Key - Stress	40
	2.4	Analy	rsis of iPEBB Shell	43
		2.4.1	iPEBB Shell - Top Face Analysis	43
		2.4.2	iPEBB Shell - Side Face Analysis	47
	2.5	Dynai	mic Loading	50
		2.5.1	Dynamic Loading Calculations	51

		2.5.2	Key	54
		2.5.3	Cold Plate and Shell	55
3	Hin	ge Sec	curing Mechanism	57
	3.1	Hinge	Mechanism Overview	57
		3.1.1	Layout	58
		3.1.2	Key Features	58
	3.2	Analy	sis of the Securing Mechanism with iPEBB Inserted	59
		3.2.1	Thermal Pad Clearance	62
		3.2.2	Bolt Loading Calculations	65
		3.2.3	Analysis of Elbow Bracket	67
		3.2.4	Required Torque to Tighten Screw	69
		3.2.5	Bolt Strength	72
		3.2.6	Bolt Thread Strength	76
	3.3	Lockir	ng Mechanism Analysis	81
		3.3.1	Locking Mechanism Design	81
		3.3.2	Locking Mechanism Design Analysis	83
4	Imp	act of	Material Selection	87
	4.1	Restri	ctions on iPEBB	87
	4.2	Mater	rial Review	90
		4.2.1	Copper and Its Alloys	90
		4.2.2	Nickel and Its Alloys	93
		4.2.3	Aluminum	94
		4.2.4	Titanium	94
		4.2.5	Austenitic Steels	95
	4.3	Base 1	Material Used for Analyses	95
	4.4	Select	ing the Ideal Material	98
	4.5	Impac	et on iPEBB	101

5	Rec	ommendations and Conclusions	105
	5.1	Results	105
		5.1.1 Review of iPEBB Design	105
		5.1.2 Review of Hinge Design	106
		5.1.3 Alternate/Clamp Design	107
	5.2	Conclusion	108
	5.3	Future Topics	109
	5.4	Design Changes	110
A	Cor	nponent Weights	115
В	Soli	dWorks Analysis	119
	B.1	Cold Plate	119
		B.1.1 Cold Plate - Static Loading	119
		B.1.2 Cold Plate - Dynamic Loading	121
	B.2	PEBB Shell - Side Face	122
		B.2.1 Side Face - Static Loading	123
		B.2.2 Side Face - Dynamic Loading	123
С	List	of Variables Used	125
D	Cal	culations Performed	127
	D.1	PEBB Shell - Roark's Formulas	127
		D.1.1 Cold Plate - Stress and Deflection	127
		D.1.2 PEBB's Shell Sidewall - Buckling	128
	D.2	Dynamic Loading	130
${f E}$	MA	TLAB Code	133
	E.1	PEBB Shell - Top Plate - Navier Solution	133
	E.2	PEBB Shell - Side Plate - Equilibrium Method	135
$\mathbf{F}$	Elb	ow Analysis	137
	F.1	Bolt Hole	137

	F.1.1	Bolt Hole - Deflection	138
	F.1.2	Bolt Hole - Stress	139
F.2	Front	Hinge Hole	140
	F.2.1	Front Hinge Hole - Shear Stresses	140
	F.2.2	Front Hinge Hole - Tension Stresses	141
	F.2.3	Front Hinge Hole - Bearing Stresses	142
	F.2.4	Front Hinge Hole - Shear Tear Out Stresses	143

## List of Figures

1-1	Projected Power Demand [1]	18
1-2	Change in Power Requirement for Future Ships [34]	19
1-3	Comparison of Traditional and Future Responses to Next-Generation	
	Systems[35]	20
1-4	Proposed Power Corridor Layout [36]	23
1-5	Current iPEBB Design [23]	24
2-1	Views of Modeled iPEBB	30
2-2	Force Analysis of iPEBB - Front View	32
2-3	Resulting Forces on iPEBB's Key-like Structure in Scenario Two	33
2-4	Diagram of relationship of Forces and Distances When iPEBB not Fully	
	Inserted	34
2-5	iPEBB with Detailed View of Key (Dimensions in mm)	35
2-6	Front Overhead View of iPEBB Support and Electrical Alignment	
	Structure	35
2-7	Front Inner View of Keyway	36
2-8	Components of a Keyed Shaft [2]	36
2-9	Detailed View of a Key[29]	37
2-10	Cross-Sectional View of Key, Keyseat, and Keyway[29]	38
2-11	Second Moment of Area[5]	39
2-12	Simply Supported Plate with Uniform Normal Loading [47]	45
2-13	Simply Supported Plate Loaded in Single Patch on Plate [47]	46
2-14	Force Analysis of iPEBB	48

2-15	Locations of Power Corridor on Model Ship[22]	51
2-16	Generic Ship Axes [40]	53
3-1	Model of Hinge Design. Image (a) shows the fixture with the iPEBB	
	inserted and locked into place. Image (b) shows the fixture with the	
	iPEBB inserted, the retaining brackets unlocked and rotated out of the	
	way, and the cold plates rotated to the open position	57
3-2	Hinge Securing Mechanism with Bolts	60
3-3	Shore 00 Hardness to Modulus of Elasticity (Young's Modulus) [31] .	63
3-4	Side Profile View Hinge Design With iPEBB Inserted	64
3-5	Scenarios Evaluated for Clearance Analysis	64
3-6	Loading Profile of a Typical Bolt [5]	67
3-7	Close up Views of Elbow Bracket	68
3-8	Loading Profile on Square Bolt Threads[5]	70
3-9	Thread Angle and Effect on the Thread Force $[5]$	71
3-10	Frustum: Observation to Model [5]	74
3-11	Side Cutaway View of Front of Hinge Design	74
3-12	Basic Thread Profile of a Typical Nut and Bolt [3]	77
3-13	Application of Securing Force on Threads	80
3-14	Locking Mechanism with Components Labeled	82
3-15	Locking Mechanism in Open and Closed Positions	82
3-16	Force Balance for Cold Plate	84
3-17	Diagram of Tab Supporting the Elbow Bracket	84
4-1	Strength vs Density for Various Materials [5]	89
A-1	PEBB Drawing and Dimensions	115
A-2	Cold Plate Drawing	116
A-3	Front and Side Beam Drawings and Dimensions	116
A-4	Elbow Bracket Drawings and Dimensions	117
B-1	SoldWorks Simulation Analysis of Cold Plate Deflection	120

B-2	SoldWorks Simulation Verification Analysis of Cold Plate Deflection	
	for Static Loading	121
B-3	SoildWorks Simulation Verification Analysis of Cold Plate Stress with	
	Dynamic Loading	122
B-4	SoildWorks Simulation Analysis of Side Plate Buckling with Static	
	Loading	123
B-5	SoildWorks Simulation Analysis of Side Plate Buckling with Dynamic	
	Loading	124
D-1	Simply Supported Plate With Uniform Loading [48]	128
E-1	MATLAB Generated Deflection for Cold Plate (in cm)	135
F-1	Representation of Elbow for Bolt Hole Analysis	138
F-2	Shear Stress on Front Hinge Hole	141
F-3	Tension Stress on Elbow Bracket	142
F-4	Bearing Stress on Elbow Bracket	143
F-5	Shear Tear-Out Stress on Elbow Bracket	144

### List of Tables

2.1	Typical Mechanical Properties of 1060 Aluminum [16]	41
2.2	Ship Characteristics	52
3.1	Metric Mechanical-Property Classes for Steel Bolts, Screws, and Studs [5]	61
3.2	Clearances from Top of Uncompressed Pad to Cold Plate	65
3.3	Torque Factors to use with Eqn 3.21 [5]	73
3.4	Diameters and Areas of Coarse-Pitch and Fine-Pitch Metric Threads[5]	75
3.5	Metric Mechanical Properties for Grade 8.8 Steel Bolts [5]	76
3.6	Dimensions of Hexagonal Nuts[5]	78
3.7	Bearing Pressure [5]	78
4.1	Strength-to-Weight Ratio for Remaining Materials	96
4.2	Area of Shell With No Thickness	96
4.3	iPEBB Shell Thickness for Various Metals	97
4.4	Comparison of Viable Aluminum Alloys[16]	101
A.1	PEBB Weight	115
A.2	Cold Plate Weight	116
A.3	Thermal Pad Weight	116
A.4	Elbow Bracket Weight	117
D.1	$\alpha$ and $\beta$ Factors Based on $\frac{a}{b}$ Ratio	128
D.2	K Value Based on $\frac{a}{b}$ Ratio [48]	130
D.3	Notional Ship Motion Characteristics	131
D.4	Loading Factors in the Principle Directions	131

D.5	Design Load in Principle Directions	132
F.1	Key Values for Elbow Analysis	138

### Chapter 1

### Introduction

This thesis is centered around the problem of securing a power conversion module. This section introduces the background necessary to understand the relevance of this problem. In doing so, the associated constraints used to confine this thesis are laid out. Finally, an overview of the remaining chapters of this thesis is presented.

#### 1.1 Background

For over three decades, the US Navy has been looking to transform the possibility of electric ships from a lofty goal to the usual path for future ships. The traditional method for propulsion is to mechanically couple the shaft of an engine (diesel, gas turbine, and steam). In 1992, the US Navy began investing in developing the Integrated Power Systems (IPS) as the path forward for an electric ship [24]. Electric ships use larger electric generators to provide electric power to propulsion, weapons, sensors, and other electric loads. As a result, electric ships have significantly larger electrical generation and distribution capabilities than traditional, non-electrically propelled ships. IPS was the first system in modern warships to combine the power generation capabilities from the propulsion and electrical systems into one combined system; it was successfully configured and implemented on USS ZUMWALT (DDG-1000) [24].

This desire for larger electrical generation and distribution capabilities stemmed from warfighters needing more power to fully utilize the next-generation systems for weapons, sensors, and Electronic Warfare (EW) equipment. As shown in Figure 1-1, the projected electrical power needed for ship service and mission systems will increase much more than the power required for propulsion. To fully operate this

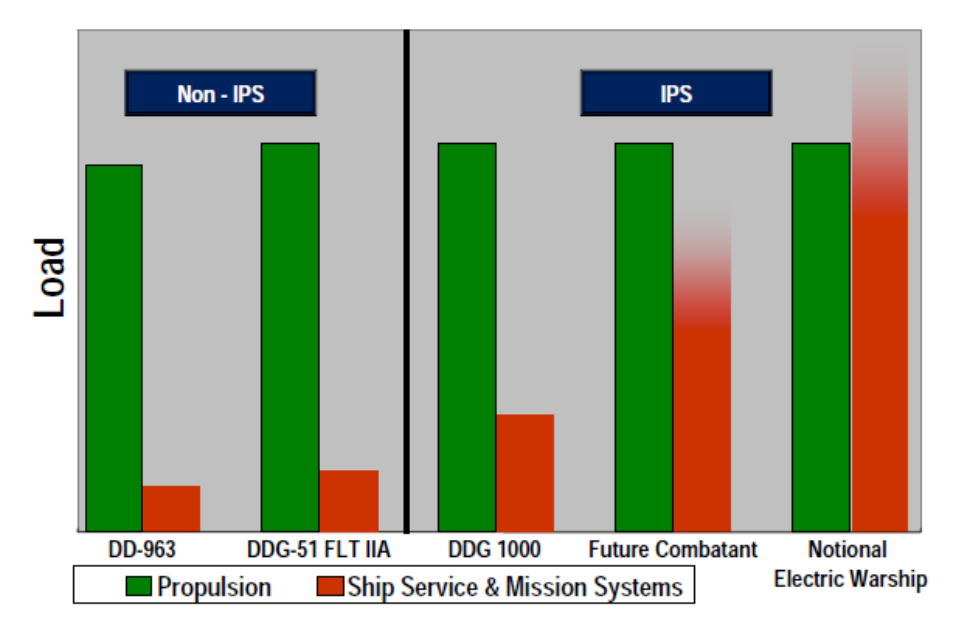


Figure 1-1: Projected Power Demand [1]

new equipment, future power distribution systems will need more power generation capabilities (shown in Figure 1-2a) and support different power demand profiles than previously used (shown in Figure 1-2b).

This need for additional power margin is difficult to quantify as some of those next-generation systems have not been built. However, as seen in Figure 1-2a, it can be estimated. To accomplish this goal, PMS 320 Electric Ships Office created the 2019 Naval Power and Energy Systems (NPES) Technology Development Roadmap (TDR) which outlined the strategy to meet the challenges imposed by these novel systems [1]. This comprehensive strategy developed the path forward for power generation, distribution, storage, and control systems architecture. This thesis will focus solely on the distribution system. The rest of this section will explore new distribution systems, focusing on the proposed Power Electronic Power Distribution System (PEPDS) made possible by Silicon-Carbide (SiC) semiconductors developed by the Office of Naval Research (ONR) [41].

#### 1.1.1 Integrated Power and Energy System

The first system proposed to handle the increased demand for power to meet the need of future systems was the Integrated Power System (IPS). IPS is based on Medium Voltage Alternating Current (MVAC) architecture [35]. As shown in Figure 1-2a, the power demanded by future ship classes is expected to increase rapidly. IPS solved that problem by adding larger generators and making the power from those generators available for either propulsion or ship service loads.

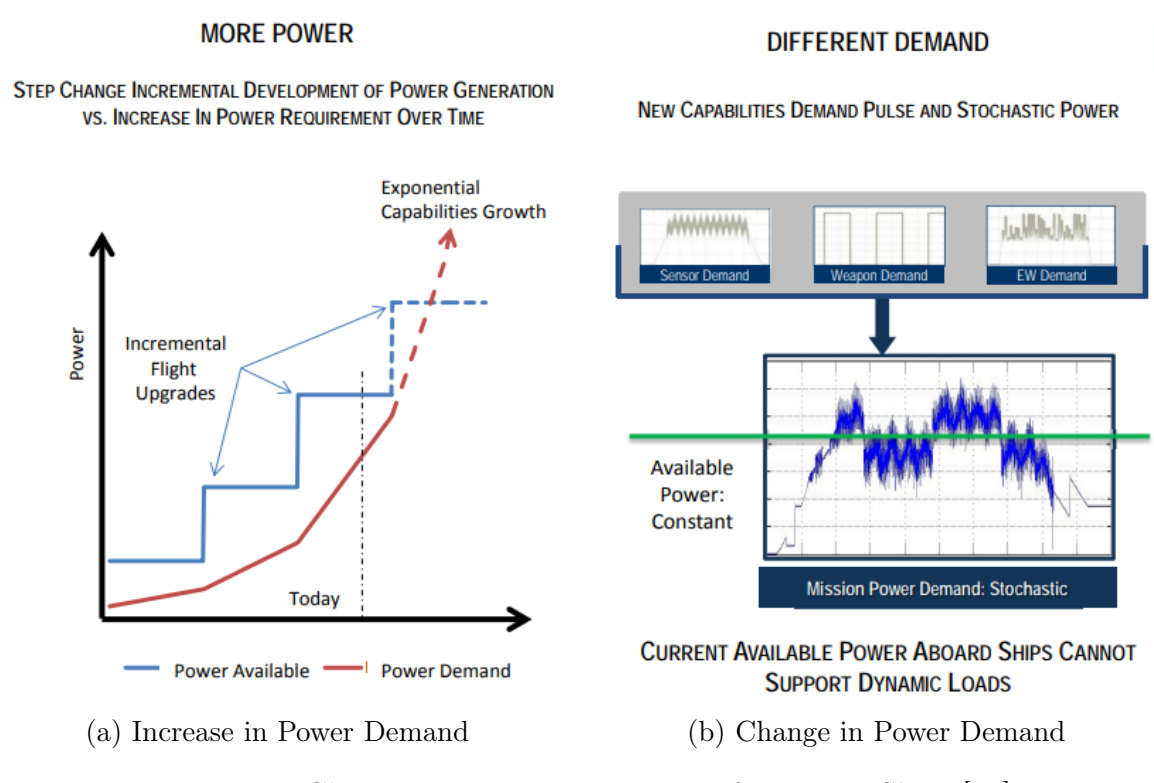


Figure 1-2: Change in Power Requirement for Future Ships [34]

Figure 1-2a does not tell the whole story. In addition to more total power, next-generation technologies have different power demand profiles. Traditional loads, such as pumps and fans, generally run at a steady-state resulting in constant, known demand, as shown in Figure 1-3a. The demand by the next-generation systems results in more unpredictability, as shown in Figure 1-2b. Figure 1-2b shows the required power based on loading (y-axis) versus time (x-axis). The horizontal green line represents the available constant power. Legacy distribution systems, solely relying on electrical generators, are not designed to handle these complex loads' pulsation/ripple profiles

[1]. Moreover, subjecting legacy systems to these complex loads results in excessive thermal stresses (overheating) and negative torques on the generators (mechanical stresses).

To alleviate these harmful issues, the next distribution system needed to incorporate advanced controls, power storage systems, or both [1]. The next step in power distribution systems was to integrate both advanced electrical controls and energy storage into the IPS distribution system [35]. This new system was called Integrated Power and Energy System (IPES) and was based on MVAC and MVDC integration. Using both of these alleviation strategies, the complex next-generation loads were

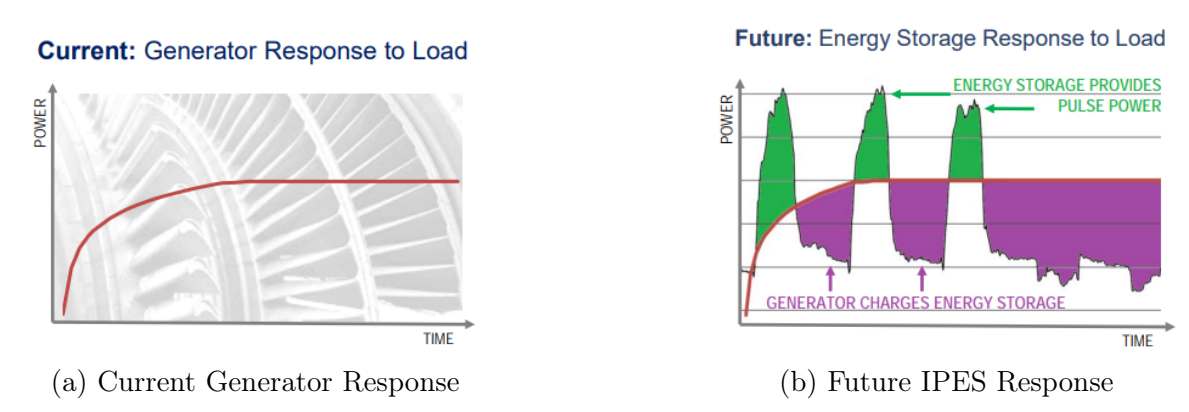


Figure 1-3: Comparison of Traditional and Future Responses to Next-Generation Systems[35]

adequately supplied with power as shown in Figure 1-3b. IPES uses advanced controls, known as Tactical Energy Management (TEM), and can take full advantage of the ship's power and energy resources. These advanced controls enable changing system guidance to operate at maximum efficiency or performance based on the situation. Additionally, this control system uses active state anticipation, reducing storage capacity and overall power requirements [35].

The main drawback of the current IPES system is that it operates on either AC or DC for power distribution. In the future, power will need to be distributed on AC, DC, or both to fully utilize all of the resources onboard the ship [41].

#### 1.1.2 Power Electronic Power Distribution System

Power Electronic Power Distribution System (PEPDS) is the next generation IPES. It is designed to be a power/energy management and distribution system that coordinates with both AC and DC power generators, converts power as needed, and delivers power to AC and DC loads.

As a management system, it can simultaneously control and coordinate with many different types of loads (AC, DC, simple and complex profiles) and sources (AC and DC). This functionality goes beyond TEM's control capability. As a distribution system, it can acquire power from AC and DC sources at the same time in the same system and deliver to AC and DC loads [41]. When a source or load is plugged into PEPDS, the system will recognize it and adapt to provide power and control functions as required performing all of the conversions required for the source or load. Some of these control functions are for the safety of the source or load. Some of these protections include over-current protection, over-voltage protection, and short circuit protection [41]. It is important to note that PEPDS is the system of the future and is not currently available today. Its current proposed form is a hybrid of MVAC and MVDC Architecture [41].

Ideally, PEPDS would be designed into a new ship so that the crucial components would be grouped together. The space that houses all of the key components of the distribution system is known as the power corridor. In addition, there are multiple power corridors onboard for redundancy purposes. For PEPDS, the essential piece of hardware contributing to the functionality of this system is the integrated Power Electronic Building Block (iPEBB), and many are housed in each power corridor.

#### 1.1.3 Power Corridor

The power corridor is a single entity that contains the components for the electrical distribution system. This means that functionally, each power corridor has the means necessary for power distribution, conversion, isolation, and storage. Physically, each power corridor contains stacks of iPEBBs, a thermal management system (pump,

heat exchanger, and piping), sensors, cables, circuit breakers, and energy storage. The circuit breaking functionality may be performed by a combination of the iPEBB controlling the flow of power and a no-load disconnect. The thermal management system's actual arrangement, specifications, and design are detailed in Reference [43]. There are multiple power corridors onboard the ship, and an example layout is shown in Figure 1-4. During the initial planning stages, the reserve space design concept is employed to allocate sufficient space for the amount of electrical power that the ship is designed to utilize [7]. The main driving factors favoring its implementation are:

- 1. Logistics and training simpler for a single design component with multiple uses. Technicians are able to handle a variety of problems. Repair parts for standard multi-function equipment are easier to obtain.
- 2. Installation, maintenance, and repair performed easier and cheaper for modular design. Installation of design can be performed off-hull to ensure all parts are on hand. Components can be built onsite to minimize interference material removed. Modular design allows for parts to be swapped as needed.
- 3. Sailor safety Keeps all high voltage equipment in a contained space.
- 4. Survivability Increased functional redundancy by geographically separating corridors while maintaining each power corridor's independent functionality. Additionally, the iPEBBs are interchangeable so they can be replaced if the surrounding equipment is in working order. This allows for a slower, graceful degradation of the equipment [17].
- 5. Costs Decreased in production, installation, supplies, and training areas. Modules are constructed off-hull and assembled on the ship, minimizing cost and manhours for rigging. Modules can be built off the ship and tested prior to installation, reducing the chance of defective parts and subsequent troubleshooting. iPEBBs are identical, leading to reduced formal training and repair parts for each device [17]. Additionally, in the early planning stages, the reserve space

concept is used to determine the amount of space required for the power corridor and tailored to sources and loads in that section [7].

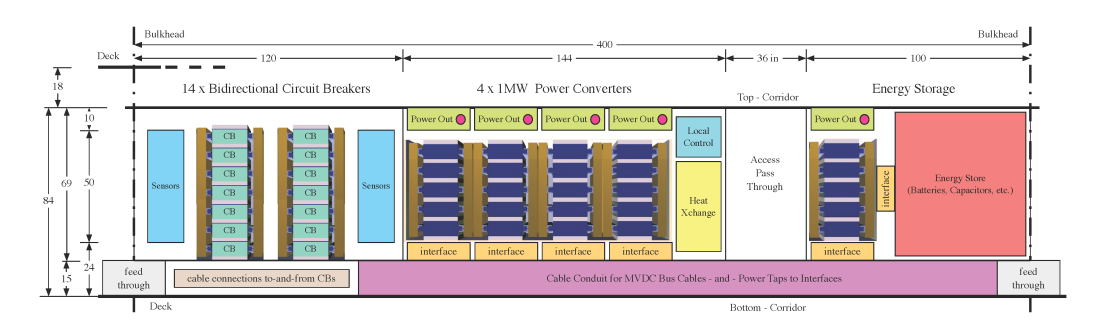


Figure 1-4: Proposed Power Corridor Layout [36]

As shown in Figure 1-4, the central fixture of the power corridor is the Power Converter, also known as the integrated Power Electronic Building Block (iPEBB).

#### 1.1.4 Power Electronic Building Block

One of the key components for the PEPDS and power corridor is the iPEBB. The iPEBB is a modular, programmable power converter essential for accepting power from either AC or DC sources and converting it, as desired, for AC and DC loads on the ship. This modular universal converter is characterized physically by being able to be carried by a single sailor and self-contained [7]. This thesis assumes that the iPEBB is made from 1060 Aluminum, weighs 16 kgs, and has the dimensions shown in Figure 1-5.

The PEPDS has sensors in every iPEBB. Using solid-state switches, PEPDS can control power in the microsecond range. This is a significant upgraded version compared to the traditional mechanical switches and gears. This integration of PEPDS within the iPEBB allows for a central system to control the flow of power in the system from all sources to all loads [41].

The iPEBB results from ONR-funded studies spanning over two decades, aiming to reduce converters' size, weight, and cost. As mentioned in Section 1.1.1, this reduction in size, weight, and cost are due to SiC semiconductors' development. Due to the recent emergence of this technology, the iPEBB has been designated as the

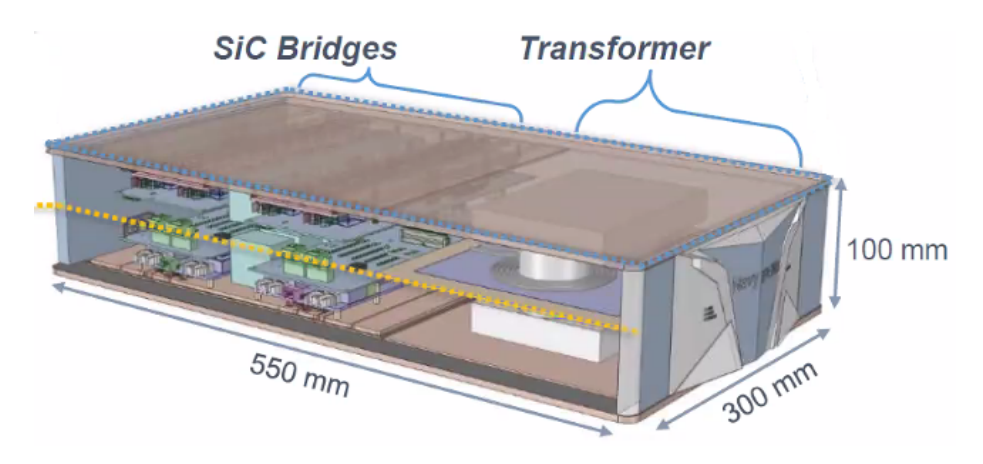


Figure 1-5: Current iPEBB Design [23]

Least Replaceable Unit (LRU). If there are problems with an iPEBB, it will be sent off ship for troubleshooting and a new iPEBB will take it place [41].

iPEBBs interface with four support systems for thermal management, electrical power, data, and mechanical support. Heat is removed from the iPEBB via conduction on the top and bottom faces. Electrical power is supplied and removed from the back face. Electromagnetic interference was not accounted for during this analysis. It was assumed that the active filters installed to control the noise generation would remove the interference. The mechanical and structural interface is designed to be reusable and facilitate the insertion and removal of the iPEBBs as required. The data connection must be safe and secure to allow for expedient control and prevent any cyber threat [41].

#### 1.2 Securing Mechanism for iPEBB

As shown by Section 1.1, PEPDS is the way of the future. PEPDS relies heavily on the proper operation of the iPEBB. The iPEBB is the critical component of the next-generation power distribution system. For that reason, there is a need to design an anchoring mechanism to secure the iPEBB properly.

#### 1.2.1 Reasons for Needing Anchoring Mechanism

In order to implement PEPDS, all of the components must be organized and arranged so that the system is connected correctly. Unlike land-based units, the components must all stay connected through various sea states. iPEBBs are designed to be easily changed by the ship's crew while the ship is underway and robust enough to remain in place for long periods without maintenance [41]. The iPEBB needs to be securely anchored when electrical power is moving on the ship from source to load. Thus, the anchoring mechanism should be hardy enough for constant operation regardless of the sea state, stand up to the associated wear, and be easily operated for repeatedly changing out iPEBBs. Finding the solution to properly anchoring the iPEBBs is a key step to implementing PEPDS.

#### 1.2.2 Mechanical Constraints

iPEBBs interface with multiple systems that should not interact with the anchoring mechanism as described in Section 1.1.4. Specifically, the electrical, thermal, and data interfaces are connected during the insertion process, maintained while the iPEBB is in place, and disconnected when removing the iPEBB. Despite any shocks and vibrations, temperature changes, potentially corrosive atmospheric conditions, and sea states, these connections must remain actively linked underway [41].

Several additional constraints affect the mechanical characteristics of the designs. The material used in the securing mechanism must inherently resist corrosion or be coated for corrosion resistance. All edges in the design must be rounded with a minimum radius of 1mm. At the same time, exposed corners must be rounded with a minimum radius of 13mm, if practicable. Finally, all bolts in the design must be Grade 5 or stronger [14].

#### 1.2.3 Thermal and Electrical Constraints

As a power conversion device, the iPEBB generates a significant amount of heat that would cause significant damage if not removed. A design constraint was imposed

that prohibited introducing fluids into the interior of the iPEBB itself. Therefore, the top and bottom plates of the iPEBB were designed to transfer the heat to the thermal management system via conduction. While conduction is excellent for heat transfer, ensuring proper, uniform contact over such a large surface is difficult due to surface roughness and cleanliness issues. Surface roughness issues are mitigated by a surface finishing process, such as buffing. Any debris could become wedged between the thermal management system and the top and bottom of the iPEBB and impact the heat transfer rate. To maximize heat transfer, a thermal pad was added to the top and bottom of the iPEBB and secured to the surface of the iPEBB. The thermal pad was added to envelop any stray debris and to help evenly distribute the heat generation for its removal. For optimum heat transmission when using this thermal pad, a self-imposed requirement mandated that a minimum of ten psi shall be applied to the thermal pad by the cold plate. The force to provide this pressure is referred to as the securing force for the rest of this thesis. Additionally, a significant amount of heat will be built up from all of the iPEBBs in the power corridor. The heat will need to be removed by the chill water system. For more information, see Reference [43].

Electrically, exposure to an MVAC/MVDC system is lethal [12]. Therefore, caution must be taken when working on this system. The electrical connectors were sized for working with medium voltages and are rigid and expected to be longer than the iPEBB is tall. Due to the length of the electrical connectors, the iPEBB must provide electrical connection ports in the back. Thus, the iPEBB was limited to strictly horizontal motion when being inserted. Additionally, accomplishing the motion for insertion and removal fulfills the requirement that guide pins or equivalent shall be used for alignment [13]. If the iPEBB is designed to be swappable, then the electrical connections must be quick connection types. Using quick connections could pose a problem if these quick connections failed and disconnected while the iPEBB was in operation. Accidental disconnections are mitigated by ensuring a proper securing force is applied to the iPEBB when in use.

#### 1.3 Focus of Thesis

This thesis focuses on the analysis of the hinge anchoring mechanisms for the iPEBB. This is strictly on the mechanical viability, stresses, and deflections for this problem. Dynamic loading was used to evaluate the sea states that this securing mechanism is expected to encounter. Shock testing was not performed but should be tested in accordance with [38].

The structure of this thesis was to relegate a chapter to each topic for in-depth analysis. In Chapter 2, the focus is on the stress and strain analyses performed on the iPEBB. Chapter 3 presents the stress analyses to prove the viability of the hinge design. Chapter 4 presents the analyses pertinent to material selection for the iPEBB. Finally, Chapter 5 presents the results, conclusion, and future topics of interest.

### Chapter 2

### iPEBB Analysis

#### 2.1 Physical Characteristics of the iPEBB

The iPEBB shell, as shown in Section 1.1.4, is treated as a hollow, rectangular box measuring 550 mm long by 300 mm wide by 100 mm high. The representation of the iPEBB that was used in modeling is shown in Figure 2-1.

The weight limit for the iPEBB is 16 kg total. This shell houses 14 kg of electrical components that support power conversion capability. Thus, the weight limit of the shell and thermal pad is 2 kg. The specific thermal pad that will be used has not been chosen. So for these analyses, the entire 2 kg weight capacity was used for the shell. The shell is made out of aluminum. The type of aluminum is not specified so generic 1060 Aluminum was assumed. This has a density of  $2705 \frac{kg}{m^3}$  [16]. The analysis assumed uniform thickness for the entire shell and the resulting iPEBB's wall thickness is 1.5 mm. The details of this are shown in Section 4.3. Further analysis should be done on the optimal material and thickness of the iPEBB's shell.

The back of the iPEBB is configured to interface with the electrical components. The top and bottom of the iPEBB interface with the cold plates for thermal management. On the left and right sides of the iPEBB, a straight, horizontal key was added to support the weight of the iPEBB.

The forces acting on the top and bottom of the iPEBB, described in Section 1.2.2, are due to applying the cold plate to the iPEBB. To aid in conducting the heat from

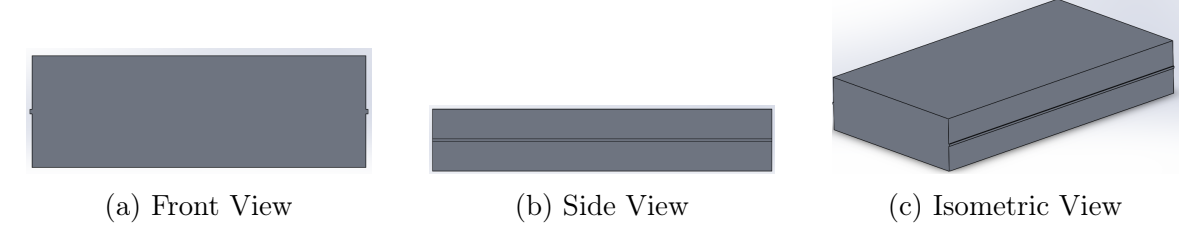


Figure 2-1: Views of Modeled iPEBB

the iPEBB, there is a thin thermal pad attached to the iPEBB interfacing with the cold plate. For the following analyses, it was assumed that the required securing pressure of 10 psi (68,948 Pa) acted on the surface area of the thermal pad. The thermal pad is aligned flush with the front of the iPEBB, covers the entire width of the iPEBB, but is offset one half inch (12.7 mm) from the back. The dimensions of the thermal pad are 537.3 x 300 x 2 mm. Thus, the contact surface area is 0.161  $m^2$  and the total force applied,  $F_A$ , is

$$F_A = (68, 948Pa)(0.161m^2) = 11,114N.$$
 (2.1)

In this chapter, the calculations performed on the key of the iPEBB are analysed. Sections 2.3.1 and 2.3.2 detail the deflection and stress of the key on the sides of iPEBB that enables the horizontal motion into the anchoring mechanism. Sections 2.4.1 and 2.4.2 show the deflection and stress on the iPEBB's shell when the securing force is applied. For this analyses, a factor of safety of two was used as the minimum unless otherwise noted.

#### 2.2 Scenarios for Analysing Stress on iPEBB Key

Before addressing the scenarios that the key was subjected to, it is important to understand why the key was used and how it could be altered. Initially, the insertion mechanism for the iPEBB was going to have both horizontal and vertical movement to secure the iPEBB to a cold plate beneath the iPEBB. This was not feasible due to rigidity and length of the electrical connections in the back of the iPEBB. Since the

electrical connections were expected to greater than 100mm, the electrical connections must attach in the rear which mandated exclusive horizontal movement. Next, the electrical components inside the iPEBB were expected to generate heat on the top and bottom of the iPEBB. So the mechanism should not interfere with the cold plate's ability to remove heat from those areas. This meant that the securing mechanism would have to provided support only on the sides of the iPEBB during the insertion and removal phases. Furthermore, depending on the design of the cold plates, the side beams (shown in Figure A-2) could overhang on the sides of the iPEBB and reduce the availability of space for to provide support. As noted in the previous section, the wall thickness for the iPEBB is 1.5mm. This is not very much material to cut into for a slot without impacting the structural integrity of the side walls of the iPEBB. Finally, to meet these functional requirements, a single lightweight key was added to the left and right sides of the iPEBB. If more support was need, additional keys could be symmetrically added to the sides or the single key could be increased in size.

Three scenarios were evaluated: (1) force from the weight of the iPEBB (normal conditions), (2) combined forces from the weight of the iPEBB and a securing force applied only to the top of the iPEBB (worst case), and (3) the weight of the iPEBB on the iPEBB's key-like structure when partially inserted into the keyway. The following figures show the forces applied to the iPEBB from each of the scenarios. The red arrows, in Figure 2-2b, signify the combined loading as the iPEBB's key was treated as a uniformly loaded beam. The derivation of all of the weights and forces for the components used are found in Appendix A.

#### **Scenario 1: Normal Conditions**

The first scenario is during normal operating conditions where the key is supporting weight of the iPEBB (157 N), and both thermal pads (11 N per pad) for a total force of 179 N split between the two keys, on the left and right sides of the iPEBB. In this scenario, either the clamping force is not yet applied or applied equally on both sides of the iPEBB, cancelling each other out. The force is applied on surface area of each of the keys for an average force of  $F_{1,avg} = \frac{179N}{2} = 89.5N$ . This scenario is

discusses to show the general stresses on the iPEBB's key. This is expected to be much less loading than scenario two. The force diagram is shown in Figure 2-2a. As shown in Figure 2-2b, when l=2 mm, the uniform load, W, on the beam is  $W_1=\frac{89.5}{2mm}=44,750\frac{N}{m}$ .

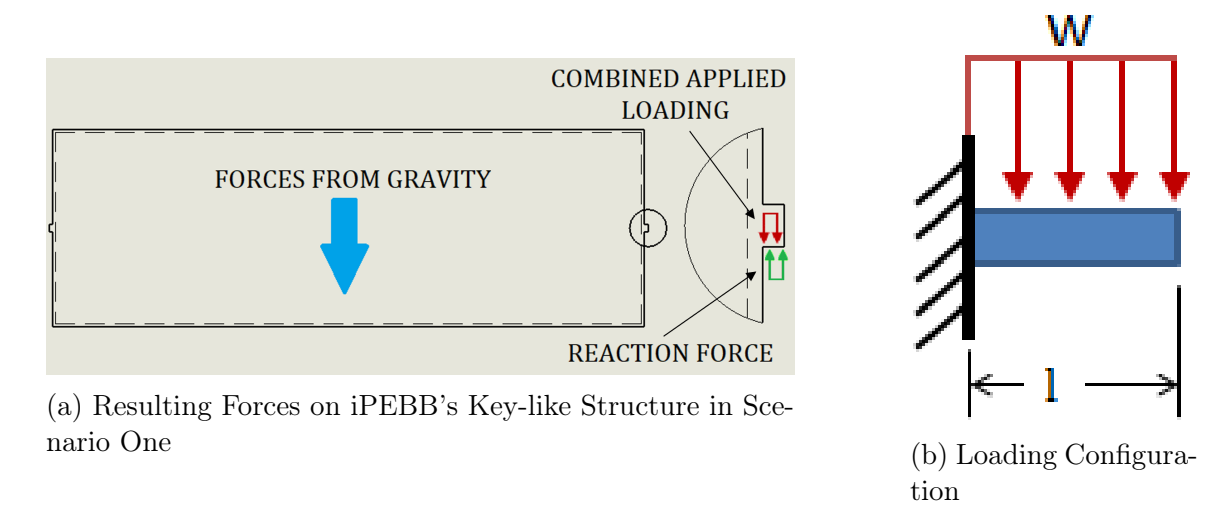


Figure 2-2: Force Analysis of iPEBB - Front View

#### Scenario 2: Unilateral Load

In the second scenario: the securing force from the top cold pate on the iPEBB (11,114N), weight of the elbow brackets (6N total), and the weight of cold plate (225N) are added to the forces observed in the first scenario. This scenario is plausible only when the securing force can be applied unilaterally. The hinge design in Chapter 3 does not fit this situation as it applies the securing force to the top and bottom of the iPEBB simultaneously. This scenario would happen during a malfunction when the securing force was applied only by the top cold plate to the iPEBB and the bottom cold plate is not providing any support. The combined loading when the securing force is applied only from top plate is more than if the securing force was applied from the bottom plate due to the bottom plate overcoming the gravitational forces for the iPEBB and thermal pad. Since all of the forces in this scenario are pointed in the same direction (downward), they are combined and split between the two keys for an average force of  $F_{2,avg} = \frac{11,345N}{2} = 5,673N$ . The size of the beam (iPEBB's

key) has not changed, thus in a similar analysis the uniform load on the beam is,  $W_2 = \frac{5,673N}{2mm} = 2,837,000 \frac{N}{m}.$ 

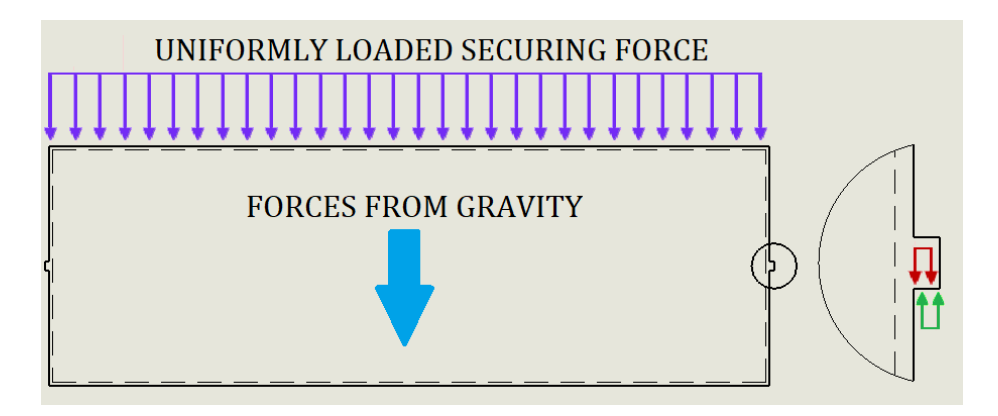


Figure 2-3: Resulting Forces on iPEBB's Key-like Structure in Scenario Two

#### Scenario 3: Partial Insertion

In the third scenario, the iPEBB is initially supported and partially inserted before removing the support. This simulates an accident scenario when the operator is not able to fully insert the iPEBB. The goal of this scenario is to find the minimum insertion distance needed to insert the iPEBB when no damage (deformation or exceeding yield stress) occurs. Since the iPEBB is not fully inserted, the only forces on the iPEBB is the the weight of the iPEBB (157 N) and the attached thermal pads (11 N per pad). These forces are combined and applied at the centroid. This problem is significantly different than the first two scenarios. Figure 2-4 shows the relationship between forces and distances at a specific moment in time. Since the majority of the iPEBB was not in the keyway, the gravitational force,  $F_G$ , was applied as a point force at the centroid of the part of the iPEBB that was not inserted. This means that the distances,  $d_{out}$  and  $d_{in}$ , changed depending on how far the iPEBB was inserted. It was assumed that the magnitude of  $F_G$  did not change no matter how far the iPEBB was inserted. This was balanced by a counter force,  $F_{CF}$ , applied at the centroid of section that had been inserted. The magnitude of  $F_{CF}$  is thus a ratio of the gravitational force.

For example, if the iPEBB was inserted 25 mm, the force due to the weight of the

iPEBB and thermal pads,  $F_G$ , would be applied at  $d_{out} = \frac{(550mm - 25mm)}{2} = 262.5mm$ . And the counter force would be applied at  $d_{in} = \frac{25mm}{2} = 12.5mm$ . The resulting magnitude of this counter force is

$$F_{CF} = F_G \frac{d_{out}}{d_{in}} = (157N + 22N) \frac{262.5mm}{12.5mm} = 3759N$$
 (2.2)

This counter force is split between the keys on the left and right sides of the iPEBB. It was assumed to be applied as a uniform load on a beam. Thus the restoring load is

$$W_3 = \frac{3759N}{(2Rails) \cdot (2mmWidth)} = 940,000 \frac{N}{m}.$$
 (2.3)

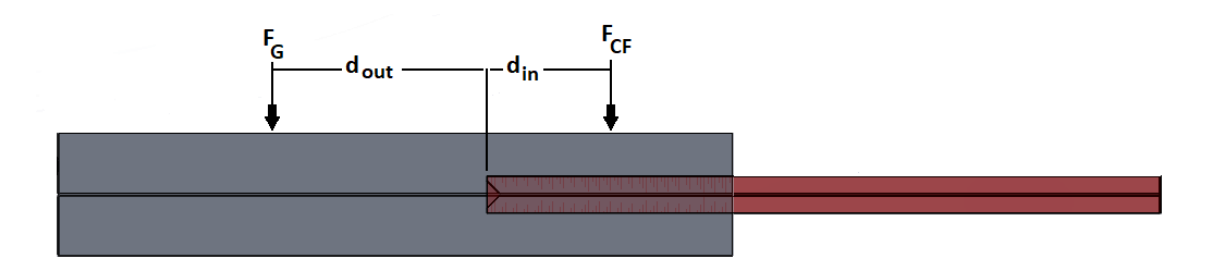


Figure 2-4: Diagram of relationship of Forces and Distances When iPEBB not Fully Inserted

#### 2.3 Analysis of iPEBB Key

The key was added to the iPEBB to (1) limit the motion of the iPEBB to the horizontal plane to fit the electrical connections (2) act as equivalent to guide pins for proper electrical alignment, and (3) support the weight of the iPEBB regardless of the status of the cold plates. It is made from the same material as the iPEBB's shell and is best seen in Figure 2-5. The dimensions of the key are 550 x 2 x 4 mm. The weight added by this feature 0.024 kg which is less than 2% of the 2 kg weight limit. The key was designed to support the worse case situation, scenario 2. The key on the iPEBB aligns with the keyway on the support structure (in red in Figures 2-6 and 2-7).

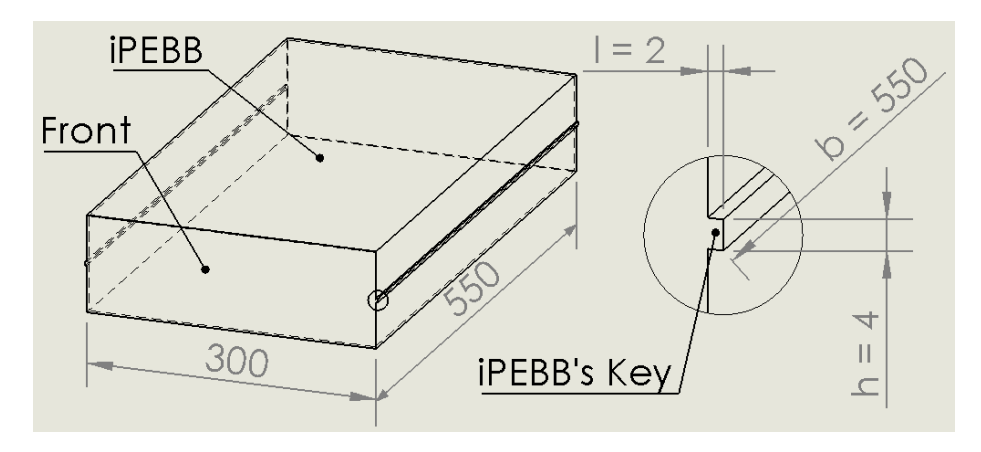


Figure 2-5: iPEBB with Detailed View of Key (Dimensions in mm)

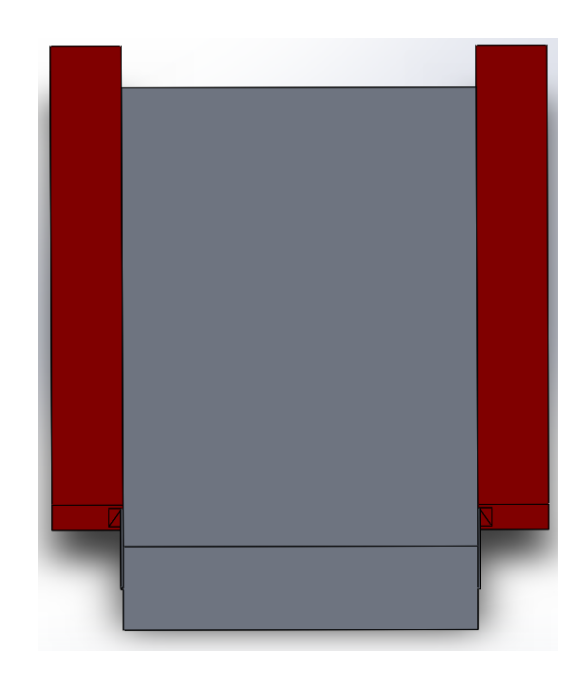


Figure 2-6: Front Overhead View of iPEBB Support and Electrical Alignment Structure  $\,$ 

A bevel was added at the entry to the keyway to aid in inserting the iPEBB into this supporting structure, as shown in Figure 2-7. The keyway runs the length of the support structure and is assumed to made of out the same material at the iPEBB. The associated measurements are illustrated in Figure 2-5.

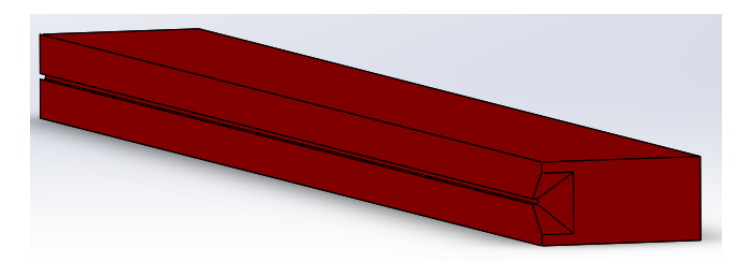


Figure 2-7: Front Inner View of Keyway

For both deflection and stress analysis the modulus of elasticity, E, is  $6.9(10^{10})Pa$ . The forces applied to the key of the iPEBB are shown in Figures 2-2 though 2-4.

The tolerance of the associated keyway in the support structure was found using ISO R 773:1969 Rectangular or Square Parallel Keys and Their Corresponding Keyways [29]. This manual is normally used to design keys and keyways between coupled shafts with their associated tolerances. Given the similarities in the key/keyway design for coupling shafts and the key-like structure on the sides of the iPEBB, it was prudent to use already established standards for the keyway.

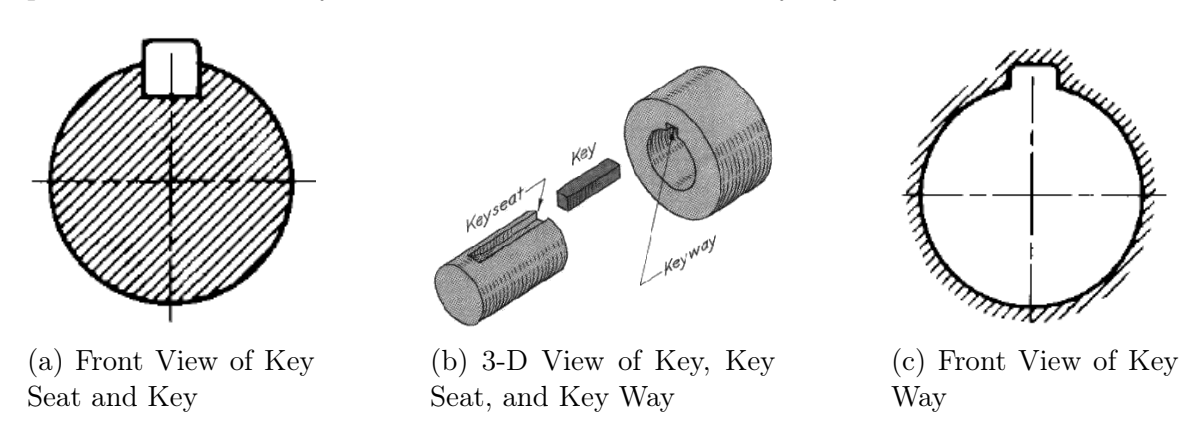


Figure 2-8: Components of a Keyed Shaft [2]

As shown in Figure 2-8b, the components included when using a key are: the keyseat, keyway, and the key itself. Keys are made with a square or rectangular cross-section with chamfered edges as shown in Figure 2-9.

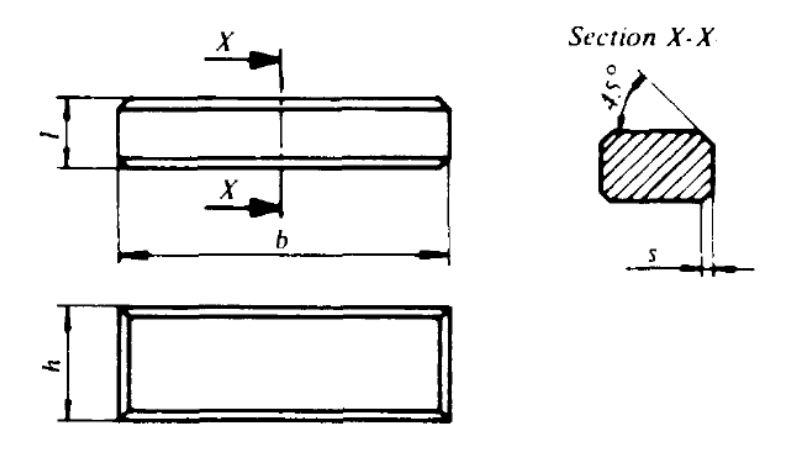


Figure 2-9: Detailed View of a Key[29]

A key with a square cross-section was used because standard sized keys are square until the key has a width (l in Figure 2-9) greater than 6mm. A typical 4x4 mm key is associated with shaft diameters of 10 to 12mm, a 45° angle chamfer with  $s = .205 \pm .045mm$ , a keyseat depth of 2.5mm, and keyway depth of 1.8 mm [29]. The important thing to note is that the depths are measured from the same point. This relation is better shown in Figure 2-10 where  $t_1$  is the depth of the keyseat and  $t_2$  is the depth of the keyway.

The difference in depth between the keyway and the keyseat is due to the components that keys are usually joining, two circular shafts. Said in another way, after accounting for the curvature the shaft, for 10mm shaft diameters, the sides of the keyway actually measure 2.0 mm. This means that the interaction between the shafts (circled in red in Figure 2-10) usually happens near the middle of the key. The actual keyway depth of 2mm shown in Figure 2-5 is comparable to the keyway depth of 2mm used to support and guide the iPEBB, shown in Figure 2-7.

When repurposing this for our needs, key and keyseat are permanently combined on the side of the iPEBB such that only the key protrudes from the side of the PEBB. The key juts out half of the usual height (l in Figures 2-5, 2-9, and 2-10). Thus, instead of 4x4 mm key, the iPEBB's key will have dimensions 4x2mm, as shown in Figure 2-5.

As far as the manufacturability of the key on the iPEBB's shell, there are many

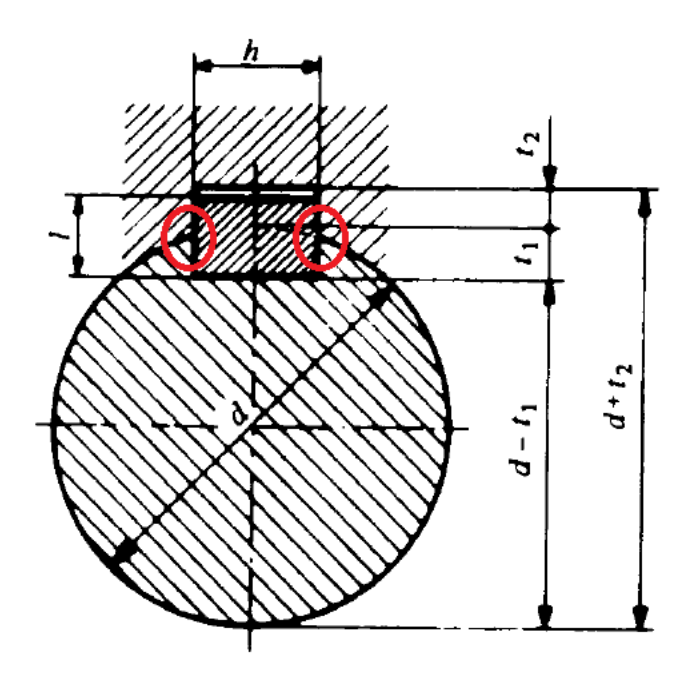


Figure 2-10: Cross-Sectional View of Key, Keyseat, and Keyway [29]

ways this could be constructed. For example, it could be welded on during the assembly of the PEBB or the material around this feature could be removed leaving the key as the raised feature on the sides of the iPEBB. If this feature was welded on, the strength and quality of the weld would need to be considered for design calculations and thoroughly examined during construction. Additionally, mitigating the stress concentration at the corners of the key by a fillet was not examined. The structural impacts on the iPEBB's key for any production method were not investigated. The material was assumed to be homogeneous and that failure of the key would occur either via bending or shear similar to solid structure. Similarly, the impact on the iPEBB's shell was not investigated for any production method.

The associated keyway for the key on the outside of the iPEBB, shown in Figure 2-7, runs the length of the iPEBB and is also sized to fit a 4x4 mm key. The machining tolerance the key is -0.03 mm and keyway is +0.03 mm [29]. This means that the range of widths of the key (labeled "h" on Figure 2-9) are 3.97 - 4 mm. The range of widths of the keyway (also labeled "h" on Figure 2-10) are 4 - 4.03 mm The combined tolerance for the smallest key and largest keyway is 0.06 mm. For all of the scenarios for this analysis, it was assumed that the loading on the key would be uniform. For

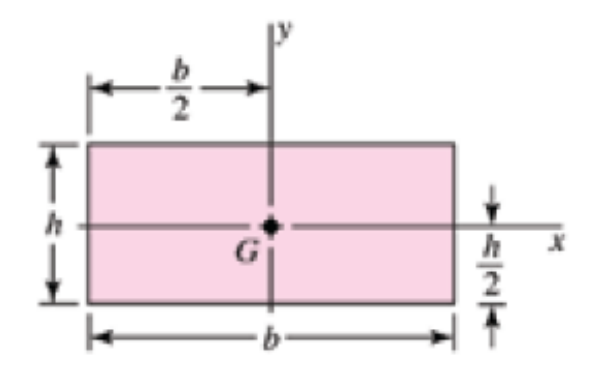


Figure 2-11: Second Moment of Area[5]

this assumption to be valid in scenario three, the iPEBB must be nearly flat to have uniform loading. Assuming the iPEBB's key is rigid, after inserting the iPEBB 5 mm into the keyway, it would drop less than 0.7°. This is a very small angle, and would decrease as the iPEBB was inserted. Thus the iPEBB was assumed to be flat and uniform loading is justified for calculations performed later in this chapter.

## 2.3.1 iPEBB Key - Deflection

The value or method for finding the value of the uniform load, W, was shown in Section 2.2. With that known, the next step in finding the deflection is to determine the second moment of inertia, I. To correctly find I, the shape of the rectangular key must be taken into account. As shown in Figure 2-11, the relevant parameter are height, h, and width, b. The height is h = 4mm and the width is b = 550mm. The dimensions of the key are best shown in Figure 2-5.

Putting this all together, the second moment of inertia, I, was determined using

$$I = \frac{bh^3}{12} = \frac{(550mm)(4mm)^3}{12} = 2.93(10^{-9})m^4$$
 (2.4)

Finally, the deflection was found using

$$Y = \frac{Wl^4}{8EI} = \frac{W(2mm)^4}{8(6.90)(10^{10}Pa)(2.93)(10^{-9}m^4)} = (W)(9.88)(10^{-15})\frac{m^2}{N}$$
(2.5)

Based on Eqn 2.5, for scenarios one and two the total deflections are  $Y_1$ 

 $4.42(10^{-10})m$  and  $Y_2 = 2.80(10^{-8})m$  respectively. Using a similar method but inserting the iPEBB 25mm, the second moment of area becomes

$$I = \frac{(25mm)(4mm)^3}{12} = 1.33(10^{-10})m^4 \tag{2.6}$$

The resulting deflection for scenario three is  $Y_3 = 2.05(10^{-7})m$ . This shows that very little deformation will happen under these scenarios. Failure in scenario three depends more on the bending and shear stresses than the deflection. This number was given for reference.

## 2.3.2 iPEBB's Key - Stress

This analysis was performed to evaluate the bending stress and shear stresses for this design. While finding the amount of stress on the key of the iPEBB, only scenarios two and three were examined. Scenario two had a similar analysis but more loading was applied compared to scenario one. The loading configuration for all scenarios analyzed was assumed to be uniformly loaded.

Starting with scenario two, the maximum bending stress occurs when the maximum moment,  $M_{MAX}$ , is produced for this reaction. To find the maximum moment for a uniformly loaded beam, the magnitude of the uniform force was applied at the centroid as a point force. In this case, the centroid is located at  $\frac{l}{2}$ . The equation below provides an example of this using the values for scenario two.

$$M_{2,MAX} = (Force)(Length) = (W_2 l)(\frac{l}{2}) = \frac{(2,837\frac{kN}{m})(.002m)^2}{2} = 5.67N \cdot m$$
 (2.7)

The largest bending stresses occur at the top and bottom of the key-like structure, at a distance of  $\frac{h}{2}$  from the midline. For reference, this is shown in Figure 2-5. Again using the values for scenario two, the equation for bending stress is

$$\sigma_{2,MAX} = \frac{M \cdot c}{I} = \frac{(M_{2,MAX})(\frac{h}{2})}{I} = \frac{(5.67N \cdot m)(\frac{.004m}{2})}{2.93(10^{-9})m^4} = 3.87MPa$$
 (2.8)

As seen in Table 2.1, the yield strength of Al 1060 is 28 MPa [16]. Thus the

Table 2.1: Typical Mechanical Properties of 1060 Aluminum [16]

	Tensile strength		Yield strength		Elongation(a),	Hardness,	Shear strength		Fatigue limit(c)	
Temper	MPa	ksi	MPa	ksi	%	HB(b)	MPa	ksi	MPa	ksi
0	69	10	28	4	43	19	48	7	21	3
H12		12	76	11	16	23	55	8	28	4
H14	97	14	90	13	12	26	62	9	34	5
H16	110	16	103	15	8	30	69	10	45	6.5
H18	131	19	124	18	6	35	76	11	45	6.5

bending Factor of Safety,  $FOS_{2,bending} = \frac{28MPa}{3.87MPa} = 7.24$  when fully inserted under the highest stress scenario of unequal loading applied by the cold plates.

To find the shear stress, the formula for the shear stress for beams in bending was used and is shown below. The shear force, V, is the combined force,  $(F_{2,avg})$ , applied on one side of the iPEBB's key-like structure.

The shear area,  $A_S$ , is the product of the length (b) and thickness (h) from Figure 2-5. The maximum shear stress,  $\tau_{max}$ , was found as follows:

$$\tau_{2,max} = \frac{3V_2}{2A_S} = \frac{(3)(5673N)}{(2)(.0022m^2)} = 3.87MPa \tag{2.9}$$

The factor of safety was found by relating the calculated maximum shear stress to the yield strength in shear. The conservative Maximum Shear Stress (MSS) method for ductile materials implies that the yield strength in shear is half of the tensile yield strength [5]. However, from testing performed to generate Table 2.1, the shear strength is known. In keeping with the conservative nature, the yield strength in shear,  $S_{sy}$  was estimated to be half of the shear strength given in Table 2.1,  $S_{sy} = \frac{48MPa}{2} = 24MPa$ . The resulting factor of safety is  $FOS_{2,shear} = \frac{24MPa}{3.87} = 6.20$ .

For scenario three, the process was performed after re-arranging Eqns 2.7-2.9 with a minor difference. The force due to gravity,  $F_G$ , takes into account only the weight of the iPEBB and the attached thermal pads for a total of  $F_G = 179N$ . This scenario was calculated differently because the length, b, of the insertion of the iPEBB was not initially known. Instead of having a goal distance to meet, these calculations were performed by working backwards, starting with a reasonable factor of safety.

The other main difference was applying the force due to gravity and this was already discussed in Section 2.2.

Starting of with the minimum safety factor = 2, the max bending stress was found to be:  $\sigma_{3,MAX} = \frac{S_{sy}}{2} = 14MPa$ . Next, Eqn. 2.8 was rearranged to include the insertion length,  $b_{in}$  as shown below:

$$\sigma_{3,MAX} = \frac{(M_{MAX})(\frac{h}{2})}{I} = \frac{(F_{CF}\frac{l}{2})(\frac{h}{2})}{\frac{b_{in}h^3}{12}} = \frac{3lF_G}{b_{in}h^2} \left(\frac{550 - b_{in}}{(b_{in})}\right)$$
(2.10)

It is worth mentioning again that similar to Eqn 2.8, this analysis assumes uniform surface contact and loading. This led to the quadratic equation necessary to solve for  $b_{in}$ . Only the positive root from this equation is useful.

$$\left(\frac{4(\sigma_{3,MAX})(h^2)}{3(l)(F_G)}\right)b_{in}^2 + b_{in} - .550 = 0 : b_{in,bending} = 35.13mm$$
(2.11)

Thus  $b_{in}$  must be larger than 36 mm to prevent failure due to bending stress with a factor of safety of two.

For shear stress, a safety factor = 2 was again used to determine minimum insertion length. Thus  $\tau_{3,max} = 24MPa$ . Using  $A_S = b_{in}h$ , Eqn 2.9 was rearranged to solve for  $b_{in}$ .

$$\tau_{3,max} = \frac{3V}{2(b_{in}h)} : V = F_G\left(\frac{.550 - b_{in}}{b_{in}}\right) : \tau_{3,max} = \frac{3F_G}{2h}\left(\frac{.550 - b_{in}}{b_{in}^2}\right)$$
(2.12)

This led to the quadratic equation necessary to solve for  $b_{in}$ . Only the positive root from this equation is useful.

$$\left(\frac{2h\tau_{3,max}}{3F_G}\right)b_{in}^2 + b_{in} - .550 = 0 : b_{in,shear} = 27.04mm$$
(2.13)

Thus  $b_{in}$  must be larger than 27 mm to prevent failure due to shear stress with a factor of safety of two. In this scenario, the bending stress is more limiting. It is recommended to ensure that the iPEBB has been inserted a minimum of 36 mm before releasing the iPEBB. The best practice would be to fully insert or remove the

iPEBB.

This meets the design standard of obtaining a factor of safety of at least 2 for this section. The reason for analysing the shear and bending stresses is to determine the weak areas of this design and determine failure before it happens.

# 2.4 Analysis of iPEBB Shell

The lightweight shell is designed to contain and protect the power conversion components. As described in Section 2.1, the shell of the iPEBB is uniformly 1.5 mm thick. The shell also conducts the heat, generated inside by the electrical components, to the thermal pad and cold plate. For this thesis, it was assumed that the iPEBB would be water cooled as this method has the capacity to remove the heat generated. Other heat removal methods may work but were not considered.

Conduction is most effective when the two surfaces are firmly connected to each other without air gaps and debris. The thermal pad is more flexible than the Al 1060 shell and thus better at maximizing the contact area between the iPEBB and the cold plate. To further improve the thermal conductivity of the thermal pad, the cold plates are secured with 10 psi of pressure on both the top and bottom by the cold plates.

The resulting structural impact on the iPEBB from the clamping pressure is evaluated next. This section will examine two cases. Case one is the impact on the top of the shell and case two is the impact on the sides of the shell. The goal of case one analysis is to limit the deflection to minimize impact to interior electrical components. The goal of the case two analysis is to ensure that the sides of the iPEBB will not buckle.

# 2.4.1 iPEBB Shell - Top Face Analysis

The first step in the analysis of the shell begins with the top and bottom cold plates. The primary force on these plates is the securing force applied through the cold plate and then the thermal pad to the top and bottom faces of the iPEBB's shell. In addition to the securing force (11,114 N), the weights of top cold plate (225 N) and thermal pad (11 N) are added to the total force pressing down onto the top of the iPEBB. The size of the thermal pad is discussed in more detail in Section 3.2.1. The top face of the iPEBB is the limiting side and thus the rest of the analysis is performed on the top plate.

As mentioned previously, the securing force is first applied to the cold plate. For this analysis, the exact dimensions of the aluminum cold plate are assumed to be 550 x 300 x 25.4 mm. Next, the cold plate is classified by the ratio of thickness (h) to another plate dimension (a) [47]. For example, the cold plate is 550 mm in length and is 25.4 mm thick. This ratio  $\frac{a}{h} = \frac{550mm}{25.4mm} = 21.7$ . Ratios between 10 and 80 are classified as thin plates. In general, the term thin plate is understood to mean a stiff plate in which the loads applied are carried two dimensionally by internal bending and twisting moments, and transverse shear forces [47].

Next, the securing force was assumed to be applied uniformly over the cold plate. The deflection of the cold plate was analysed using Navier's Method (double series solution) and checked with both *Roark's Formulas for Stress and Strain* as well as SolidWorks Simulation. The stress on the cold plate was computed via *Roark's Formulas for Stress and Strain* as well as SolidWorks Simulation. For Navier's Method, the following assumptions were made [47]:

- 1. The plate is initially flat.
- 2. The material, aluminum, is elastic, homogeneous, and isotropic.
- 3. The deflection is small compared to the thickness of the plate.
- 4. Straight lines, initially normal to the middle plane remain normal to the middle plane during and after deformation.
- 5. Normal stress in the transverse direction is small compared with other stress component and can be disregarded.
- 6. The middle surface remains unstrained after bending.

Using Kirchhoff's assumptions, contained in the assumptions above, Lagrange introduced the governing differential equation for plate deflections shown in Eqn 2.14. Navier posed that a solution to this governing equation for the deflection at any point was in the form of an infinite Fourier series. This is shown in Eqn 2.15. The deflection is found from the force of distributed surface load, p(x,y), and is shown in Eqn 2.16. In this section, u, v, and w are components of the displacement vector occurring in the x, y, and z directions respectively, and p is the flexural rigidity of the plate (shown in Eqn 2.22). Additionally, p and p are positive in downward directions.

$$\nabla^4 w = \frac{d^4 w}{dx^4} + 2\frac{d^4 w}{dx^2 dy^2} + \frac{d^4 w}{dy^4} = \frac{p}{D}$$
 (2.14)

Where w is a displacement vector

$$w(x,y) = \sum_{m=1}^{\infty} \sum_{n=1}^{\infty} w_{mn} sin(\frac{m\pi x}{a}) sin(\frac{n\pi y}{b})$$
(2.15)

$$p(x,y) = \sum_{m=1}^{\infty} \sum_{n=1}^{\infty} p_{mn} sin(\frac{m\pi x}{a}) sin(\frac{n\pi y}{b})$$
 (2.16)

In Eqn 2.16, m and n are indexing variables and a and b are the side lengths of the plate. Figure 2-12 is helpful to view a generic simply supported plate with the origin at the corner referencing the variables used.

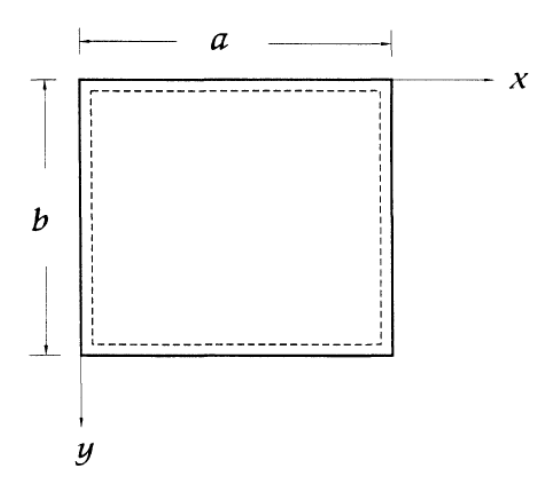


Figure 2-12: Simply Supported Plate with Uniform Normal Loading [47]

The cold plate was assumed to be simply supported on all four edges. Boundary conditions for simply supported edges are shown in Eqn 2.17 along the edge when x=0.

$$w = 0|_{x=0} : \frac{d^2w}{dx^2} = 0|_{x=0}$$
 (2.17)

When developing the solution, it was not known if the surface load would be uniformly applied on the entire area or a patch of it. To be more versatile, the expression was determined for the situation when the surface load was applied to a single patch. In this analysis, the exact placement of the patch can vary and surface load was assumed to produce the equivalent of 10 psi of securing pressure on the iPEBB. A representation of this situation is shown in Figure 2-13. After inserting Eqn 2.17 into Eqn 2.15 and performing some routine simplification detailed [47], the resulting expression for deflection is shown in Eqn 2.18.

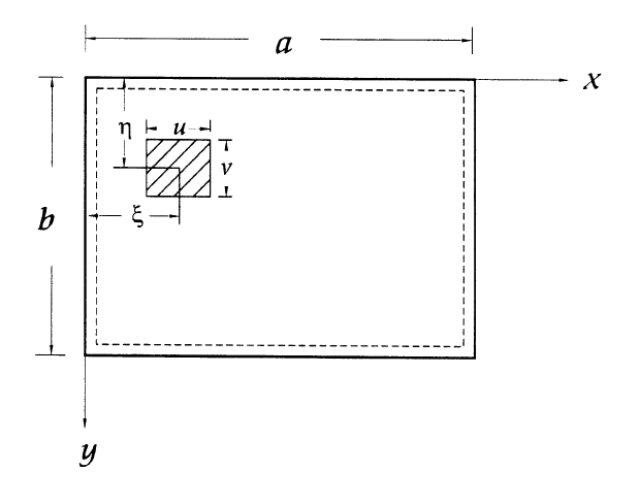


Figure 2-13: Simply Supported Plate Loaded in Single Patch on Plate [47]

$$w(x,y) = \frac{16p_0}{\pi^6 D} \sum_{m=1}^{\infty} \sum_{n=1}^{\infty} \frac{\sin(\frac{m\pi\xi}{a})\sin(\frac{m\pi\eta}{b})\sin(\frac{m\pi\eta}{2a})\sin(\frac{m\pi v}{2b})\sin(\frac{m\pi x}{a})\sin(\frac{m\pi y}{b})}{mn[(\frac{m}{a})^2 + (\frac{n}{b})^2]^2}$$
(2.18)

Using MATLAB, the resulting deflection was found to be the highest when there was one node, m = n = 1. Under this loading condition, the maximum plate deflection was  $y_{N,max} = 0.053mm$ . The associated code is found in Appendix E.1. This result was cross referenced with Roark's Formulas for Stress and Strain. From this analysis,

the stress at the center was  $\sigma_{R,max} = 5.60MPa$  and the displacement was  $y_{R,max} = .052mm$  [48]. The associated calculations are shown in Appendix D.1.1 The next step was to model this situation in SolidWorks and determine the result. From SolidWorks, the stress at the center was  $\sigma_{S,max} = 4.842MPa$  and the deflection was  $y_{S,max} = .04996mm$ . The SolidWorks analysis is detailed in Appendix B.1.1. The yield strength of aluminum alloy 1060 is 28 MPa [16]. Thus, based on the stress from Roark's analysis, the Factor of Safety is 4.9. The difference in the stress calculations is in-part due to the difference in edge conditions. The solution obtained by the Navier Analysis and Roark's Formulas assume that the sides are simply supported. When using SolidWorks, the edges had to have additional constraints to effectively model the scenario and the results can vary depending on the size of the mesh. The more conservative approach is to base the factor of safety on Roarks analysis since it has been used to verify various SolidWorks models and had the higher stress value.

From these calculations, the maximum that the plate will deform is 0.053mm. Earlier, it was assumed that the cold plate material is isotropic. This assumption is carried forward when combining the cold plate, thermal pad, and top face of the shell to all layers are assumed to be isotropic and that sliding between them is prevented. This is a common assumption for multilayered materials [47]. Furthermore, since the shell of the iPEBB and the cold plate are made out of the same material, their deformations should be similar. The result of these assumptions is that the iPEBB's shell will not deform any more than the cold plate.

## 2.4.2 iPEBB Shell - Side Face Analysis

The next step is to ensure that the sides of the iPEBB's shell are strong enough to withstand the compressing forces. This analysis consisted of determining the minimum compressive edge load that causes bucking and comparing it to the compressive load that is acting on the edge. This was done following the Equilibrium Method outlined in [47].

To solve this problem, the equilibrium method was used to conduct the linear buckling analysis. This method was used due to the rectangular nature of the iPEBB's side plates. The assumptions for this method, taken from [47], are:

- 1. The plate is initially flat and all loads act strictly on the middle of the plate.
- 2. States of stress are described by equations of the plane elasticity.
- All loads applied are dead loads; they do not change in value when the plate deforms.
- 4. Plate bending is described by Kirchoff's plate bending theory.

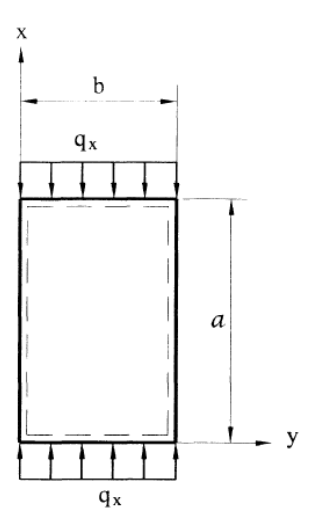


Figure 2-14: Force Analysis of iPEBB

Figure 2-14 shows the plate, associated parameters, and their orientation.

The general governing differential equation for plate is shown below:

$$\frac{d^4w}{dx^4} + 2\frac{d^4w}{dx^2dy^2} + \frac{d^4w}{dy^4} = \frac{1}{D}\left(N_x \frac{d^2w}{dx^2} + 2N_{xy} \frac{d^2w}{dxdy} + N_y \frac{d^2w}{dy^2}\right)$$
(2.19)

In this analysis, we assume that the sides are simply supported and there are only forces compressing the plate in the y-direction. This leaves the internal forces  $(N_i)$  with the following values:

$$N_x = -q_x : N_y = N_{xy} = 0 (2.20)$$

Eqn 2.19 is simplified after inserting the simply supported boundary conditions (Eqn 2.17) and the internal forces from Eqn 2.20. The resulting simplification is shown below:

$$D\nabla^2\nabla^2 w + N_x \frac{d^2 w}{dx^2} = 0 (2.21)$$

The general solution to the above equation is in the form of Eqn 2.15. After inserting Eqn 2.15 into Eqn 2.21 and performing routine simplification detailed in [47], the resulting equation had three parts and the product of which is zero. Disregarding the trivial solution when  $w_{mn} = 0$  (meaning no buckling and the plate is flat) and the trigonometric functions (used to satisfy the boundary conditions), the remaining part is set equal to zero. It was rearranged to find the edge load,  $q_x$ , as shown below:

$$q_x = \frac{\pi^2 D}{b^2 h} \left( \frac{mb}{a} + \frac{n^2 a}{mb} \right)^2 : D = \frac{Eh^3}{12(1 - v^2)}$$
 (2.22)

For the plate flexural rigidity, D, the Poisson Ratio, v = 0.333, iPEBB shell thickness h = 1.5mm, and modulus of elasticity, E = 69.3GPa.

This edge load has been determined by the properties of the plate. This value is the load that, when exceed, will cause buckling of this plate. The design must take into account the critical value, that is the smallest applied loading that will cause buckling. This occurs when m = n = 1 on the larger side plate and the value is shown below for the side plates (Eqn 2.23) and front and back plates (Eqn 2.24).

$$q_x = \frac{\pi^2(21,827N \cdot m)}{(550mm)^2(1.5mm)} \left(\frac{(1)(550mm)}{100mm} + \frac{(1)^2(100mm)}{(1)(550mm)}\right)^2 = 15.32 \frac{N}{mm}$$
 (2.23)

$$q_x = \frac{\pi^2(21,827N \cdot m)}{(300mm)^2(1.5mm)} \left(\frac{(1)(300mm)}{100mm} + \frac{(1)^2(100mm)}{(1)(300mm)}\right)^2 = 17.73 \frac{N}{mm}$$
 (2.24)

The loading on the sides of the plate was determined by summing the forces on the iPEBB shell's top plate. The forces are the clamping force (11,114 N) and the weight of the cold plate and thermal pad (236N). Next, it was assumed that edges would be loaded with a uniform distributed load. The total length of the edge is (2\*550mm) + (2\*300mm) = 1700mm. Thus the uniform distributed load was

determined to be  $q_{x,applied} = \frac{11,350N}{1700mm} = 6.68 \frac{N}{mm}$ . This is less than the minimum load required to cause bucking in the sides of the iPEBB. The factor of safety for bucking is  $FOS_{buckling} = \frac{15.3 \frac{N}{mm}}{6.68 \frac{N}{mm}} = 2.29$ . The MATLAB code used for the analysis of the side plate can be seen in Appendix E.2. To provide an additional analyses of the buckling of the plate, SolidWorks and Roark's formulas were used as described in Appendixes B.2 and D.1.2 respectively. The result from SolidWorks analysis was  $FOS_{buckling} = 4.0276$ . When working with the SolidWorks tools, the answers varied based on the size of the mesh and edge conditions. For example, even with no lateral forces, the SolidWorks analysis would find lateral movement/displacement by the plate. This led to additional constrains applied to the plate that may not be representative of actual conditions. This was not present in the other two calculations.

From Roark's formulas, only the front and back plate were able to be reliably analysed. From this analysis, the critical unit component stress was  $q' = 18.12 \frac{N}{mm}$  (compared to Eqn 2.24) and its  $FOS_{buckling} = 2.71$ . The results from SolidWorks and the Equilibrium Method indicate that all of the side faces are safe from buckling. The analysis from Roark's formulas can only truly claim the front and back faces are safe from buckling. For the side face, the length to width ratio (a/b ratio) is not contained in the reference table. Thus to get the critical stress, values would have to be extrapolated vice interpolated and the shape of the graph outside the bounds is not known. It is worth noting the similar values for the critical component unit stress for the front and back sides of the iPEBB's shell from the Equlibrium Analysis and using Roark's formulas.

# 2.5 Dynamic Loading

Until now, the loading discussions have used static loading to determine the feasibility of the design. It would not make sense to test a structure dynamically if it failed statically. Likewise, since this electrical distribution system is to be mounted on a ship, dynamic loads must be considered. Naval Sea Systems Command (NAVSEA) has approved a standard defining the interface requirements for structures, systems,

and equipment that are affected by ship motion and attitudes. This standard takes into account the motions and attitudes of the ship, with the exception of sway, to find the loading factors. Sway is not considered due to its small magnitude. The loading factor is a calculated acceleration dependent on the location in the ship of the structure or equipment, the type of ship, and in what sea state the ship is present. For these calculations, it was assumed that the ship is notional 10,000 ton destroyer-type vessel as described in Ref [8]. The possible locations in the ship are shown in Figure 2-15. The locations further from the center of gravity of the ship are subject to higher accelerations thus the highest and furthest forward and aft locations were evaluated. The electrical system needs to work in all sea states so Sea State 8 motions and attitudes were used for these calculations. The structure or equipment evaluated is the iPEBB.

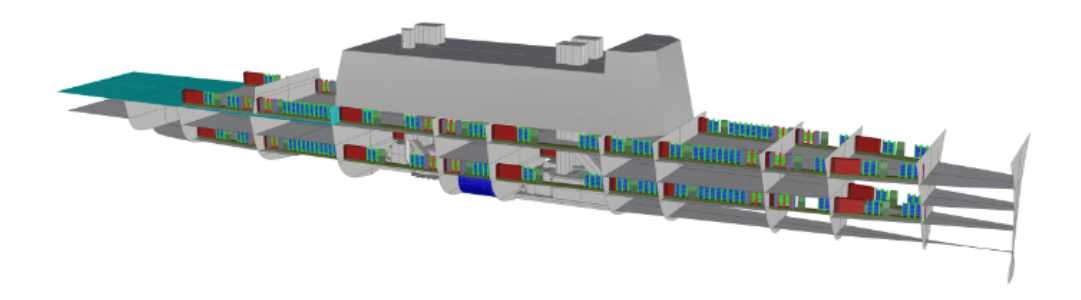


Figure 2-15: Locations of Power Corridor on Model Ship[22]

After the loading factors for both forward and aft locations were found, they were multiplied by the mass of the iPEBB to find the design loads. Finally, the magnitude of the resultant design load was calculated and added to the static loading for further analysis.

## 2.5.1 Dynamic Loading Calculations

This section is a high level summary of the process used to determine the resulting dynamic force acted on the iPEBB. In-depth calculations are provided in Appendix D.2 and are in line with the latest Department of Defense Standards [11]. The ship chosen to model the dynamic load considerations on was the notional 10,000 ton

destroyer-type vessel [8]. Relevant characteristics are shown in Table 2.2.

Metacentric Height

Value Symbol В 24 m

GM

1.30

m

Constants Units Beam (at waterline) Length Between Perpendiculars L 184  $\mathbf{m}$ Τ Draft 16 m Displacement Δ 10,000 mton

Table 2.2: Ship Characteristics

The roll constant, C, for ships is determined experimentally. For the World War II era destroyers (DDs), the roll constant was C = 0.82. For older aircraft carriers (CVs), C = 0.725 [11]. It was assumed that the notional ship had a roll constant similar to a older DDs but were more stables thus C = 0.78 was used for calculations.

After finding the ship's characteristics, the next step was to determine the load factors,  $(A_{(i)})$ . The load factors are determined in principal directions (i = x, y, or z)are as follows:

$$A_x = gsin(\theta) + s + \frac{4\pi^2}{T_P^2}\theta^2 X + \frac{4\pi^2}{T_P^2}\theta Z$$
 (2.25)

$$A_y = gsin(\phi) + \frac{1}{2} \cdot \frac{4\pi^2}{T_P^2} \theta X + \frac{4\pi^2}{T_r^2} \phi^2 Y + \frac{4\pi^2}{T_r^2} \phi Z$$
 (2.26)

$$A_z = g \pm \left( h + \frac{4\pi^2}{T_P^2} \theta X + \frac{4\pi^2}{T_r^2} \phi z \right)$$
 (2.27)

where g is the gravitational constant  $(9.807\frac{m}{s^2})$ ,  $\theta$  is the max pitch angle (radians),  $\phi$  is the maximum roll angle (radians),  $T_P$  and  $T_r$  are the pitch and roll periods respectively (seconds), h and s denote the respective heave and surge accelerations  $(\frac{m}{s^2})$ , and X, Y, Z are the distances (in meters) from the center of gravity of the ship along their respective axis to the location of the structure. The principal directions for a generic ship are shown in Figure 2-16 where the origin is located at the ship's center of gravity. The load factor in the z-direction, is different than the rest as it contains a plus-minus sign based on the direction of the force. When the force is acting downward (negative z-direction), it is a positive and all of the components are summed together. When the plus-minus become a negative, the load is acting upwards in the positive z-direction.

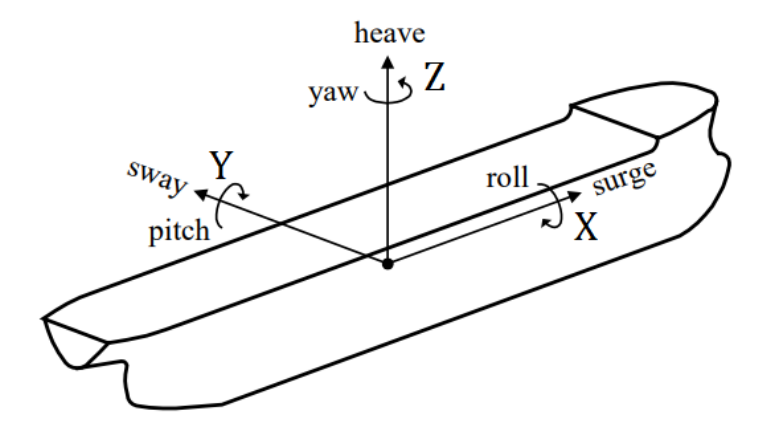


Figure 2-16: Generic Ship Axes [40]

The design load is the product of the loading factor and the weight of the structure or equipment. The formula is shown below:

$$F_{(i)} = \frac{W}{q} \cdot A_{(i)} \tag{2.28}$$

Where  $F_{(i)}$  is the design load in the principal direction (x, y, or z), and W is the weight of the iPEBB (N).

The magnitude of the total design load or dynamic force,  $F_{dyn}$ , was found using the formula below:

$$F_{dyn} = \left(F_x^2 + F_y^2 + F_z^2\right)^{1/2} = \left((73.0)^2 + (154)^2 + (336)^2\right)^{1/2} = 376.3N$$
 (2.29)

Over the entire range of the possible values for C, the magnitude of  $F_{dyn}$  only varies by 10 N. More directly, the lower the value of the roll constant, the larger the total dynamic force. Thus, having a lower roll constant for better crew comfort will not greatly affect the dynamic loading. For the remaining section in Chapter 2, the dynamic force will be added to the deflection and stress calculations previously covered in this chapter and a final factor of safety will be calculated.

## 2.5.2 Key

The iPEBB's key was first analyzed for deflection under dynamic loading. In Section 2.2, the average applied force in scenario two,  $F_{2,avg}$ , was composed of the force applied only by the top plate and the weights of the iPEBB, cold plate, and thermal pad onto on of the iPEBB's keys. For this analysis, only the component of the dynamic force acting in the same direction as the forces compiled in  $F_{2,avg}$  was considered. In this scenario,  $F_z$  in the downward direction was applied equally between both iPEBB keys. Evaluating the resulting deflection from the dynamic forces results in a new total force, uniform load, and deflection are as follows:

$$F_{t,dyn} = F_{2,avg} + F_z = (5,673N) + \left(\frac{336N}{2}\right) = 5,841N$$
 (2.30)

After determining the uniform loading from the this increased force,  $W_{2,dyn}$  was substituted into Eqn 2.5 to find the deflection as shown below.

$$W_{2,dyn} = \frac{5,841N}{2mm} = 2.92 \frac{MN}{m} : Y_{2,dyn} = 2.89(10^{-8})mm$$
 (2.31)

The analysis for scenario three was not performed. It was assumed that that operator would be inserting and removing the iPEBB in a smart and efficient manner.

The iPEBB's key was then analysed for stress under dynamic loading. In Section 2.3.2, the maximum moment was determined by the bending stress on the key. This static force consisted of the force applied only by the top plate and the weights of the iPEBB, cold plate, and thermal pad. For this analysis, the addition of the total design load is again only from the z-direction. The new maximum moment, bending stress, and factor of safety were determined in the same manner as before from Eqns 2.7 and 2.8.

$$M_{MAX,dyn} = \frac{(2,920\frac{kN}{m})(.002m)^2}{2} = 5.841N \cdot m \tag{2.32}$$

$$\sigma_{2,dyn} = 3.983MPa : FOS_{bend} = 7.0$$
 (2.33)

This shear force consisted of the force applied by the top plate, dynamic loading

in the downward direction, and the weights of the iPEBB, cold plate, and thermal pad. It was again assumed to loaded uniformly on both of the keys (left and right sides) of the iPEBB. The shear stress was based on the shear force, V = 5.841KN. The new shear force leads to a new shear stress of:

$$\tau_{2,max} = 3.983MPa : FOS_{shear} = 6.0$$
 (2.34)

### 2.5.3 Cold Plate and Shell

The top face for the shell was again analysed by finding the deflection of the cold plate. The iPEBB Shell analysis performed in Section 2.4.2 has been modified to include the addition of dynamic loading of 335.5N in the negative z-direction. This results from the MATLAB script was a maximum deflection of  $y_{dyn,max} = 0.053mm$ . This is a similar value to the deflection without the dynamic forces. This result makes sense due to the magnitude of the dynamic loading compared to the securing force. Using Roark's Formulas for Stress and Strain, the resulting stress was  $\sigma_{dyn,max} = 5.73MPa$  and the displacement was  $y_{dyn,max} = -0.055mm$ . From SolidWorks, the stress at the center was  $\sigma_{dyn,max} = 5.011MPa$  and displacement was  $y_{dyn,max} = 0.05171mm$ . Using the max stress found by Roark's analysis, the minimum Factor of Safety for bending is  $FOS_{bending} = 4.89$ .

The side faces of the iPEBB were analysed for buckling with the addition of the dynamic loading. Similarly to the cold plate analysis, only the dynamic load in the Z-direction was included in this analysis. Based on the MATLAB code explained in Section 2.4.1, the edge forces increased to  $7.063\frac{N}{mm}$ . The force required to cause bucking didn't change and thus the new Factor of Safety for bucking is  $FOS_{Bucking} = 2.17$ . As detailed in Appendix B.2.2, the resulting Factor of Safety from SolidWorks was  $FOS_{Bucking} = 3.884$ . Using the same process for Roark's Formulas for the static loading (found in Appendix D.1.2), the resulting Factor of Safety was  $FOS_{Buckling} = 2.57$  for the front and back plates. The results from SolidWorks and the Equilibrium Method indicate that all of the side faces are safe from buckling under dynamic loading. As already explained, the analysis from Roark's formulas can only claim the

front and back faces are safe from buckling under dynamic loading.

# Chapter 3

# Hinge Securing Mechanism

In this chapter, the analysis specific to proving the feasibility of the hinge design for the securing mechanism is shown. Section 3.1, explains the design overview. Section 3.2 addresses how the securing force is applied to the iPEBB when inserted. Section 3.3 address the locking mechanism for the cold plates when not in use.

# 3.1 Hinge Mechanism Overview

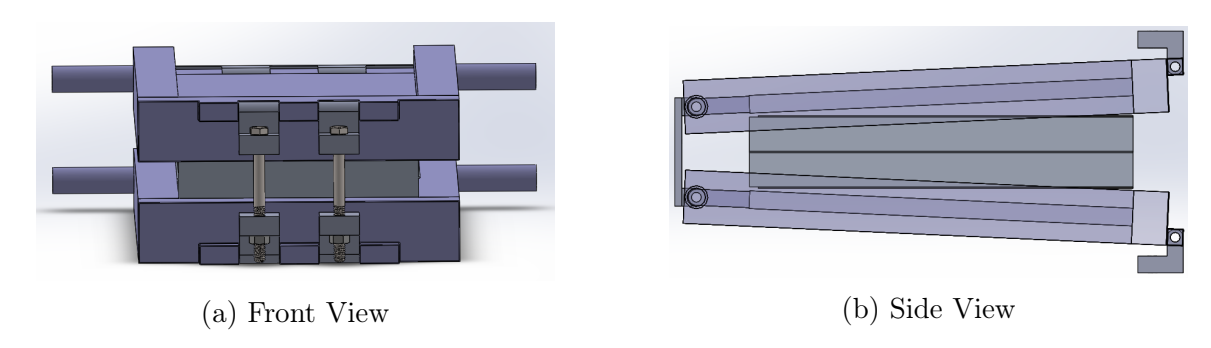


Figure 3-1: Model of Hinge Design. Image (a) shows the fixture with the iPEBB inserted and locked into place. Image (b) shows the fixture with the iPEBB inserted, the retaining brackets unlocked and rotated out of the way, and the cold plates rotated to the open position.

### 3.1.1 Layout

The hinge securing mechanism is named by the differentiating feature by which the cold plates are anchored in the rear to the cabinet, the hinge, as shown in Figure 3-1. By placing the hinge in the rear of the cold plate, the front of the cold plate can be raised and lowered allowing easy access to insert and remove the iPEBB as desired <sup>1</sup>. The cold plate and the anchor plate are connected by a hinge. The anchor plate is then connected to the cabinet. The hinge is offset from the cabinet to ensure unimpeded rotation of the cold plate. The hinge provides structural support and is as wide as the iPEBB. Along the same axis of rotation lies the entrance and exit piping for the cooling water system. This means that there is no displacement of the cooling water piping when the cold plates rotate. A swivel joint is installed in the piping that allows for rotation while keeping the system sealed. More information about the cooling water system can be found in [43].

In the front of the cold plate, two elbow brackets are used to secure the iPEBB. These elbow brackets rotate along a similarly sized hinge as in the rear. When the iPEBB is inserted, the brackets are rotated closed, as shown in Figure 3-1a, to allow for a bolt to be inserted connecting the top and bottom cold plates. These bolts are then tightened to provide the required securing force. When the iPEBB is removed, the elbows are rotated open, as shown in Figure 3-1b, to attach the cold plates to the cabinet via the locking mechanism. This prevents damaging the cold plates when not in use. More is shown in Section 3.3.

## 3.1.2 Key Features

The hinge design is meant to be a simple design. There are few moving parts required to apply the necessary securing force. The spaces on the sides of the iPEBB inside the cabinet is left unobstructed for better air flow and to minimize the width of the cabinets. The ideal placement for the securing mechanism would occupy only on the top and bottom of the iPEBB. This is accomplished with this design.

<sup>&</sup>lt;sup>1</sup>Access to the electrical equipment shall be from the front for replacement and maintenance[13]

By placing the hinge in the back, the axis of rotation aligns with the entry and exit of the cooling system fluid. This achievement improves the range for which the colds plates can rotate. The hinge is designed to have an appropriate margin to failure and reduces the force to lift the cold plate. The cold plates are large pieces of metal with tubing embedded to direct the flow of the cooling water. If made out of aluminum, the cold plates would still weigh more than 40 lbs. When aligned correctly, the cold plates will lay flat on the thermal pad after the securing force is applied. Finally, by placing the hinge in the back, all of the moving parts needed to be accessed are in the front allowing for more a more accessible design.

In the front, the elbow brackets provide the securing force by the cold plates. Since the top elbow bracket has a matching bottom elbow bracket, the clamping force is formed in a symmetric manner. When aligned correctly, the securing bolts will be vertical. When the securing mechanism is not in use, the cold plates can be secured in the open position by the locking mechanism which is discussed more in Section 3.3.

# 3.2 Analysis of the Securing Mechanism with iPEBB Inserted

Figure 3-1, shows the hinge design that will be discussed in this section. A closer, more accurate view can be seen in shown in Figure 3-2.

In this section, the analyses of the hinge anchoring mechanism are shown. In Section 3.2.1, the clearance for the thermal pad attached to the iPEBB is discussed. Section 3.2.2 shows the bolt development and calculates the necessary pre-loading. Section 3.2.3 analyses relevant stresses on the elbow bracket. Section 3.2.4 takes an in-depth look at the torque required for the bolts to secure the cold plates in position. Section 3.2.5 shows the strength of the bolt under load with factor of safety of 2 for this design. It also shows the grade and size of bolts that meet this standard. Finally, Section 3.2.6 looks at the the bending stress at the root of the screw threads to ensure that the threads will not shear and evaluates the probability of failure from the thread

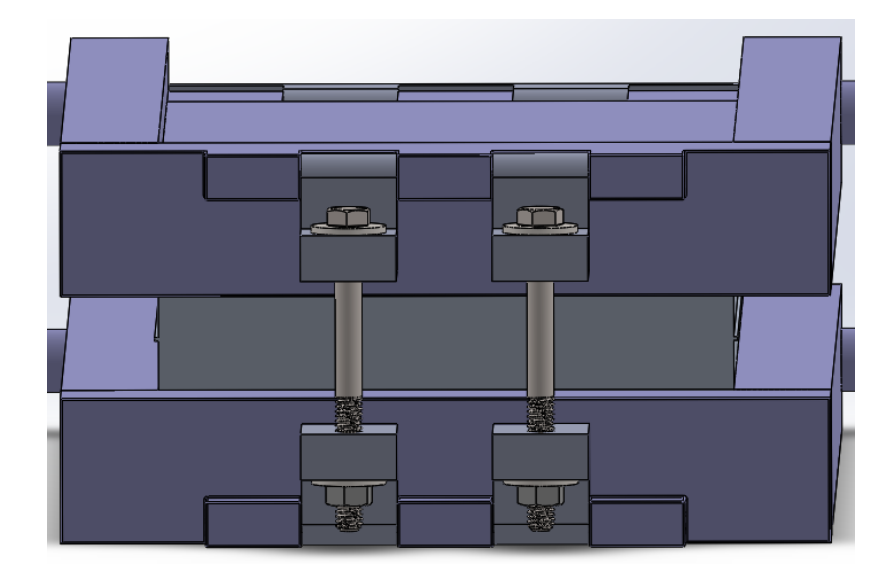


Figure 3-2: Hinge Securing Mechanism with Bolts

strength of the bolt.

For these analyses, the following assumptions were made:

- 1. The bolt used is a common bolt classified as a single threaded M14mm x 75mm Grade 8.8 zinc plated steel. Per MIL-DTL-917F [14], bolts must be Grade 5 or stronger.
- 2. The bolt is coarse threaded with a pitch of 2mm. Per MIL-DTL-917F [14], threads shall be from the coarse-thread series, unified form, class 2A/2B.
- 3. The coefficient of friction for both the threads and head is 0.25 [5].
- 4. The mean collar diameter,  $d_c$ , is 14mm.
- 5. The Proof, Tensile, and Yield strengths are in accordance with Table 3.1.
- 6. The minimum pressure adhering the cold plate to the thermal pad and iPEBB is 10 psi (68.95 kPa).
- 7. There are two angle brackets on each cold plate to secure them on the front side shown in Figure 3-2.

Table 3.1 shows the mechanical properties for steel bolts for common grades. Other bolts may be used if they exceed the strength of the bolt used for this design or if appropriate calculations show them to be safe and in accordance with [14] and [37].

Table 3.1: Metric Mechanical-Property Classes for Steel Bolts, Screws, and Studs [5]

Property Class	Size Range, Inclusive	Minimum Proof Strength,† MPa	Minimum Tensile Strength,† MPa	Minimum Yield Strength, <sup>†</sup> MPa	Material	Head Marking
4.6	M5-M36	225	400	240	Low or medium carbon	4.6
4.8	M1.6-M16	310	420	340	Low or medium carbon	4.8
5.8	M5-M24	380	520	420	Low or medium carbon	5.8
8.8	M16-M36	600	830	660	Medium carbon, Q&T	8.8
9.8	M1.6-M16	650	900	720	Medium carbon, Q&T	9.8
10.9	M5-M36	830	1040	940	Low-carbon martensite, Q&T	10.9
12.9	M1.6–M36	970	1220	1100	Alloy, Q&T	12.9

<sup>\*</sup>The thread length for bolts and cap screws is

$$L_T = \begin{cases} 2d + 6 & L \le 125 \\ 2d + 12 & 125 < L \le 200 \\ 2d + 25 & L > 200 \end{cases}$$

where L is the bolt length. The thread length for structural bolts is slightly shorter than given above.

<sup>†</sup>Minimum strengths are strengths exceeded by 99 percent of fasteners.

### 3.2.1 Thermal Pad Clearance

The iPEBB is cooled on the top and bottom by the cold plates. This process relies on conduction to cool the internal components. Conduction works best when two surfaces are in complete contact with each other. If there are any gaps in the interface surface, the rate of heat transfer decreases. For the iPEBB, this could lead to hot spots and overheating the internal electrical components. To mitigate this problem, a thermal pad is placed on the top and bottom of the iPEBB and interfaces with the cold plates as shown in Fig 3-4. The thermal pad is a thermally conductive material that specializes in being the conduction interface between two materials. It is placed between the two materials to fill any small voids and smooth uneven surfaces thereby reducing the resistance to heat transfer. The thermal pad used for this analysis was T-Global Technology's TG-A1780 Ultra Soft Thermal Pad. In order to do its job effectively, the thermal pad must have a low modulus of elasticity. This was not provided on the data sheet, but was calculated below. Additionally, the clearance in the back of the iPEBB must be high enough to not have the thermal pad touch the cold plate when inserting the iPEBB. Failure to do so could decrease the life of the thermal pad. The appropriate calculations to mitigate this risk are shown below.

The TG-A1780 Ultra Soft Thermal Pad's spec sheet did not include the modulus of elasticity [9]. This is an important property to compare thermal pads and ensure that they are softer than the materials that will be joined. The goal hardness was  $70\pm10$  as measured on the Shore 00 test. The hardness on the data sheet was 65 [9]. The Shore 00 hardness scale is used to measure rubbers and soft gels. From the data sheet, the thermal pad uses silicone as the base material and adds a thermal conductive powder (mostly aluminum) to increase the thermal conductivity [9]. For some silicones, the modulus of elasticity could be estimated from their durometer hardness [31]. This method is not exact but a rough value was desired for this material. Larson [31] plotted the tested material's nominal Shore 00 Hardness and Young's Modulus, and found the line of best fit. For the Shore 00 Materials, the plot is shown in Figure 3-3.

From the line of best fit in Figure 3-3, using the goal Shore 00 value of 70, the

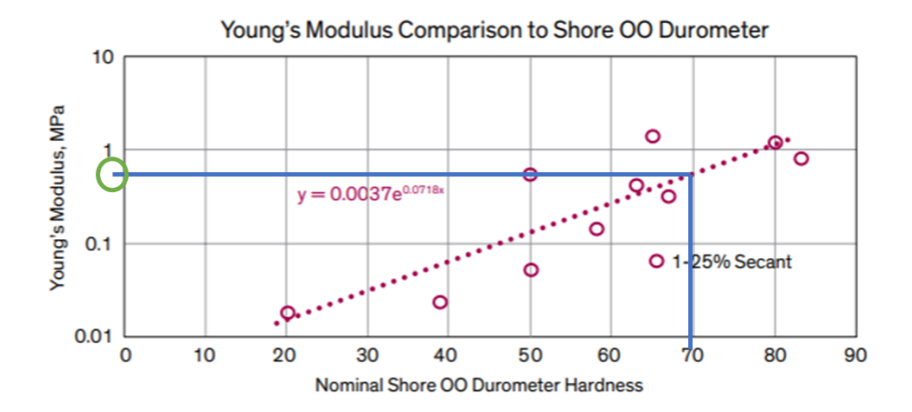


Figure 3-3: Shore 00 Hardness to Modulus of Elasticity (Young's Modulus) [31]

modulus of elasticity was determined to be

$$E = 0.0037e^{0.0718x} = 0.0037e^{0.0718 \cdot 70} = 0.563MPa.$$
(3.1)

Through the range of the hardness goal  $(70\pm10)$ , the modulus of elasticity varied from E = 0.275 - 1.156MPa. This is sufficiently smaller than the typical modulus of elasticity for metals (more aptly measured in GPa; see Chapter 4 for more details). This shows that the thermal pad is softer than the metals and will minimize voids better then an interface between just the metals.

Thermal pads of 2 mm thickness will be placed on the top and bottom of the iPEBB. With the hinge design, when the cold plates are in the open position for inserting and removing the iPEBB, the smallest clearance will be in the back as can be seen in Figure 3-4 (left side). It was assumed that the cold pate could be raised a maximum of one inch in the front (right side of Fig 3-4). It is from this conservative assumption that  $\overline{DE}$  is limited to 1in. It was assumed that the cold plates, represented by blue rectangles on top and bottom of iPEBB and thermal pad in Figs 3-4 and 3-5, would remain rigid when rotated.

Fig 3-5 shows the diagram for this analysis. In the position shown, the cold plate is flat and level, resting on the thermal pad. It was assumed that the thermal pad maintained its height of 2 mm under the loading of the weight of the cold plate. From this position, the elbow on the right side would be rotated down to secure the

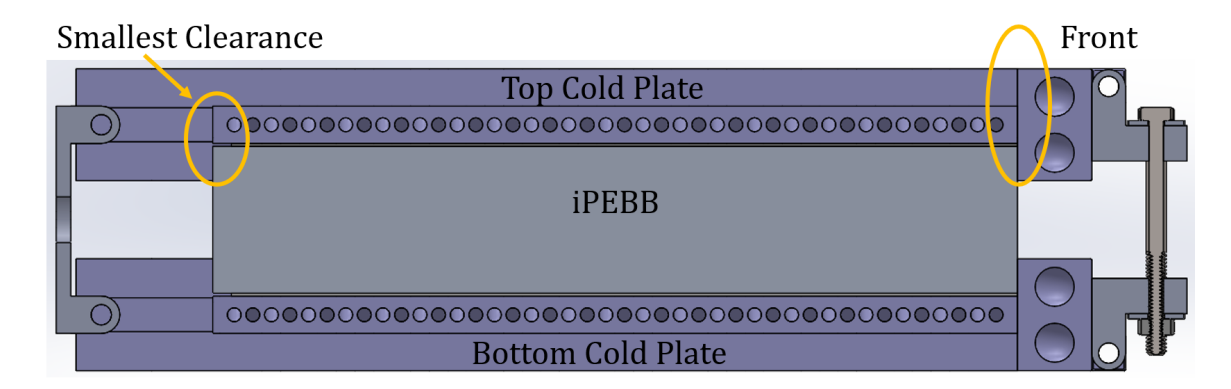


Figure 3-4: Side Profile View Hinge Design With iPEBB Inserted

iPEBB in place. Length  $\overline{AB}$  is the distance from the center of rotation of the hinge to the start of the iPEBB. Length  $\overline{BF}$  is the distance from the edge of the iPEBB to the start of the thermal pad. When  $\overline{BF}=0$ , points B and F are in the same spot. The maximum height that the cold plate can be raised in the front is  $\overline{DE}=1in$ . Length  $\overline{FG}$  is the minimum distance from the cold plate to the thermal pad for that configuration.

The minimum clearance distance,  $\overline{FG}$ , was found by comparing similar triangles  $\triangle ADE$  and  $\triangle AFG$ . For every situation, lengths  $\overline{AD}$ ,  $\overline{DE}$ , and  $\overline{AF}$  were known. Additionally, angles  $\angle DAE$  and  $\angle FAG$  are the same. To find  $\overline{FG}$ , the ratio method of similar triangles was used as shown below.

$$\overline{FG} = \frac{\overline{AF} \cdot \overline{DE}}{\overline{AD}} \tag{3.2}$$

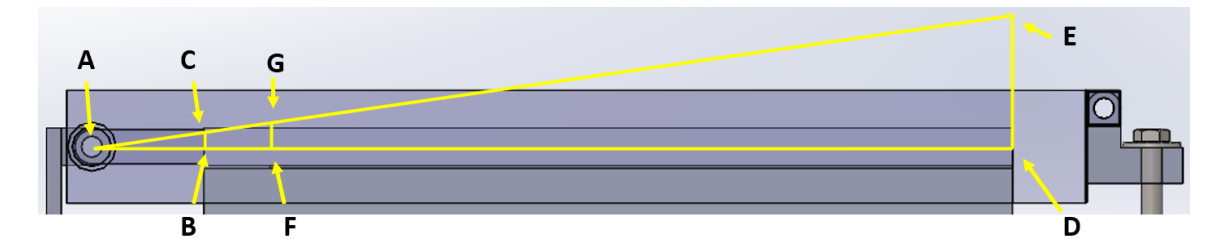


Figure 3-5: Scenarios Evaluated for Clearance Analysis

The next part was to constrain the analysis. The goal was to have a minimum clearance  $\overline{FG} = 2mm$  with 3mm preferred. The thermal pad must stretch from the front of the iPEBB to a maximum of two inches from the back edge of the iPEBB

(maximum value of  $\overline{BF}=2in$ ). Thus  $\overline{BF}$  was varied in half inch increments from 0 to 2 in. It was preferable to have the thermal pad cover the entire iPEBB.  $\overline{AB}$  was varied in half in increments from 2-5 in. The minimum value, 2, was chosen as it was close to the minimum desired clearance without having to adjust the length of the thermal pad. It was unnecessary to continue evaluating  $\overline{AB}$  greater than five inches as there were many solutions that would easily fit the desired minimum clearance and to keep the length of the housing cabinet reasonable. Applying those constraints, the analysis was performed and the results are shown in Table 3.2.

Table 3.2: Clearances from Top of Uncompressed Pad to Cold Plate

For DE = 1 inch: Clearance From Top of Uncompressed Pad to Cold Plate (mm)

AB (in)	at BF = 0.0 in	at BF = 0.5 in	at BF = 1.0 in	at BF = 1.5 in	at BF = 2.0 in
2.0	1.91	2.44	2.98	3.52	4.06
2.5	2.39	2.91	3.44	3.97	4.49
3.0	2.85	3.37	3.88	4.40	4.91
3.5	3.29	3.80	4.30	4.81	5.31
4.0	3.72	4.22	4.71	5.21	5.70
4.5	4.13	4.62	5.10	5.59	6.07
5.0	4.52	5.00	5.48	5.95	6.43

The minimum clearance chosen was  $\overline{FG} = 3.37mm$ , when  $\overline{AB} = 3in$  and  $\overline{BF} = .5in$ . The thermal pad dimensions are 300 x 537.3 x 2 mm. With a density of  $3500\frac{kg}{m^3}$ , the weight of the sample thermal pad is 1.13 kg (see App A for details) [9]. If permanently attached to the iPEBB, this may lead to a issue with weight as discussed in Section 4.1; new thermal pad materials should be investigated with weight considerations in mind.

## 3.2.2 Bolt Loading Calculations

This section addresses finding the load on each bolt, which will be used to calculate the required torque to adequately secure the cold plates to the iPEBB, and to assess the strength of the bolt and threads.

First the magnitude of the force must be found. In this case, the magnitude of the force is found from knowing the required pressure on the cold plate, specifically 68.95 kPa (10 psi from assumption 6), and the dynamic loading associated with the cold plates. The dimensions of the top and bottom faces of the iPEBB are given in Section 1.1.3. As discussed in Section 3.2.1, the thermal pad is expected to be slightly shorter than the total length of the iPEBB (537.3 mm vs 550 mm). Thus the total surface area is .16119  $m^2$ . The force due to pressure,  $F_p$  is found using the equation below

$$F_p = Pressure \cdot Area = (68.96kPa) \cdot (.1612m^2) = 11,114N$$
 (3.3)

Next, the dynamic loading for the cold plates was calculated following a similar path as described in Appendix D.2. For this analysis, it was assumed that the weight of the iPEBB would be held in place by the iPEBB's key and thus only the weight of the cold plates and elbow brackets would be applied to the bolts. As shown in App A, each cold plate and elbow bracket weighs 21 kg and 3kg, respectively. The total weight of the structure was 42 kg. From Eqns 2.28 and 2.29, the resulting principle and total dynamic forces for the cold plates are as follows

$$F_{dyn,CP} = \left(F_x^2 + F_y^2 + F_z^2\right)^{1/2} = \left((246N)^2 + (520N)^2 + (1,132N)^2\right)^{1/2} = 1,270N$$
(3.4)

Combining the above two forces, the magnitude of the force to secure a cold plate is 11,114N+1,132N=12,246N. The cold plate is held in place by the hinge in the back and elbows/bolts in front. Assuming an even distribution of loading between the the front and back, each side would be responsible for providing 6,123N of securing force. From the analysis performed in Section 3.2.3, there will be two bolts. Assuming that each bolt carries the same loading, the combined force per bolt is

$$F_c = \frac{6,123N}{2} = 3,062N \tag{3.5}$$

Fig 3-6 shows a typical bolt profile sandwiching two sections together. The key points to notice are that the bolt is loaded in tension by equal and opposite forces, P, and that the two sections being clamped by the bolts are touching. The total force,

 $F_c$ , is shown in Figure 3-6.

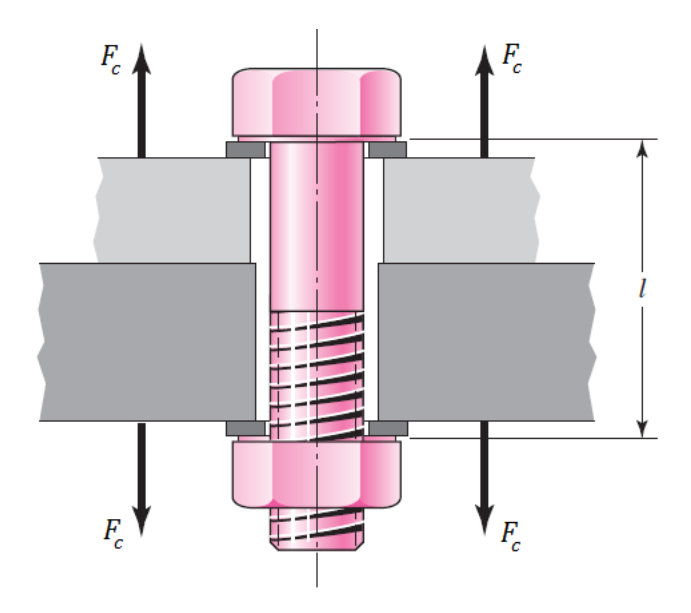


Figure 3-6: Loading Profile of a Typical Bolt [5]

## 3.2.3 Analysis of Elbow Bracket

There are four elbow brackets for the securing mechanism: two on the top cold plate and two on the bottom cold plate. They are connected to the cold plate via a solid aluminum rod. To secure the iPEBB and place the necessary loading on the iPEBB, opposing pairs (one from the top and one from the bottom plate) were bolted together. For the following analyses, the elbow bracket material is assumed to be aluminum. The elbow bracket has a total width of 65 mm, height of 62.3 mm and total depth, b, of 50 mm. The width and height are best viewed in Figure 3-7a, and the depth is shown in Figure 3-7b. The stresses and deflections of the elbow bracket were categorized by hole, first the bolt hole and lastly the hole for the aluminum rod (centered at pt L in Figure 3-7a). The rest of this section will refer to the latter hole as the front hinge hole.

The first analysis is from the forces applied to the bolt hole. The deflection calculations are shown in Appendix F.1.1. The resulting deflections, y, are

$$y_{\overline{HJ}} = -3.15(10^{-3})mm : y_{\overline{IJ}} = -3.15(10^{-3})mm$$
 (3.6)

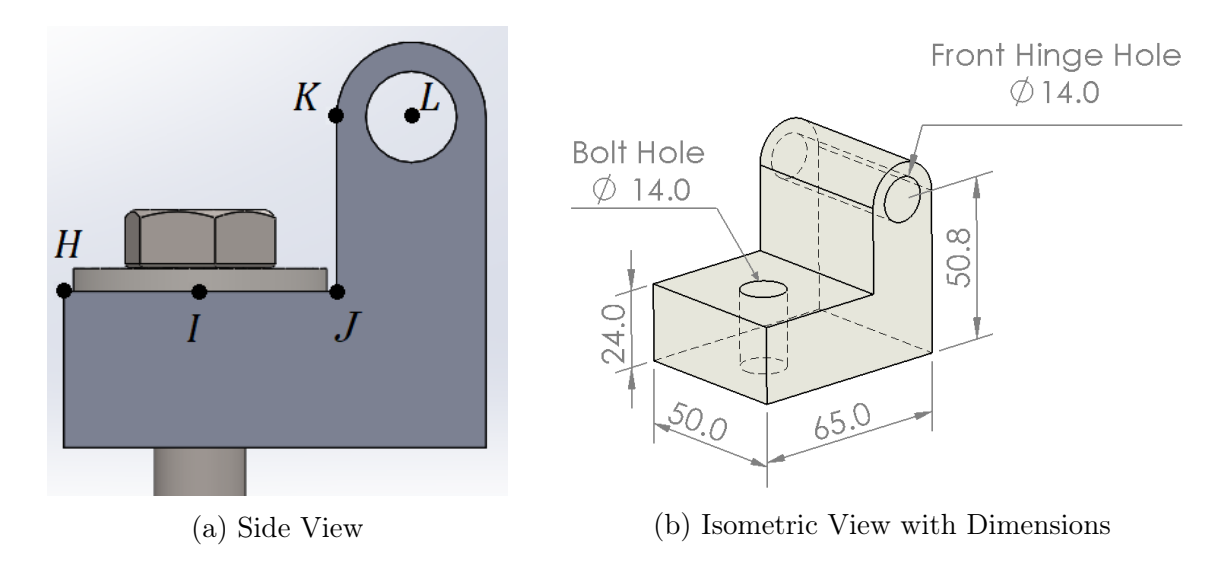


Figure 3-7: Close up Views of Elbow Bracket

The stress calculations are shown in Appendix F.1.2. The resulting bending  $(\sigma_{bending})$  and shear  $(\tau_{shear})$  stress are

$$\sigma_{bending} = 10.84MPa : \tau_{shear} = 2.55MPa \tag{3.7}$$

The associated factors of safety for bending  $(\eta_{bending})$  and shear  $(\eta_{shear})$  stress are

$$\eta_{bending} = \frac{28MPa}{6.94MPa} = 2.58 : \eta_{shear} = \frac{32.2MPa}{2.04MPa} = 18.8$$
(3.8)

The hinge hole was evaluated on four different types of failure methods using four different stresses. The process started with finding the shear stress on the connecting rod. Then on the elbow bracket, the other modes of failure were from tension on the remaining material, bearing stress, and shear tear out. The calculations and associated diagrams are shown in Appendix F.2.

The resulting shear  $(\tau_{shear})$  stress and Factor of Safety  $\eta_{shear}$  are

$$\tau_{shear} = 19.9MPa : \eta_{shear} = \frac{48MPa}{19.9MPa} = 2.41$$
(3.9)

The resulting tension ( $\sigma_{tension}$ ) stress and Factor of Safety  $\eta_{tension}$  are

$$\tau_{tension} = 6.80MPa : \eta_{tension} = \frac{48MPa}{6.80MPa} = 4.12$$
(3.10)

The resulting bearing  $(\tau_{bearing})$  stress and Factor of Safety  $\eta_{bearing}$  are

$$\tau_{bearing} = 4.37MPa : \eta_{bearing} = \frac{28MPa}{4.37MPa} = 6.40$$
(3.11)

The resulting shear tear out  $(\tau_{tear})$  stress and Factor of Safety  $\eta_{tear}$  are

$$\tau_{tear} = 3.36MPa : \eta_{tear} = \frac{48MPa}{3.36MPa} = 14.31$$
(3.12)

The most limiting stress was the shear stress on the solid aluminum rod on the hinge hole. It was from this calculation that the minimum number of elbow brackets needed for this design was confirmed to be two. This affirms assumption #7 at the beginning of this chapter. For this design, all factors of safety were greater than two.

## 3.2.4 Required Torque to Tighten Screw

An in-depth guide for developing the equations that determine the torque required to tighten and loosen a bolt are shown in [5]. The following overview is presented for orientation and to understand the assumptions made.

Developing these equations works best when using square threads and then converting to the Unified National (UN) coarse pitch (UNC) series. This analysis will be analyzing the interaction due to friction between (1) the bolt and the nut along the threads and (2) the nut and washer. It was assumed that the head of the bolt was held stationary.

Starting with the interaction of the bolt and the nut along the threads, the force diagram for tightening the nut is shown in Figure 3-8. In this diagram,  $F_c$  is the compressive force, f is the coefficient of friction, N is the normal force,  $\lambda$  is the lead angle, and P is the load required to tighten the nut. To loosen the nut, the direction of fN and P would be reversed.

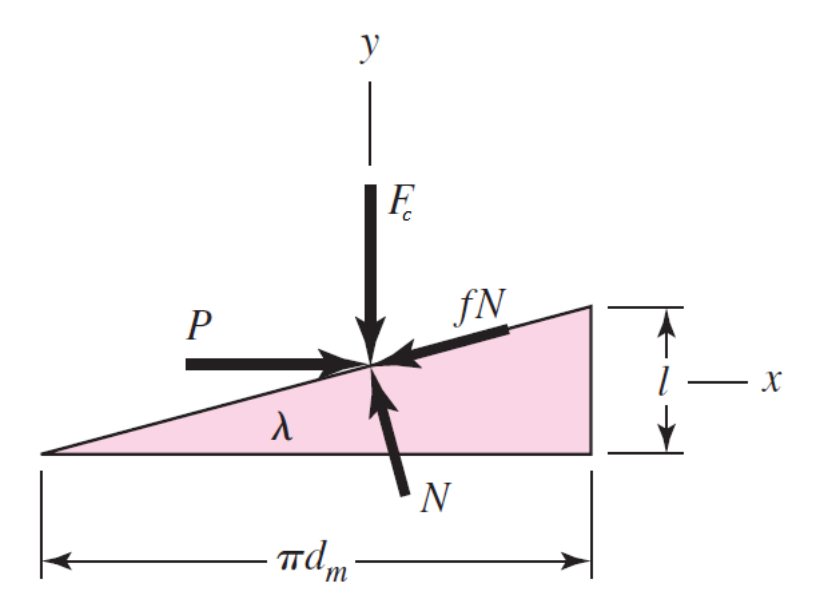


Figure 3-8: Loading Profile on Square Bolt Threads[5]

The forces are summed in the x-direction and y-direction and set equal to zero.

$$\sum F_x = P - N\sin(\lambda) - fN\cos(\lambda) = 0 \tag{3.13}$$

$$\sum F_y = -F_c - fN\sin(\lambda) + N\cos(\lambda) = 0 \tag{3.14}$$

The force of interest is P. The equations above are combined by eliminating N. The resulting equation solved for P is

$$P = \frac{F_c(\sin(\lambda) + f\cos(\lambda))}{\cos(\lambda) - f\sin(\lambda)}$$
(3.15)

The next step in solving for the torque to tighten the bolt is to simplify Eqn 3.15 by dividing both the numerator and denominator by  $\cos(\lambda)$ . Torque is defined by multiplying the distance from center of rotation by the perpendicular component of applied force. In this case, the radius of a generic bolt,  $\frac{d_m}{2}$  is multiplied by the force to tighten the nut, P. The resulting equation after all of the simplifications is shown below

$$Torque = \frac{F_c d_m}{2} \left( \frac{\tan(\lambda) + f}{1 - f \tan(\lambda)} \right)$$
 (3.16)

Earlier, the bolt was assumed to have square threads. This is not the case; it has

UNC series threads which have an inclination due to the lead angle,  $\lambda$ , and thread angle,  $\alpha$ . A representation of the thread angle is shown in Figure 3-9. The lead angle is usually small compared to the thread angle and thus neglected. The effect of the inclination is accounted for by the thread angle where the compressive force is divided by the  $\cos(\alpha)$  in Eqn 3.16. The result is shown in the first term of Eqn 3.18.

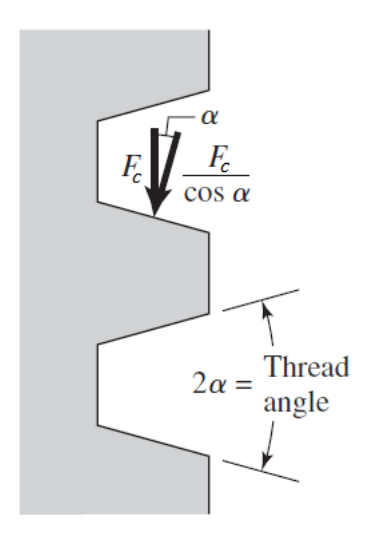


Figure 3-9: Thread Angle and Effect on the Thread Force [5]

The second component of torque is overcoming the friction between the nut and washer. The distance changes to the radius of the collar  $\frac{d_c}{2}$ . Since the force components are applied solely in the vertical direction, the normal force is equal in magnitude but opposite in direction compared to the applied force. Thus the frictional force is  $f_c N = f_c F_c$ . Putting this all together, the torque between the nut and washer is shown below

$$Torque = \frac{F_c f_c d_c}{2} \tag{3.17}$$

Putting both of these concepts together, the relationship between the required torque to tension,  $T_T$  and the compressive force,  $F_c$ , is:

$$T_T = \frac{F_c d_m}{2} \left( \frac{\tan(\lambda) + f \sec(\alpha)}{1 - f \tan(\lambda) \sec(\alpha)} \right) + \frac{F_c f_c d_m}{2}$$
(3.18)

Where d is the bolt diameter,  $d_m$  is the average of the major and minor bolt diameters,  $\lambda$  is the lead angle, f is the co-efficient of friction on the threads, and  $f_c$  is the co-

efficient of friction on the collar. In general, lead angles,  $\lambda$ , are small and usually only the effect of the thread angle,  $\alpha$ , is considered. This is shown in Eqn 3.18 by multiplying select terms by  $\sec(\alpha)$ .

Standard tools shall be used when constructing and working on the securing mechanism [14]. For this application a high degree of reliability is needed and thus the parts (nuts, bolts, etc.) shall conform to commercial standards [37]. For standard hex head bolts, the major diameter is one and a half times as large as the minor diameter. The mean collar diameter is  $d_c = \frac{d+1.5d}{2} = 1.25d$ . Eqn 3.13 can then be re-arranged to

$$T_T = \left[ \left( \frac{d_m}{2d} \right) \left( \frac{\tan(\lambda) + f \sec(\alpha)}{1 - f \tan(\lambda) \sec(\alpha)} \right) + 0.625 f_c \right] F_c d \tag{3.19}$$

To simplify this, define K, the torque coefficient, as

$$K = \left[ \left( \frac{d_m}{2d} \right) \left( \frac{\tan(\lambda) + f \sec(\alpha)}{1 - f \tan(\lambda) \sec(\alpha)} \right) + 0.625 f_c \right]$$
(3.20)

Simplified, Eqn. 3.19 can be written as

$$T_T = KF_c d (3.21)$$

On average,  $f = f_c = 0.15$ , and, from Table 3.3 for zinc plated bolts, K = 0.20 regardless of bolt size and thread type (fine or course) [5]. From assumption 1, d = 14mm. The result is the required torque to place 68.95kPa (10 psi) on the top plate is

$$T_T = KF_c d = (0.2)(3062N)(14mm) = 8.57N \cdot m.$$
 (3.22)

# 3.2.5 Bolt Strength

The strength of the bolts depends on the strength of the threads and of the bolt itself. This section evaluates the axial stress on the bolt, and its associated factor of safety.

Normally, to find the axial stress on the bolt, the stiffness of the bolt and material

Table 3.3: Torque Factors to use with Eqn 3.21 [5]

Bolt Condition	K
Nonplated, black finish	0.30
Zinc-plated	0.20
Lubricated	0.18
Cadmium-plated	0.16
With Bowman Anti-Seize	0.12
With Bowman-Grip nuts	0.09

must be taken into account. The stiffness of the frustum,  $k_f$ , is treated like the stiffness of a spring, obeying Hooke's law. The bolt stiffness,  $K_b$ , is found by combining the stiffness of the threaded and unthreaded portions in series. The stiffness of the these portions depends on the length of the threaded and unthreaded portions of the bolt that are clamped together and their associated cross-sectional area. The material stiffness,  $K_m$ , depends on the clamped zone area and material properties. The clamped zone is known is known as the frustum and extends from the top of the bolt to the nut as shown in Figure 3-10. This becomes important when there are more than two layers and/or the layers do not have equal thicknesses. In Figure 3-10b, the layers are of different thickness so there would be three stiffnesses: (1) Top material and top frustum, (2) Bottom material and top frustrum, and (3) bottom material and bottom frustum. They would then be combined in series to form  $K_m$ . The bolt and material stiffnesses are then combined in parallel to form the frustum stiffness,  $k_f$ .

Under normal circumstances, it is assumed that the bolt is physically clamping two connected pieces such that these pieces develop concentrated areas of stress from this contact. During pre-loading of the bolt, the bolt is stretched and the member materials are compressed. When an external load is applied, the bolt stretches further but also the materials decompresses. Typically, the bolt will carry around 20% of the total load from the interaction and the remaining 80% will be carried by the clamped materials [5]. For this design, shown in Figure 3-11, the will be no frustum since the material being clamped is not touching. Thus the bolt will be carrying all of the load.

The bolt was thus assumed to fail at the threaded section where the bolt has the

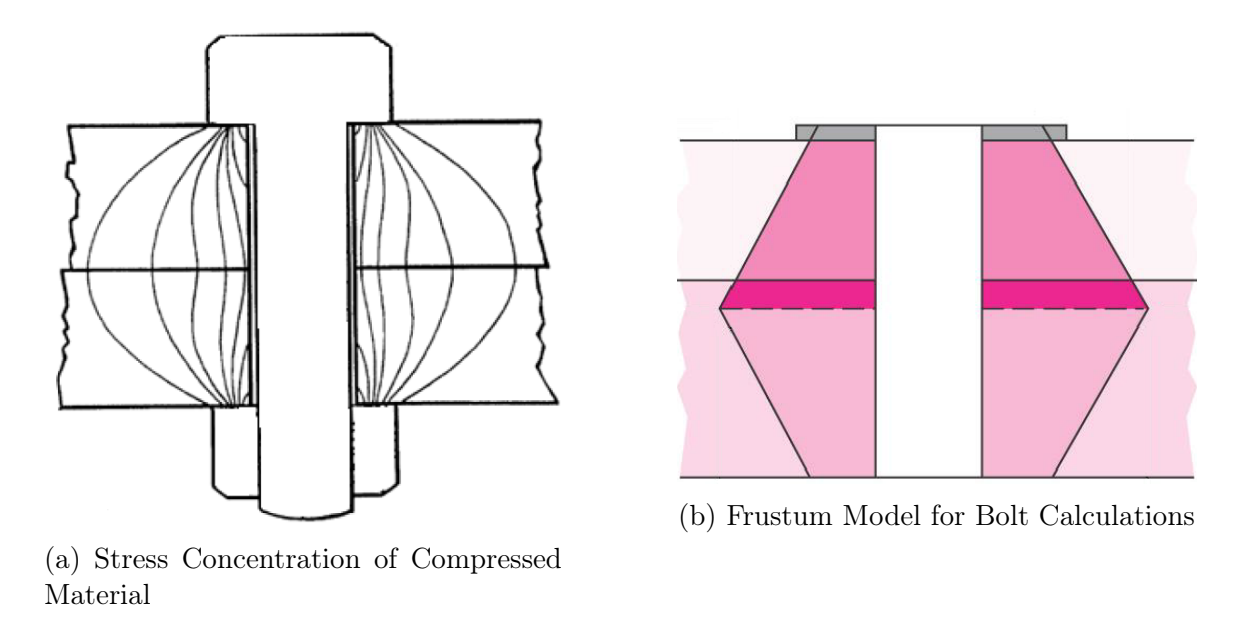


Figure 3-10: Frustum: Observation to Model [5]

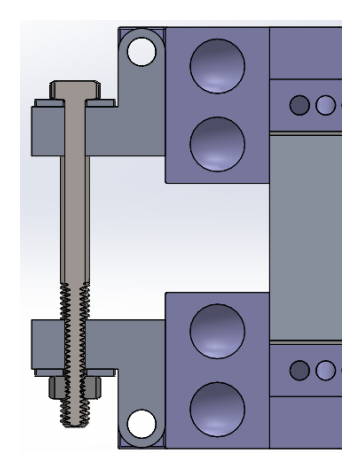


Figure 3-11: Side Cutaway View of Front of Hinge Design

smallest cross-section area. Experimentally, the cross-sectional area for the threaded section of a bolt has been found to have a larger tensile strength than the cross-sectional area using just the root diameter. The effective cross-sectional area is similar to an area from a diameter between the minor/root diameter and the pitch diameter [5]. From Table 3.4, the cross-sectional threaded area,  $A_t$ , of a M14 bolt is  $115mm^2$ . Using assumption #7, the force on the bolt is  $F_b = 3.062kN$ . The stress on the bolt in the threaded portion,  $\sigma_b$ , is

$$\sigma_b = \frac{F_b}{A_t} = \frac{3062N}{115mm^2} = 26.63MPa. \tag{3.23}$$

Table 3.4: Diameters and Areas of Coarse-Pitch and Fine-Pitch Metric Threads[5]

Nominal Major	C	oarse-Pitch Tensile-	Series Minor-	ı	Fine-Pitch S Tensile-	Pitch Series sile- Minor-	
Diameter d mm	Pitch P mm	Stress Area A <sub>f</sub> mm <sup>2</sup>	Diameter Area A <sub>r</sub> mm <sup>2</sup>	Pitch P mm	Stress Area A <sub>t</sub> mm <sup>2</sup>	Diameter Area A <sub>r</sub> mm <sup>2</sup>	
1.6	0.35	1.27	1.07				
2	0.40	2.07	1.79				
2.5	0.45	3.39	2.98				
3	0.5	5.03	4.47				
3.5	0.6	6.78	6.00				
4	0.7	8.78	7.75				
5	0.8	14.2	12.7				
6	1	20.1	17.9				
8	1.25	36.6	32.8	1	39.2	36.0	
10	1.5	58.0	52.3	1.25	61.2	56.3	
12	1.75	84.3	76.3	1.25	92.1	86.0	
14	2	115	104	1.5	125	116	
16	2	157	144	1.5	167	157	
20	2.5	245	225	1.5	272	259	
24	3	353	324	2	384	365	
30	3.5	561	519	2	621	596	
36	4	817	759	2	915	884	
42	4.5	1120	1050	2	1260	1230	
48	5	1470	1380	2	1670	1630	
56	5.5	2030	1910	2	2300	2250	
64	6	2680	2520	2	3030	2980	
72	6	3460	3280	2	3860	3800	
80	6	4340	4140	1.5	4850	4800	
90	6	5590	5360	2	6100	6020	
100	6	6990	6740	2	7560	7470	
110				2	9180	9080	

From assumption #1, a grade 8.8 bolt was chosen, with characteristics shown in

Table 3.5.

Table 3.5: Metric Mechanical Properties for Grade 8.8 Steel Bolts [5]

Crede of Polt	Minimum Proof	Minimum Tensile Strength (MPa)	Minimum Yield	
Grade of Bolt	Strength (MPa)	Strength (MPa)	Strength (MPa)	
8.8 600		830	660	

From assumptions # 1 and 5, the proof strength,  $S_p$ , of this bolt is 600 MPa. The Factor of Safety for the bolt was found by comparing the proof strength of the bolt to the nominal stress acting on the bolt. This is shown below

$$\eta_b = \frac{S_p}{\sigma_b} = \frac{600MPa}{26.63MPa} = 22.5 \tag{3.24}$$

This is a large factor of safety, much greater than the minimum value of 2. From this analysis, the design meets the requirements and should not fail due only to axial stress.

## 3.2.6 Bolt Thread Strength

As stated previously, the strength of the bolts depends on the strength of the threads and of the bolt itself. This section covers the interaction between the nut and bolt by evaluating the bearing stress, root bending stress, and shear stress.

The bearing stress is the resulting pressure, from the force developed in Section 3.2.2, applied over the contact area of the engaged threads. Figure 3-12 shows the basic profile for metric thread. In this figure,  $d_i$  is the inner/minor diameter,  $d_r$  is the root diameter, d is the major diameter, and t is the thickness of the nut. Moving forward, H will be used as the nut thickness. Metric threads use ISO 68 profile which dictates a thread angle of  $\alpha = 60^{\circ}$  (see Figure 3-9). It is important to note the space between  $d_i$  and  $d_r$ . The relationship between the root diameter and major diameter as a function of pitch, p, is known,  $d_r = d - 1.227p$  [5]. The relationship between the other diameters and  $d_i$  is not as well known. For the rest of this section, a good approximation of  $d_i = d - p$  is used.

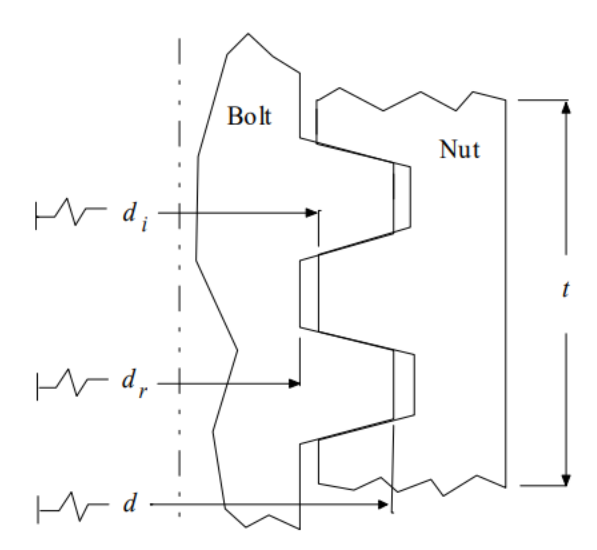


Figure 3-12: Basic Thread Profile of a Typical Nut and Bolt [3]

For square threads, the bearing stress,  $\sigma_B$ , is shown in the equation below[5]

$$\sigma_B = \frac{F}{\pi d_m n_t p/2} \tag{3.25}$$

Where  $d_m$  is the mean diameter,  $n_t$  is the number of engaged threads, and p is the pitch. These variables can be broken down into simpler parts as shown in the equation below

$$d_m = \frac{d+d_i}{2} : n_t = \frac{H}{p} {3.26}$$

The contact area of the engaged threads for a square threaded bolt is  $A_{c,sq} = \pi d_m n_t p/2$ . The area must modified to represent the increased contact area due to the thread angle. For square threads,  $\frac{p}{2}$  represented the width of the contact area as it wound around the circumference of the mean diameter. For metric threads, the width is  $\frac{p}{2 \cdot \cos(\alpha/2)}$ . Taking into account Eqn 3.26 and the increased contact area width for metric threads, the bearing stress is

$$\sigma_B = \frac{2F \cdot \cos(30^\circ)}{\pi d_m H} \tag{3.27}$$

The next step was to find a bolt that would not fail under this load. This was done by evaluating common bolts starting at a nominal major diameter of 14 mm.

The relevant bolt properties for a 14 mm metric bolt are shown in Table 3.4. The relevant nut properties for a 14 mm regular metric nut are shown in Table 3.6.

Table 3.6: Dimensions of Hexagonal Nuts[5]

		Height <i>H</i>			
Nominal Size, in	Width W	Regular Hexagonal	Thick or Slotted	JAM	
M5	8	4.7	5.1	2.7	
M6	10	5.2	5.7	3.2	
M8	13	6.8	7.5	4.0	
M10	16	8.4	9.3	5.0	
M12	18	10.8	12.0	6.0	
M14	21	12.8	14.1	7.0	
M16	24	14.8	16.4	8.0	
M20	30	18.0	20.3	10.0	
M24	36	21.5	23.9	12.0	
M30	46	25.6	28.6	15.0	
M36	55	31.0	34.7	18.0	

The bearing stress for a 14mm nut and bolt is calculated below

$$\sigma_B = \frac{2F \cdot \cos(30^\circ)}{\pi d_m H} = \frac{2(3062N)\cos(30^\circ)}{\pi (13mm)(12.8mm)} = 10.15MPa$$
 (3.28)

Comparing this stress to Table 3.7, choosing a medium strength low speed bronze nut would be best. The factor of safety is  $\eta_{Bearing} = \frac{23.0}{10.15} = 2.3$ .

Table 3.7: Bearing Pressure [5]

Screw Material	Nut Material	Safe Pb (MPa)	Notes
Steel	Bronze	17.2 - 24.1	Low Speed
Steel	Bronze	11.0 - 17.2	$\leq 305 \text{ cm/min}$
Steel	Cast Iron	12.4 - 17.2	$\leq 245 \; \mathrm{cm/min}$
Steel	Bronze	5.5 - 9.6	610-1220  cm/min
Steel	Cast Iron	4.1 - 6.9	610-1220  cm/min
Steel	Bronze	1.0 - 1.6	$\geq 1525 \text{ cm/min}$

Next, the remaining forces at the thread interface are the root bending stress and shear stress. To find the root bending stress a few assumptions were made:

- The force is applied in the center of the thread (along  $d_m$ )
- The thread is treated as a linearly tapered beam

- The material is isotropic, homogeneous, and obeys Hooke's law
- The plane has an access of symmetry in the plane of bending
- The second moment of area, I, at the point where the force is applied is a representative of the tapered beam

The second moment of area, I, initially given by Eqn 2.4, but in this case the base, b, is the circumference of the root diameter and multiplied by the number of turns. The height, h, is calculated at the middle of the thread. The distance from the mid-line to the top edge, c, is half of the height (the height at the bolt is labeled b in Figure 3-13).

$$I = (\frac{1}{12})bh^3 = \frac{1}{12}(\pi d_m n_t)(\frac{p}{2}\tan(30^\circ))^3 : c = (\frac{p}{4})\tan(30^\circ)$$
 (3.29)

Simplifying these two equations, the section modulus, Z = I/c, becomes

$$Z = (\frac{\pi}{24})d_m n_t p^2 \tan^2(30^\circ). \tag{3.30}$$

As stated previously, the moment is the force applied multiplied by the distance. Because the threads are angled, only the vertical applied force is considered for the moment.

$$M = F\cos(30^\circ) \left(\frac{p}{4}\right) \tag{3.31}$$

The equation for bending stress is given by Eqn 2.8. Putting Eqns 3.30 and 3.31 together and simplifying the trigonometric terms, the resulting bending stress for a metric bolt is shown in Eqn 3.32. From Table 3.4 for a nominal major bolt diameter of 14 mm, the pitch is p = 2mm and the mean diameter is  $d_m = d - p/2 = 13mm$ . From Table 3.6 and Eqn 3.5, the number of engaged threads is  $n_t = H/p = 12.8/2 = 6.4$ . If the threads uniformly support the force, the bending stress is

$$\sigma_b = \frac{M}{Z} = \frac{F\cos(30^\circ)(p/4)}{(\pi/24)d_m n_t p^2 \tan^2(30^\circ)} = \frac{9\sqrt{3}F}{\pi d_m n_t p} = \frac{9\sqrt{3}(3062N)}{\pi(13mm)(6.4)(2mm)} = 91.3MPa$$
(3.32)

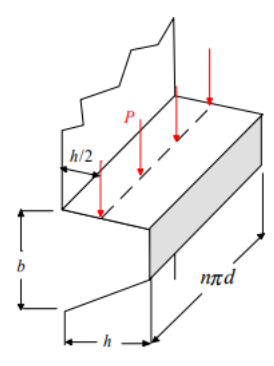


Figure 3-13: Application of Securing Force on Threads

Some experiments showed that the load is not uniformly distributed across the threads. These experiments claim that the first three threads carry 81% of the load with the highest being the first thread with 38% of the load [5]. If this is the case, the highest bending stress is

$$\sigma_b = \frac{9\sqrt{3}(0.38F)}{\pi d_m n_t p} = \frac{9\sqrt{3}(0.38 \cdot 3062N)}{\pi (13mm)(1)(2mm)} = 222.1MPa$$
 (3.33)

The factor of safety for this first thread is

$$\eta_{b,1stThread} = \frac{Yield/ProofStrength}{ActualLoad} = \frac{600MPa}{222.1MPa} = 2.7$$
(3.34)

The final stress analysed is the shear stress on the threads of the bolt. The shear stress takes into account the shear force, V, and shear area,  $A_s$ . The maximum shear force,  $V_{max}$  is the vertical stress on the first thread assuming uneven loading. The shear force is applied along  $d_m$ . Thus the shear area is the thickness of the thread at  $d_m$  multiplied by the circumference,  $\pi d_m$ . Using the assumption stated earlier in this section, the shear stress is described by

$$\tau = \frac{3V_{max}}{2A_s} = \frac{3(0.38F\cos(30^\circ))}{\pi d_m n_t p} = \frac{3(0.38 \cdot 3062N\cos(30^\circ))}{\pi (13mm)(1)(2mm)} = 37.0MPa$$
 (3.35)

The shear strength is found by multiplying the ultimate strength (from Table 3.1)

of the bolt by 0.67. The factor of safety for this first thread is

$$\eta_{s,1stThread} = \frac{ShearStrength}{ActualLoad} = \frac{830 \cdot 0.67MPa}{37.0MPa} = 15.0$$
(3.36)

# 3.3 Locking Mechanism Analysis

### 3.3.1 Locking Mechanism Design

The locking mechanism is made out of steel. Aluminum would be the material of choice however relying on threading in aluminum material should be avoided, where practicable, by the use of through bolting [14]. Steel can be threaded with no issues. With limited space around the locking mechanism to maneuver, it was critical for the bolt to screw into this component. If aluminum is desired to be used to save on weight, bolts must be removed for routine maintenance [14]. Additionally, there are few materials that do not need any further processing to be used in corrosive environments. The specific type of steel is briefly discussed later in this section and more in-depth in Section 4.1. The locking mechanism was designed to be attached to both sides in the front of the cabinet and to secure the cold plate when not in use. Each locking mechanism was designed to secure one cold plate; thus, one locking mechanism is located above and one below the cold plates. As shown in Figure 3-14, the locking mechanism is shaped like a hollow bar. It is hollow to minimize weight. It was rectangular on the outside to be easily stacked and on the inside to better conform to the shape of the elbow bracket. The locking mechanism consists of two parts, a holder and a slider. On average, each piece is 3mm thick. Combined, the two pieces weigh 2.87 kg.

To operate the locking mechanism, the slider is moved horizontally. There are two positions, open and closed. In the closed position, the slider is also locked into place with one of the bolts used to secure the iPEBB. More is discussed below. When in the open position, the elbow can be lifted directly into the locking mechanism. Then the slider is moved to the closed position. In the closed position, the elbows are supported by the slider which is prevented from moving by the bolt. The open (top)

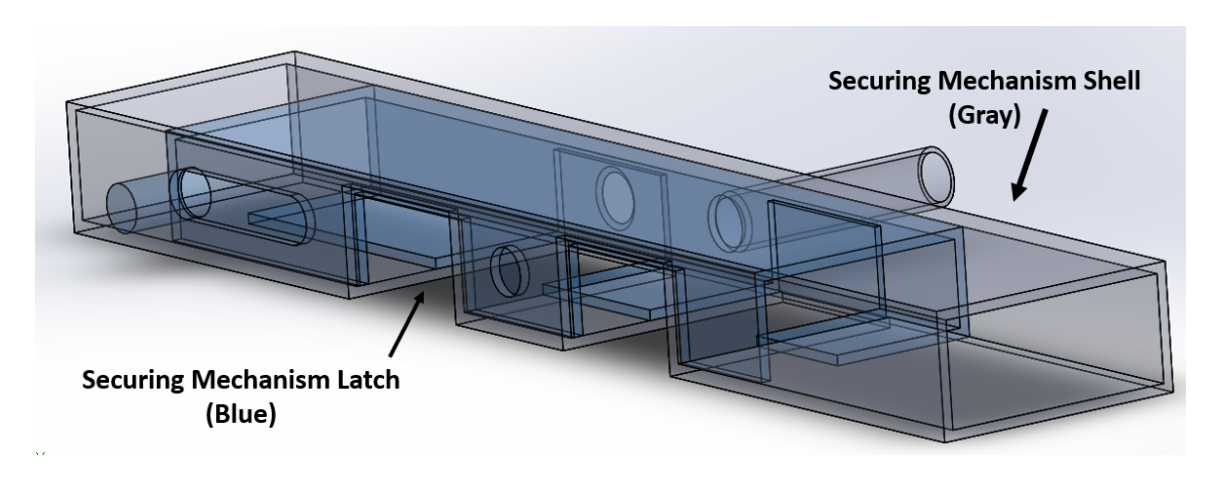


Figure 3-14: Locking Mechanism with Components Labeled

and closed (bottom) positions are shown in Figure 3-15.

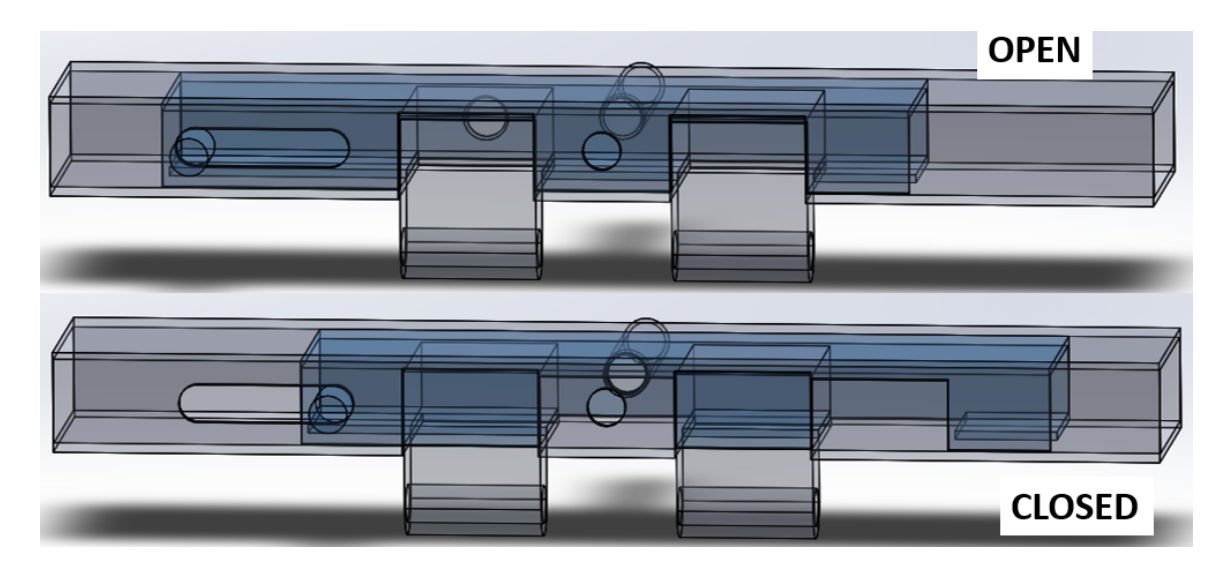


Figure 3-15: Locking Mechanism in Open and Closed Positions

This locking mechanism has an important feature in addition to doing its main function of locking the cold plates in place. Each locking mechanism stores a nut, two washers, and a bolt when not in use. The handle was sized and threaded so that the nut can be stored there. Both washers can be stored on the bolt. When the elbows have been rotated into place, the latch is slid laterally to secure the cold plate in place. After the latch has been fully repositioned, the hole for the bolt is aligned allowing for the bolt to be stored in the cabinet. This feature minimizes the number of parts necessary for this design and allows for on-site storage of the parts. The bolt

should be hand-tight to keep the locking mechanism in place.

### 3.3.2 Locking Mechanism Design Analysis

The performance of this mechanism is based on its ability to secure the the cold plates in place. This was evaluated based on bending and shear stress factors of safety. Using Austenitic steel Type 316 for the locking mechanism, the modulus of elasticity is 193GPa with the ultimate and yield tensile strength being 515MPa and 205MPa, respectively. This is significantly stronger than the aluminum that was previously used but comes at a much higher density of  $8\frac{g}{cm^3}$ . Since the cold plate has been modeled in SolidWorks and with symmetry, it was relatively easy to find the centroid. From the back hinge, it was located  $x_c = 346.0mm$ . From the back hinge, the center of the front hinge was located  $x_{FH} = 708.6mm$ .

The next task was to find force to secure the cold plate transmitted through the elbows to the locking mechanism. This is shown in Figure 3-16. To balance out the torque from weight of the cold plate, an equivalent torque was applied to support the cold plate via a force at the elbow,  $F_{elbow}$ . In addition to the weight of the cold plate, the weight of both elbows (3.0N per elbow) and the dynamic loading were included. Calculations were performed for the dynamic loading regarding the cold plate that were similar to the example for the iPEBB shown in Appendix D.2. The only change was to modify the weight to that of the cold plate, 232 N. The resulting dynamic forces are

$$F_{dyn,cp} = \left(F_x^2 + F_y^2 + F_z^2\right)^{1/2} = \left((132)^2 + (279)^2 + (608)^2\right)^{1/2} = 682N$$
 (3.37)

In this case only the z-direction component of the dynamic force is relevant to the analysis and was applied in the same direction as the weight. The locking mechanism for the top cold plate was analyzed because it has more limiting stress than the bottom locking mechanism. The equation to find the  $F_{elbow}$  is given below

$$F_{elbow} = F_p \frac{x_c}{x_{FH}} = (226N + 608N + 6.0N) \frac{346.0mm}{708.6mm} = 410N$$
 (3.38)

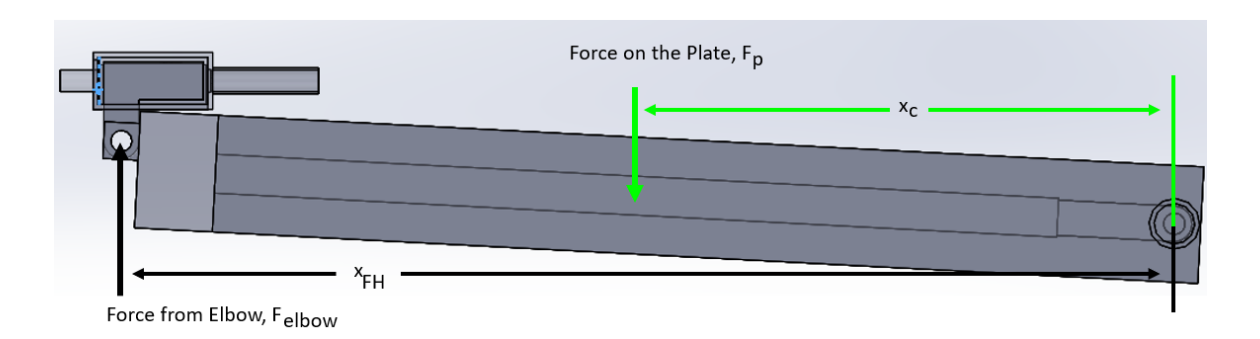


Figure 3-16: Force Balance for Cold Plate

This force was then used to analyze for bending and shear stress applied to the top locking mechanism. Similar to the analysis in Section 3.2.6, first the second moment of area, I, was found. Then the maximum moment  $M_{max}$  and the section modulus, Z = I/c were determined. And, finally, the bending stress,  $\sigma_{bending}$  which was compared to the yield stress  $\sigma_{yield}$ . For both analyses, it was assumed that each elbow would carry half of  $F_{elbow}$  and each elbow bracket would be supported by a beam-like tab with a base, b = 50mm, height h = 3mm and length, l = 42mm. It was assumed that the load applied by the elbow would be uniformly distributed on the beam like supporting tab. For this analysis, the uniform loading was condensed to a point load applied at the middle of the length,  $x_m = 21mm$ . Clarifying diagram is shown in Figure 3-17.

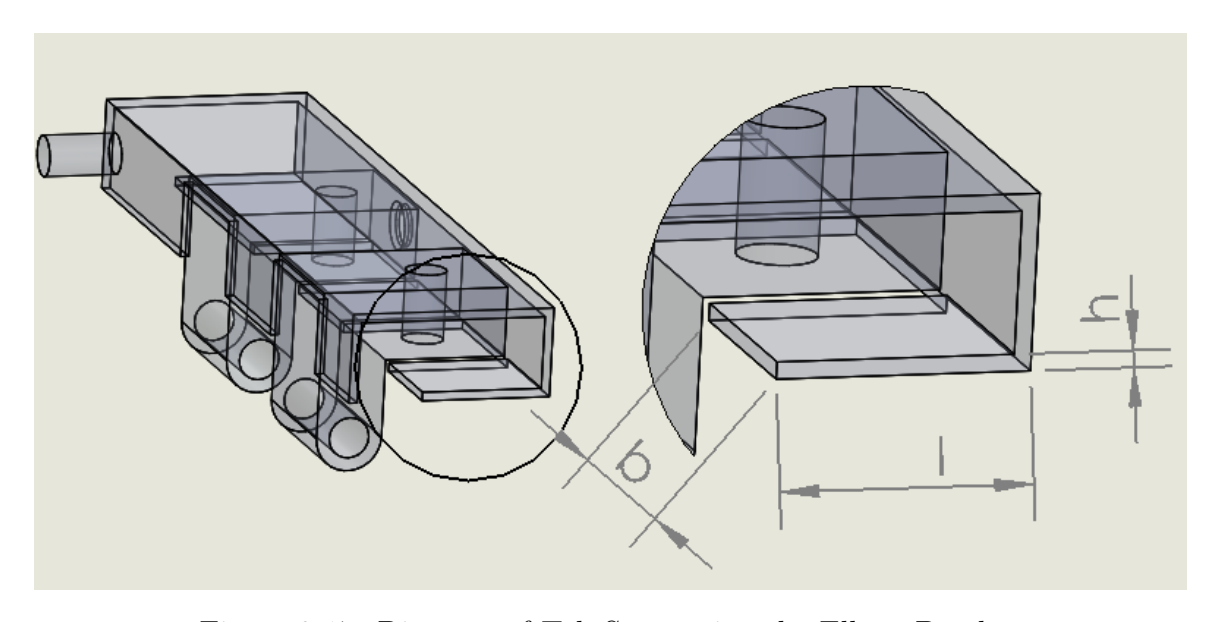


Figure 3-17: Diagram of Tab Supporting the Elbow Bracket

Beginning with the second moment of area,

$$I = \left(\frac{1}{12}\right)bh^3 = \frac{1}{12}(50 \cdot 3^3) = 112.5mm^4 : c = \frac{h}{2} = 1.5mm$$
 (3.39)

Next the section modulus and bending stress becomes

$$Z = \frac{I}{c} = \frac{112.5mm^4}{1.5mm} = 75mm^3 : M = F \cdot x_m = \frac{410N}{2} \cdot 21mm = 4.31kN - mm \quad (3.40)$$

Everything is known to calculate the bending stress on the beam. The equation for bending stress is

$$\sigma_{bending} = \frac{M}{Z} = \frac{4.31kN - mm}{75mm^3} = 57.5MPa \tag{3.41}$$

The factor of safety for bending stress is

$$\eta_{bending} = \frac{\sigma_{yield}}{\sigma_{bending}} = \frac{205MPa}{57.5MPa} = 3.56 \tag{3.42}$$

This shows that this is a safe design and should not fail by bending.

Next, the shear area and shear stress are found and compared to allowable shear stress. Since this is modeled as a cantilever beam, the bending stress should be more limiting. The shear force, V, is half of the  $F_{elbow}$ . The shear area,  $(A_S)$ , is the base, b multiplied by the height, h.  $A_S = (50mm) \cdot (3mm) = 150mm$ .

$$\tau_{max} = \frac{3V_2}{2A_S} = \frac{3(205N)}{2(150mm)} = 2.05MPa \tag{3.43}$$

The allowable shear stress is nominally calculated as two-thirds of the ultimate tensile strength or  $(0.67) \cdot 515MPa = 345MPa$ . The actual shear stress is just over 2 MPa. While there is a possibility of this mechanism failing by shear stress, the likelihood of this is quite small. As expected, the bending stress was more limiting. In general this design has adequate factors of safety and may even be overbuilt. If desired to reduce the weight, there are modifications that could be made. From the analysis, this appears to be a safe design.

# Chapter 4

# Impact of Material Selection

This section covers the reasoning behind and implications of selecting the right material for the iPEBB's shell. First the requirements for the housing of the iPEBB are discussed. Next, the justification for selecting a preferred material (in this case aluminum was the metal of choice). Then, the list of suitable alloys was reduced to the top three and each was compared. Finally, the total weight needed for one of the remaining aluminum alloys to fully function as the iPEBB's shell was determined. In the event that the iPEBB is not housed in an aluminum shell, the methodology from this analysis works.

# 4.1 Restrictions on iPEBB

The iPEBBs are meant to be lifted and operated by a single person. The upper weight limit for an individual item to be moved by a single person is 16 kg [39]. As mentioned in Section 2.1, the assumed weight of the electrical components is 14 kg. This leaves a maximum of 2 kg for the weight of the shell to contain and protect the electrical components. Not all materials were initially considered. There is a list of prohibited materials (e.g., asbestos) and other not suitable for design (e.g., leather) [14]. Additionally, the enclosure is required to be rigid and not deform under a firm touch [10].

The shell of the iPEBB is subjected to the clamping force securing the cold plates

to the iPEBB. The force, as detailed in Section 2.1, is derived from applying 10 psi to the cold plate, facilitating the removal of heat generated by the power conversion components. As previously mentioned, the shell can weigh a maximum of 2 kg, thus the material must have high strength-to-weight ratio and good thermal conduction properties. The value for thermal conductivity varies greatly (four orders of magnitude) among all materials. Materials like glass, foam, natural materials, and most plastics are not good thermal conductors; metallic materials in general, are excellent conductors [42] [5]. Some ceramics, excluding oxides, have thermal conductivity values similar to metals [42]. For this design a minimum thermal conductivity of  $40 \frac{W}{m \cdot K}$  was used to separate the acceptable materials.  $40 \frac{W}{m \cdot K}$  was shown to provide adequate heat removal to avoid violating any thermal limits of the internal electrical components.

The shell of the iPEBB must resist deforming significantly to prevent damaging internal components. As in seen in Figure 4-1, metals are stronger that most materials. They are also the most dense. Since the strength of the iPEBB is, in part, dictated by the weight limit, the ideal material should be strong and light. Additionally, as practicable, the materials used for construction shall be of a common variance (type, class, forms, and grade) that is readily available for normal sources of supply [14].

Next, the material must also be inherently corrosion resistant or be processed such to provide corrosion resistance [14]. The main corrosion that this design was wary of was galvanic, stress corrosion cracking, and general corrosion. Corrosion of materials will only happen in the correct settings. For example, galvanic corrosion occurs at the interface of two dissimilar conductive materials where the anodic (more active) material's corrosion rate accelerates and the cathodic (less active) material's corrosion rate decreases [15]. To minimize galvanic corrosion, the method shall include ways to exclude electrolyte interaction between the two dissimilar metals [15]. This could mean adding a separation layer which can be as simple as paint, anodizing, or powder coating [14]. Alternatively, the removal of galvanic corrosion could be accomplished by using the same material throughout the design. The process of

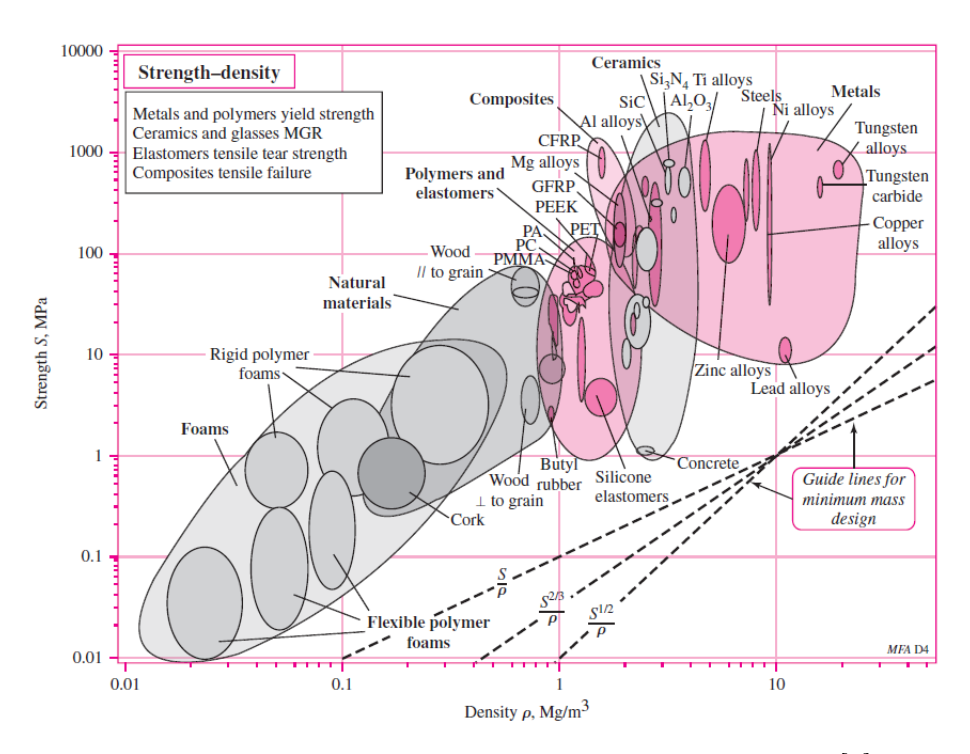


Figure 4-1: Strength vs Density for Various Materials [5]

stress corrosion cracking is not entirely known [4]. To some materials (i.e. Austenitic Stainless steels, brass, and certain aluminum alloys), it is known to occur at elevated temperatures (generally greater than 150°F) or when highly stressed. This is an issue since the maximum operating temperature for the iPEBB is 180°F. From MIL-DTL-917F, common materials that naturally resist corrosion in non-extreme environmental conditions and do not need further processing are:

- 1. Brass <sup>1</sup>
- 2. Bronze
- 3. Copper
- 4. Copper-Nickel alloy
- 5. Copper-Beryllium alloy
- 6. Copper-Nickel-Zinc alloy

<sup>&</sup>lt;sup>1</sup>Brasses containing 20 to 40 percent zinc are highly susceptible to stress corrosion cracking in marine environments when highly stressed

- 7. Nickel-Copper alloy
- 8. Nickel-Copper-Silicone alloy
- 9. Nickel-Copper-Aluminum alloy
- 10. Aluminum Alloys <sup>2</sup>
- 11. Titanium
- 12. Austenitic steels, corrosion resistant<sup>3</sup>

Materials that were not naturally corrosion resistant were discarded as the additional measures needed to make them corrosion resistant (i.e. coating like paint) would have a negative effect on the thermal conductivity. Thus, only the twelve alloys listed above were considered for analysis.

## 4.2 Material Review

From this list of twelve alloyed materials, generic material properties are explained and compared. This method was advantageous as the material to be used was not fully defined and allowed for a high level comparison of relevant material properties. The disadvantage is that not all of the nuances of each alloy are considered. This leaves open the possibility of error that there is a better type of alloy that was not considered.

## 4.2.1 Copper and Its Alloys

In general, copper and copper alloys have great thermal conductivity, wide range of good to high yield strengths, excellent corrosion resistance, and are more dense than most of the other options[21]. The density of pure copper varies around 8.9  $\frac{g}{cm^3}$  depending on the amount of could work applied to the copper. Where the more cold work imparted on the copper, the higher the density. Copper is generally alloyed

<sup>&</sup>lt;sup>2</sup>Types: 3003, 3004, 5052, 5056, 5083, 5085, 5086, 5154, 5456, 6061

<sup>&</sup>lt;sup>3</sup>Types: 202, 301, 302, 303, 304, 304L, 309, 310, 316, 316L, 321, 324A, 347

with lighter materials thus the density of the copper alloys is usually less than pure copper. The thermal conductivity of pure copper is 398  $\frac{W}{m \cdot K}$  at room temperature. This is much more than the minimum required value. The strength of pure copper depends on the work and heat treatment performed on the metal. After annealing, the yield strength ( $\sigma_{yield}$ ) is 33 MPa. After cold-drawing, the  $\sigma_{yield} = 333MPa$ , ten times higher. The modulus of elasticity for cold drawn pure copper is slightly reduced from 128GPa to 112GPa when cold drawn. Additionally the machinability rating for pure copper is 20 [21]. Machinability is the ease of cutting/shaping a material. It is defined by power consumption, tool wear rates, surface finishes, and chip formation and dependent on type of tool used, cutting fluid, and machinist's skill. These ratings have been standardized using the test described in ASTM E618 Standard Test Method for Evaluating Machining Performance of Ferrous Metals Using an Automatic Screw/Bar Machine [28]. Not all materials have been tested due to the quantity of material needed for this test and the amount of alloy and temper combinations [21]. Higher numbers are better for machinability ratings. In the case of copper and it alloys, they are compared to C36000 Free-cutting Brass which scored a 100.

Any alloys consisting of copper principal alloyed with zinc are classified as brass. Brass retains the preferable corrosion resistance and formability characteristics as copper and is noticeably stronger. A popular maritime industry metal, Muntz metal (C28000 H00), was used to compare material properties. For Muntz metal,  $\sigma_{yield} = 240MPa$  and the modulus of elasticity is 105GPa. In general, the more zinc added produces higher strengths up to the 30% range [21]. Its density is less that pure copper at  $8.39 \frac{g}{cm^3}$ . The thermal conductivity was reduced to  $123 \frac{W}{m \cdot K}$ . Corrosion resistance for brass is good; except when it contains more than 15% zinc. Then it is susceptible to stress corrosion cracking. Machinability rating is 40 [21].

Copper alloyed with tin were traditionally classified as bronze. In more recent years, the term bronze can be used with any alloying element and may not contain any tin. It simply refers to variety of copper alloy [21]. For this context, since there is no other alloying element, it is assumed that the traditional copper alloyed

primarily with tin was the desired material. Depending on the amount of tin added, the physical appearance and mechanical properties change. For example, at 10% tin, the metal appears to be yellow, while increasing the amount of tin turns the material gray around 30% tin [44]. Copper alloy 91700 is used in high strength applications where heavy loads are present. Its yield strength is between put copper and brass at  $\sigma_{yield} = 150MPa$ . The modulus of elasticity is the same as bronze at 105GPa. It has a higher density than brass at 8.75  $\frac{g}{cm^3}$ . The thermal conductivity has been further reduced from brass to 71  $\frac{W}{m \cdot K}$ . The inherent corrosion resistance is still high for this material [21].

Copper-Nickel alloys are typically used in heat exchanger tubes and condensers due to their superior ability to resist stress corrosion cracking, impingement corrosion, and corrosion in acid solutions. Has some of the best resistance to aqueous corrosion of all of the copper alloys. Specifically for Copper-Nickel C70600 OS025, its yield strength is  $\sigma_{yield} = 110MPa$  with a density of 8.94  $\frac{g}{cm^3}$ . The modulus of elasticity is higher than most copper alloys at 140GPa. Its thermal conductivity is even lower than bronze at  $40 \frac{W}{m \cdot K}$ . Additionally, the machinability rating for this alloy is 20 out of 100 [21].

Copper-beryllium alloys have the similar corrosion resistance as copper meaning that Beryllium has no effect on the corrosion resistance. Copper-Beryllium alloy C17200 is used in application when high strength, and fatigue and creep resistance are required. Additionally, when working with this metal, care has to be taken since beryllium is a potential health hazardous when airborne from dust/flames. Its yield strength is  $\sigma_{yield} = 620MPa$  with a density of 8.25  $\frac{g}{cm^3}$ . Its thermal conductivity is close to brass at 115  $\frac{W}{m \cdot K}$ . This alloy has a machinablity rating of 40 [21].

Copper-Nickel-Zinc alloy typically exhibit good corrosion resistance in salt and fresh water. Alloy C74500 OS025 is typically used in hardware and optical parts. It has a yield strength of  $\sigma_{yield} = 160MPa$  at a density of  $8.69 \frac{g}{cm^3}$ . It's thermal conductivity is similar to copper nickel alloys at  $45 \frac{W}{m \cdot K}$  with slightly lower modulus of elasticity of 120GPa. This material has excellent formability when cold working however it is poor for hot forming. [21]

### 4.2.2 Nickel and Its Alloys

Nickel is, in general, used in applications that require great corrosion resistance and heat resistance applications. Nickel can be used in corrosive environments where the are high temperatures and high stresses. Nickel and nickel based alloys are ductile and fabricated by conventional wrought and casting methods. When machining nickel and nickel based alloys it important to understand that they are stronger at metal cutting temperatures. Thus a different tool may be needed in the annealed than the hardened condition to machine the desired nickel component. Elemental nickel had a yield strength of 59 MPa, thermal conductivity of  $82.9 \frac{W}{m \cdot K}$ , and a density of  $8.902 \frac{g}{cm^3}$  [20].

Nickel-Copper alloys are resistant to a wide range of moderately aggressive corrosive environments and have a higher strength than nickel. Typically, Monel 400 (N04400), a specific Nickel-Copper alloy, is used in chemical processing and marine applications. It has a yield strength of  $\sigma_{yield} = 240MPa$  with a density of 8.8  $\frac{g}{cm^3}$ . Its thermal conductivity is  $21.8 \frac{W}{m \cdot K}$  at room temperature. In addition to great corrosion resistance in various environments such as brine, sulfuric acid, it is also immune to stress corrosion cracking [20].

Nickel-Copper-Silicon alloy are typically cast where an upper limit of 10% Silicon can be added. Most hover around 1-4%. A minimum of 3.5% Silicon is required for age hardening to be possible<sup>4</sup>. Greater that 3.8% Silicon causes the formation of brittle silicides which causes difficulty when machining that alloy. Alloy M-35-2 (dsignated by ASM; M35-2 is the ASTM designation) is similar to Monel 400 (listed above) but M-35-2 is an alloy formed by casting instead of wrought techniques. It has a yield strength of  $\sigma_{yield} = 205MPa$  and a density of 8.8  $\frac{g}{cm^3}$ [20]. Its thermal conductivity is similar to Monel 400 at 22  $\frac{W}{m \cdot K}$ [33]. Similarly to Monel 400, M-35-2 has a excellent resistance to corrosion in marine environments[20].

A Nickel-Copper-Aluminum Alloy is known as Waspaloy (N07001). It is typically used in aerospace applications and can make use of its high temperature strength and high oxidation resistance [20]. It has a yield strength:  $\sigma_{yield} = 793MPa$  [46] with a

<sup>&</sup>lt;sup>4</sup>Also know as precipitate hardening; increases strength and reduces ductility

density of 8.2  $\frac{g}{cm^3}$  [26]. Its thermal conductivity is even less that Monel 400 at 11  $\frac{W}{m \cdot K}$  [26]

#### 4.2.3 Aluminum

Aluminum alloys are known for high strength, low weight, excellent corrosion resistance. As a structural metal, they are second only to steel in their use. Aluminum has a density about one-third that of steel. Aluminum forms a passive oxide layer on its surface to prevent general corrosion and it will not rust (oxidize) as long as this layer is present. If this protective layer is scratched, it will heal itself. When correctly alloyed, it can resist corrosion from a variety of other environmental factors such as salt water [18].

From the list of aluminum alloys, Type 5052 H32 is typically is in marine applications, sheet metal work, and appliances. It has a yield strength of  $\sigma_{yield} = 193 MPa$  with a density of  $2.68 \frac{g}{cm^3}$ . It has a good thermal conductivity of  $138 \frac{W}{m \cdot K}$ . Additionally, it has a modulus of elasticity of 69.3 GPa corresponding to high fatigue strength and moderate static strength properties[16].

#### 4.2.4 Titanium

Titanium is about 40% lighter than steel and when correctly alloyed can have higher ultimate strength values than austenitic steels. It may be wrought, forged, or casted. Additionally, it may be processed by powder metallurgy (P/M) techniques.

Pure Titanium has a yield strength of  $\sigma_{yield} = 170 MPa$  at a density of  $4.51 \frac{g}{cm^3}$ . It's thermal conductivity is similar to Waspaloy at  $11.4 \frac{W}{m \cdot K}$ . It's modulus of elasticity is 120 GPa. Titanium has excellent corrosion resistance except in environments with fluoride ions. It has performed well in atmospheric condition in marine environments. Additionally, weld zones on pure titanium and many of its alloys had no impact on the corrosion resistance [25].

#### 4.2.5 Austenitic Steels

Stainless steels are iron based alloys that contain a minimum of 11% chromium. They have the "stainless" designation due to the oxide surface layer due to chromium. The austenitic stainless steel evaluated was Type 316 which means that Nickel was alloyed with the chromium. Austenitic Steel has good work-ability even in very cold temperatures.

From the list of Austenitic Steels, Type 316 (S31600) was selected. It generally has good corrosion resistance to weak bases. Stronger bases may be able to remove protective layer and cause cracking. Molybdenum was added to Type 316 to enhance its resistance to corrosion in chloride environments. It's yield strength is  $\sigma_{yield} = 205MPa$  at a density of 8.0  $\frac{g}{cm^3}$ . Its thermal conductivity is among the lower on this list at 16.2  $\frac{W}{m \cdot K}$  [19].

# 4.3 Base Material Used for Analyses

For the material analysis, the important factors are: strength-to-weight ratio, thermal conductivity, and corrosion resistance. To determine the best material to choose for the enclosure of the iPEBB, a comparison was made on the yield strength, thermal conductivity, density, and corrosion resistance.

The first evaluation was based on thermal conductivity. Initial calculations performed on the heater transfer from the internal electrical components to the heat sink have concluded that the ideal material for the shell of the iPEBB must have a thermal conductivity greater than  $40 \frac{W}{m \cdot K}$ . This would ensure that adequate heat would be transferred and with acceptable margin to thermal limits. This minimum acceptable value eliminates: Bronze, Copper-Nickel alloy, Copper-Nickel-Zinc alloy, Nickel-Copper alloy, Nickel-Copper-Silicon alloy, Nickel-Copper-Aluminum alloy, Titanium, and Austenitic steels. The remaining materials are: Brass, Copper, Copper-Beryllium alloys, and Aluminum alloys.

The second evaluation was based on the strength-to-weight ratio. This analysis directly compared the yield strength to the density of the materials. The objective

was to find the material that produced the most strength for the least amount of weight. There was no objective to meet for this analysis. From Table 4.1, the strongest material for its weight is Aluminum Alloys. Specifically, this table shows that between these remaining materials that Aluminum Alloy 5052 is the strongest for its weight with Copper-Beryllium in a close second. There may be other alloys of the other materials that are stronger per their weight. However, in order to do so, many of the copper alloys would need to more than double their yield strength without dropping below the thermal conductivity threshold.

Table 4.1: Strength-to-Weight Ratio for Remaining Materials

Material	Modulous of Elasticity	Yield Strength	Density	$\sigma_{yield}/\rho$
Material	E (GPa)	σ <sub>yield</sub> (MPa)	$\rho$ (g/cm $^3$ )	Ratio
Brass	105	220	8.40	26.2
Bronze	105	150	8.75	17.1
Copper	112	333	8.90	37.4
Copper-Nickel Alloy	140	110	8.94	12.3
Copper-Beryllium Alloys	139	620	8.94	69.4
Copper-Nickel-Zinc Alloys	120	160	8.69	18.4
Aluminum Alloys	69.3	195	2.68	72.8

Table 4.2: Area of Shell With No Thickness

Component	Length	Width	Number	Area
Component	$(mm^2)$	$(mm^2)$		$(mm^2)$
Sides	550	100	2	110,000
Front and Back	300	100	2	60,000
Top and Bottom	550	300	2	330,000
Total				500,000

Since there is a weight limit on the shell, the third evaluation compared density of the materials as it relates to resulting iPEBB wall thickness. The thickness of the sidewall based on the current assumed dimensions, given in Section 2.1, of 550 x 300 x 100 mm. From these dimensions, if the shell were deconstructed and laid flat, the area would be  $0.5 \ m^2$  or  $500,000 \ mm^2$  as shown in Table 4.2. Then, using the densities of the materials remaining, the thickness of the shell was found using Eqn 4.1.

$$WallThickness = \frac{Weight}{Area \cdot Density} = \frac{2000g}{500,000mm^2 \cdot Density}$$
(4.1)

Table 4.3: iPEBB Shell Thickness for Various Metals

Material	Area of Shell	Density	Max Weight	Thickness
Wiaterial	$(mm^2)$	$\left(\frac{g}{mm^3}\right)$	(g)	(mm)
Brass	500,000	0.00840	2,000	0.4762
Bronze	500,000	0.00875	2,000	0.4571
Copper	500,000	0.00890	2,000	0.4494
Copper-Nickel Alloy	500,000	0.00894	2,000	0.4474
Copper-Beryllium Alloys	500,000	0.00894	2,000	0.4474
Copper-Nickel-Zinc Alloys	500,000	0.00869	2,000	0.4603
Aluminum Alloys	500,000	0.00268	2,000	1.4925

Table 4.3 shows the results. For the copper and copper alloys, the wall thickness would be around 0.5 mm while the wall thickness for aluminum alloys would be around three times thicker at 1.5 mm. This is significant in the shell side face buckling calculation (Section 2.4.1). Specifically, the plate flexural rigidity, D, proportionally depends on the Modulus of Elasticity (E) and the shell thickness cubed ( $h^3$ ) (see Eqn 2.22). Looking only at the thickness of the face in question, the copper alloy's shell is three times less thick (compared to aluminum alloys). That amounts to a twenty-seven times smaller plate flexural rigidity. Thus, while the copper alloys do have a much larger modulus of elasticity, it cannot compensate for reduction in shell thickness. This means that load that would cause buckling to occur would happen at a much lower value. For example, using Eqn 2.23 for the side plates replacing the material with copper-beryllium alloy having the same properties previously discussed, the new load that would cause buckling is  $0.83 \frac{N}{mm}$ . This means that the side plates would buckle under the current loading.

The final metric for this analysis was corrosion resistance. While all of the materials listed have good corrosion resistance and most are sufficient for the environment that the iPEBB would be operating in, if there were to be any corrosion it would be best to have more material to wear down. Since these metals all have good corrosion resistance and are not required to have any additional coatings, it is assumed that the rate of corrosion would be slow and similar between all metals. Thus, it was preferred to have a thicker shell to a thinner one. It is worth mentioning again that some of the alloys, like some brass and aluminum alloys, are susceptible to stress corrosion

cracking at elevated temperatures.

Taking into account all of these factors, the ideal material is one of the aluminum alloys. This selection was primarily based on having the lowest density and highest strength-to-weight ratio.

# 4.4 Selecting the Ideal Material

Now that the general material has been selected, it is time to take a closer look into the specific alloy for the iPEBB's shell. From Section 4.1, the allowable alloys of aluminum are types: 3003, 3004, 5052, 5056, 5083, 5085, 5086, 5154, 5456, 6061. Since these all possess roughly the same density, it was important to view other factors when narrowing down the list to the acceptable metals. The ideal type of aluminum must be a common material [14], able to be produced at a thickness of 1.5mm, and resistant to stress corrosion cracking.

The first evaluation tackled two challenges at the same time. American Society for Testing and Materials (ASTM) governs manufacturing of aluminum alloys as sheets and plates among other sizes. Sheets are defined as having thickness of 0.5 to 6.3mm. Plates have thickness >6.3mm and foils have thickness < 0.5mm [27]. Thus if the alloys were on the list then they would be both a common material and about to be manufactured as a sheet. Alloys 5056 and 5085 were not covered by the ASTM standard for plates and sheets [27]. They were removed from consideration.

The next final criteria was to ensure that the alloy chosen was resistant to stress corrosion cracking. This happens when the aluminum alloy has a >3.5% concentration of magnesium and in operating environment when the temperature exceeds 65°C or 150°F [18]. As mention previously in this chapter, the iPEBB is expected to operate as high at 150°F with a maximum temp of 180°F. Using the Aluminum Association notation, aluminum alloys in the 5xxx series are primarily alloyed with magnesium and used in the marine environment due to good resistance to corrosion characteristics. If this material was going to be continuously exposed to salt water, such as on the hull of the ship, the 5xxx series would be used [18]. Since this structure

is not expected to be exposed to salt water and to avoid compounding causalities that could happen with high temperature stress corrosion cracking, the following types were removed from consideration: 5083, 5086, 5154, and 5456. The remaining types are: 3003, 3004, 5052, and 6061.

As alloys are compared, it will be necessary to fully define the alloy and any mechanical or thermal treatments that were performed on the material. In all cases, the material properties vary with these treatments. To standardize the material properties achieved, a system was developed to catalogue the properties achieved. Specific material properties are called tempers and must be registered with the Aluminum Associate Technical Committee of Product Standards. In general, tempers are alphanumeric designations following the alloy that convey the material information. The first letter in the temper designation indicates the general class of treatment. The classes are F (fabricated), O (annealed), H (strain hardened), W (solution heat treated), and T (thermally treated and not F, O, or H). The subsequent number that follow the the general class break down the thermal and/or mechanical work performed on the material [30]. This analysis chose common tempers for each material.

Up to this point, the process has mostly found which materials would not work. These remaining materials will all work for the shell of the iPEBB. Now it is about finding the reasons to select one material over the others. The best material will depend on how the iPEBB is made. Since that is not currently known, the rest of this chapter will outline the strengths, weaknesses, and typical application for each of the alloys. A summary is provided at the end in Table 4.4.

Starting with types 3003 and 3004, these alloys are general purpose alloys for architecture like applications. The are alloyed with manganese and wrought alloys are strengthened by work-hardening. These alloys are used for moderate strength applications requiring good workability. Both type 3003 and 3004 have good formability and resistance to corrosion. In terms of working with Type 3003, it has excellent soderability, good weldability, and scores an A for brazeability (generally brazeable). Its thermal conductivity is  $193 \frac{W}{m \cdot K}$  (comparing O temper). Type 3004 is often referred to having the same properties at 3003 with higher strength. When working

with Type 3004, it has good soderability and received a brazeability score of B (special techniques needed). Its thermal conductivity is  $162 \frac{W}{m \cdot K}$  (comparing O temper). When evaluating these two types, the higher thermal conductivity and workability properties would pick Type 3003 over Type 3004. If higher strength is needed the Type 3004 is the better choice. Compared two the other two aluminum alloys, Type 3003 has a better surface finish and is better for sheet metal forming.

Type 5052 is stronger than 3003 and still facilely formable. It is used in applications such as products exposed to the marine environment, electronic panels, electronic chassis, and cooking equipment. When working with Type 5052 is has good weldability but poor soderability, and scored a C (limited brazeability) on brazeability. It has good resistance to corrosion. It is strengthen by cold work and is thus work hardenable. It has the lowest thermal conductivity at 138  $\frac{W}{m \cdot K}$  but the highest fatigue strength at 115 MPa and modulus of elasticity at 70.3 GPa. This is the alloy to pick if worried about buckling of the side faces on the iPEBB's shell.

Type 6061 is the strongest of all of the types. It is used across a variety of area such as architectural extrusions, marine applications, electrical and electronic applications, recreations vehicles, and kitchen equipment. This type is easy to work with as it received a good rating for formability, soderability, and weldability. It scored an A (generally brazeable) on brazeability. It has good corrosion resistance. This alloy is heat-treatable and thus precipitation-hardenable. It's thermal conductivity is 167  $\frac{W}{m \cdot K}$ . It's yield strength is 276 MPa. This is the material to pick if strength and working with the metal are of the biggest concerns. It is better in applications that require machined parts than Type 5052 because it is more brittle. Compared to Type 3003, Type 6061 is harder to scratch and has better thermal conductivity values after 3003 has been work hardened.

Table 4.4, compare the aluminum alloys mentioned above in addition to the alloy 1060 which was used for calculations for the previous chapters. This is useful to see the possible improvement made selecting a better material. The material properties associated with assembling the shell of the iPEBB were not included for Type 1060 as it is not intended to be used for that purpose. Rather only the relevant physical

characteristics are included for comparison since these were used during prior analysis.

Table 4.4: Comparison of Viable Aluminum Alloys[16]

Ch t i - t i	1060	3003	5052	6061
Characteristics	(O)	(H14)	(H32)	(T6)
Thermal Conductivity $(\frac{W}{m \cdot K})$	234	159	138	167
Strength (MPa)	-	-	-	-
Ultimate Tensile	69	150	228	310
Tensile Yield	28	145	193	276
Fatigue	21	62	115	96.5
Modulus of Elasticity (GPa)	69.0	70.0	70.3	68.9
Density $\left(\frac{g}{cm^3}\right)$	2.705	2.73	2.68	2.7
Welding	-	Good	Good	Good
Machinability	-	Good	$\mathrm{BA}^5$	Good
Brazeability	-	A	С	A

# 4.5 Impact on iPEBB

All of the information discussed above provides the reasons to pick an aluminum alloy over other materials. Building on this discussion, this section highlights the effect on the weight of the iPEBB if it were constructed from one of the recommended alloys. From the analysis performed in Section 2.4, the analysis with the lowest factor of safety is the buckling analysis. Previous calculations were performed with aluminum type 1060 and depend mostly on the modulus of elasticity and the thickness. From Table 4.4, the modulus of elasticity and density do not change drastically between all of the aluminum alloys. The source of the weight reduction will be from requiring the buckling factor of safety to be close to, but no less than two. Assuming that the loading on top and bottom of the iPEBB are the same, the uniform distributed load on the edge is  $q_{x,applied} = 6.88 \frac{N}{mm}$ . From Section 4.3, it is clear that greatly reducing the thickness of the shell detrimentally impacts the buckling minimum load that causes buckling. Thus the remained of this section will find the find the minimum edge load to provide adequate margin to buckling, then rearrange Eqn 2.22 to solve for the

 $<sup>^{5}\</sup>mathrm{BA} = \mathrm{Below} \ \mathrm{Average}$ 

minimum thickness, and finally using that thickness determine the lowest weight of the iPEBB. Aluminum alloy Type 6061 is used for this analysis.

When  $FOS_{buckling} = 2$ , the associated minimum load required for buckling is shown in the equation below:

$$q_x = \frac{q_{x,applied}}{FOS_{buckling}} = \frac{6.88 \frac{N}{mm}}{2} = 13.76 \frac{N}{mm}$$

$$(4.2)$$

Next, rearranging Eqn 2.22 to solve for the minimum thickness and shown below:

$$h = \sqrt{\left(\frac{q_x b^2(12)(1 - v^2)}{\pi^2 E}\right) \left(\frac{mb}{a} + \frac{n^2 a}{mb}\right)^{-2}}$$
 (4.3)

Where, same as before for the longer side faces of the iPEBB, b = 550mm, v = 0.33, m = n = 1, and a = 100mm. The new modulus of elasticity, E, is given in Table 4.4. The resulting thickness is h = 1.42mm. It is assumed that this is the uniform thickness throughout the shell. Thus, multiplying this thickness by the area of the shell (shown in Table 4.2), the total volume is found to be:

$$V_{tot} = h \cdot Area = (1.42mm) \cdot (500,000mm^2) = 710,000mm^3 or 710cm^3$$
 (4.4)

Using the density from Table 4.4, the minimum weight of the iPEBB is

$$Mass = Density \cdot V_{tot} = (2.7 \frac{g}{cm^3})(710cm^3) = 1.917kg$$
 (4.5)

This shows that minimum weight for the iPEBB is 1.917 kg for these load conditions and dimensions. If looking to reduce the weight of the shell even further, (1) less securing force should be applied which would lower the applied edge load (affects the heat transferred from the electrical components) or (2) change the design of the iPEBB for better plate aspect ratios that would increase the minimum load required for buckling (affects the internal layout). Additionally, this calculation assumed that the shell is of uniform thickness, this does not necessarily need to be the case. This also shows that limiting the maximum weight for the iPEBB's case to be 2 kg for

these dimensions does limit the material selection

# Chapter 5

# Recommendations and Conclusions

## 5.1 Results

This section summarizes the results from the previous chapters and provides a brief look at an alternate design.

# 5.1.1 Review of iPEBB Design

When reviewing the iPEBB's design, the two most important factors are which material the shell is made from and its ability to resist buckling loads. To even be considered, the material had to meet the standard for corrosion resistance or be able to be coated to provide corrosion resistance [14]. Applying a coating to materials that were then used for heat transfer seemed counter-productive. Thus, only the materials that did not need to be coated were considered. The materials list was then whittled down based on their thermal conductivity and strength-to-weight ratio properties.

Looking at the design of the iPEBB's shell, three critical assumptions drove this analysis. The assumptions are that the iPEBB's shell would: (1) be of uniform thickness, (2) be of uniform material, and (3) weigh a maximum of 2 kg. These three assumptions drove the rest of the analysis. For example, the most limiting analysis was the buckling of the sides of the iPEBB. The minimum load required to cause buckling depends heavily on the shell thickness cubed  $(h^3)$  and the modulus

of elasticity (E). Using the above assumptions, the shell thickness on the sides of any material can be known once its density is known. Thus, denser materials would produce thinner shells, which may result in lower critical buckling loads depending on E.

Thus, after conducting this analysis, the essential idea moving forward is that selecting a material directly ties to the critical buckling load of the iPEBB's shell. The current assumptions greatly restrict the choices available. Under the current assumptions, an aluminum-based alloy is the best choice.

## 5.1.2 Review of Hinge Design

The hinge design fulfills the needs of the securing mechanism and integrates well with the cooling system. The critical component for the hinge design is the elbow bracket in the front. They are used to secure the iPEBB and hold up the cold plate when not in use. The elbow brackets are at the most significant risk of failure when providing the securing force due to shearing the front hinge hole and then bending at the bolt hole. However, all of the components have acceptable safety factors; the factors of safety for shear and bending stress for the elbow bracket are the lowest and would be expected to fail first.

The advantages of this design are: (1) light design, (2) accessible parts, (3) securing force is self-generated, (4) operates independently of other systems, and (5) cooling system optimized for this design. Besides the necessary parts of the iPEBB, thermal pad, and cold plates, this design only adds the front and back hinges, elbow brackets, locking mechanisms, washers, nuts, and bolts. These components do not add much additional weight to the design (<5% of the total 68 kg). Since most of these parts are movable, they are located in the front of the cabinet and are thus easy to access. The elbow brackets require 180° of rotation which is easily accomplished since the parts are in the front of the design. The cold plates are compressed together by bolts. This system does require additional material for attachment points for components that are applying the securing force. This contributes to the lightweight design. Additionally, this design is manually operated. This reduces reliance on the

status of other systems, increasing the likelihood that this system will be operational when needed. Finally, the cooling liquid enters and exits along the same axis as the rear hinge. This integration allows for more rotation of the cold plate, creating additional clearance between the iPEBB and cold plate when needed.

The disadvantages of the hinge design are: (1) there is no assistance for the heavy cold plate, and (2) the hinge in back must be appropriately aligned to apply an evenly distributed force on the iPEBB. The cold plate and elbows combined to weigh around 25.2 kg. Removing dynamic loading, the operator would need to lift and hold approximately 13 kg (29 lbf) while securing the cold plate. This is doable but would be easier with assistance. Finally, the hinge in back would need to be correctly measured and cut to ensure proper alignment for the back hinge. It would be critical to align this properly for an even distribution of force on the iPEBB.

### 5.1.3 Alternate/Clamp Design

This design is not described nor calculated in-depth in this report. However, if a clamp design were to be made, there would be some advantages and disadvantages with this design. The iPEBB would still slide in and out along the keyway and use the cold plates to remove the heat generated inside the iPEBB. The hinge and clamp designs are different because the cold plate moves in a strictly vertical motion in the clamp design while it rotates in the hinge design. The motion would be accomplished by a linear actuator attached to the cold plates, such as a jack. There could be multiple jacks per cold plate to obtain an even force distribution. The jacks for one cold plate would move synchronously and could be controlled by cranking an interconnected shaft via a motor or manually. This thought experiment assumed that four jacks were used (1 per corner) and that each cold plate was controlled via a shaft cranked manually.

The advantages of this design are: (1) smaller distance traveled by the cold plate in the front of the iPEBB, (2) the weight of the cold plate is not an issue for the operator, and (3) ensures an even distribution of force. The cold plates would only need to be raised to allow for clearance for insertions and removal of the iPEBB. This

may lead to a different design of the cold plates. Since the cold plate is attached to the jacks, the weight of the cold plate would not be supported by the operator. Using four jacks moving simultaneously, there would be an even distribution for force on the cold plate. The disadvantages of this type of design are: (1) it requires a flexible hose connections for the cooling system, (2) it requires a structure internal to the cabinet to provide securing force, and (3) this system would have more parts and would be heavier than the hinge design. Flexible hoses have specific requirements regarding how much they are allowed to bend. This would use more piping and take up additional space. This may make maintenance difficult with space restrictions. The jack must attach to an internal structure. This structure would need to be strong enough to support the jack(s) with minimal deflection. This leads to the final problem: this design would add significantly more weight than the proposed hinge design. This would not be an issue if only a few iPEBBs were used. However, with hundreds of iPEBBs projected to be onboard the vessel, the additional weight added for this design would take away from other vital components on the vessel.

## 5.2 Conclusion

In conclusion, this thesis has explained a proposed solution to the future electrical distribution problems. The current electrical distribution system is not suited for future shipboard technologies that require more power and faster response (pulses). Placing larger generators onboard would not fix both problems. Thus a new energy distribution system is needed to effectively transmit power from generators and an energy storage device (i.e., batteries, capacitor banks, etc.). In order to use power more effectively, future electrical distribution systems will need agile power conversion units. In a proposed electrical distribution system, PEPDS, these power conversation units are called iPEBBs. The iPEBB will need to be secured and cooled when in use and properly stored when not in use. Since these iPEBBs are still being researched and produced, general specifications were used, and an in-depth analysis was performed on fielding a securing mechanism that would be able to secure a iPEBB in place.

The mechanical and electrical constraints and functional requirements associated with building such a mechanism were considered when designing a securing mechanism. Then a potential design (hinge design) was analyzed based on its ability to fulfill these requirements. The result is that the hinge design can meet these requirements and is recommended due to its simplicity, cooling system integration, and minimal additional weight added. This design is not perfect but rather a positive first step towards the final design iteration. Future design should incorporate a way of reducing the weight that the operator must lift in order to secure the cold plates. While this is doable, it may be inconvenient in some situations.

#### 5.3 Future Topics

This thesis assumed that 10 psi was needed to ensure adequate contact between the cold plate and the top and bottom of the iPEBB. There are two current problems with this thermal pad: the pressure applied and its weight. Future work could look at lighter thermal pads. Furthermore, the impact of pressure on thermal pads should be considered.

Additionally, it was assumed that the cold plates would lay flat on top of the thermal pad, and the 2mm that the thermal pad could deform was not significant. This is not entirely correct. It would be expected that the thermal pad would deform under the weight of the cold plate and the applied force. The ideal height of the back hinge must be determined so that the cold plate will be level when the pressure is applied and the thermal pad is deformed. Alternatively, some flexibility in the system could assist in ensuring consistent, uniform loading. Future work could look at the magnitude of variance in pressure on the iPEBB by the cold plate as the securing force is applied when there is a slight misalignment of components.

This thesis assumed that key was able to be manufactured as designed in a homogeneous manner with no impacts structurally. This may not be the case. It may be more practicable to weld the key onto the iPEBB. This may cause structural changes to the sidewall of the iPEBB that may decrease the critical load (minimum load to

cause buckling of the sidewall).

The alternate clamp design spoken of earlier should be researched more in depth. This could provide more information than the pro/con list shown earlier. Furthermore, the ideal outcome may be a combination of clamp and hinge designs.

In the materials section, one of the factors that reduced the ideal materials was requiring a thermal conductivity value greater than  $40\frac{W}{m \cdot K}$ . The current thermal pad has a thermal conductivity value of  $17.8\frac{W}{m \cdot K}$ . If the required thermal conductivity value is relaxed, then more materials would be able to compete. Also, this analysis assumed that the iPEBB shell was of a constant thickness. The iPEBB may benefit from sections with varying thickness to save weight.

#### 5.4 Design Changes

After combining all of the components in the design, an initial assumption for the sizing of the thermal pad was that the maximum the cold plate would be able to rotate in front was one inch. This assumption was unnecessarily conservative; there is more space in the front for rotation. With more room to rotate, the thermal pad can cover the entire top of the iPEBB with no issues in the back regarding clearance between the thermal pad and the cold plate.

### Bibliography

- [1] PMS 320. Naval power and energy systems technology development roadmap. Naval Sea Systems Command, 2019.
- [2] American National Standards Institute (ASNI) and American Society of Mechanical Engineers (ASME). American national standard key and keyways for milling cutter and arbors. Standard, 1997.
- [3] Cagatay Basdogan. Static screw stresses [class handout]. Retrieved from: http://portal.ku.edu.tr/cbasdogan/Courses/MDesign/course\_notes/ScrewStresses.pdf. Istanbul, Turkey: Koc University, MECH 303.
- [4] Benjamin Floyd Brown. Stress corrosion cracking control measures. Technical report, American University Washington DC Dept of Chemistry, 1977.
- [5] R G Budynas, J K Nisbett, et al. Shigley's Mechanical Engineering Design. McGraw-Hill New York, 2011.
- [6] Michael D. Busch. Shear joints. https://www.cirruspilots.org/Publications/Articles/shear-joints, 2020.
- [7] J Chalfant, C Cooke, and C Chryssostomidis. White paper: Power corridor, 2020.
- [8] J Chalfant, M Ferrante, and C Chryssostomidis. Design of a notional ship for use in the development of early-stage design tools. In 2015 IEEE Electric Ship Technologies Symposium (ESTS), pages 239–244. IEEE, 2015.
- [9] T-Global Technology Co. Tg-a1780 ultra soft thermal pad, Revised: 06.03.2021.Data Sheet Version 17.
- [10] Naval Sea Systems Command. MIL-STD-108E: Definitions of and basic requirements for enclosures electric and electronic equipment. Department of Defense Military Standard, August 1966.
- [11] Naval Sea Systems Command. DOD-STD-1399, section 301: Ship motion and attitude. Department of Defense Interface Standard, July 1986.
- [12] Naval Sea Systems Command. Naval ship's technical manual (NSTM) chapter 300 electric plant-general, May 2012.

- [13] Naval Sea Systems Command. MIL-DTL-2036E: Naval shipboard enclosures for electric and electronic equipment. Detail Specification, February 2014.
- [14] Naval Sea Systems Command. MIL-DTL-917F: Basic requirements for electronic power equipment. Detail Specification, August 2014.
- [15] Naval Sea Systems Command. MIL-STD-889D: Galvanic compatibility of electrically conductive materials. Standard Practice, July 2021.
- [16] ASM Handbook Committee. Properties of wrought aluminum and aluminum alloys. *ASM Handbook*, 1990.
- [17] C Cooke, C Chryssostomidis, and J Chalfant. Modular integrated power corridor. In 2017 IEEE Electric Ship Technologies Symposium (ESTS), pages 91–95. IEEE, 2017.
- [18] Joseph R Davis et al. Alloying: Understanding the Basics. ASM international, 2001.
- [19] JR Davis et al. Stainless Steels. ASM Specialty Handbook, 1994.
- [20] JR Davis et al. Nickel, Cobalt, and Their Alloys. ASM specialty handbook, 2000.
- [21] JR Davis et al. Copper and Copper Alloys. ASM Specialty Handbook, 2001.
- [22] José del Águila Ferrandis, J Chalfant, C Cooke, and C Chryssostomidis. Design of a power corridor distribution network. In 2019 IEEE Electric Ship Technologies Symposium (ESTS), pages 284–292. IEEE, 2019.
- [23] Christina DiMarino. Navy integrated power electronics building block (iPEBB). In Office of Naval Research iPEBB Program Review, November 2020.
- [24] N Doerry and K McCoy. Next Generation Integrated Power System: NGIPS Technology Development Roadmap. Naval Sea Systems Command, 2007.
- [25] MJ Donachie. Titanium: A Technical Guide. ASM International, 2nd edition, 2000.
- [26] Ulbrich Stainless Steels & Special Metals Inc. Waspaloy®, UNS N07001. https://www.ulbrich.com/uploads/data-sheets/Waspaloy%C2% AE-Wire-UNS-N07001.pdf, accessed: 03.20.2022. Brochure.
- [27] ASTM Interantional. B209M-14 Aluminum and Aluminum-Alloy Sheet and Plate, 2014.
- [28] ASTM International. ASTM E618-07:Standard Test Method for Evaluating Machining Performance of Ferrous Metals Using an Automatic Screw/Bar Machine, 2018.

- [29] ISO. Rectangular or Square Parallel Keys and Their Corresponding Keyways, 1969.
- [30] J G Kaufman. Understanding the aluminum temper designation system. *Introduction to Aluminum Alloys and Tempers*, 2000. ASM International.
- [31] Kent Larson. Can you estimate modulus from durometer hardness for silicones. Dow Corning Corporation, 2016.
- [32] Michael R Lindeburg. Mechanical engineering reference manual for the PE exam. Professional Publications, Inc., 13th edition, 2013.
- [33] MakeItFrom.com. Grade M35-2 (J04020) Cast Nickel. https://www.makeitfrom.com/material-properties/Grade-M35-2-J04020-Cast-Nickel, accessed: 03.20.2022. Brochure.
- [34] S Markle. IPES harnessing total ship energy & power. Sea-Air-Space Exposition, 2018.
- [35] S Markle. Naval power & energy systems: Way forward. 32nd Annual National Symposium, Surface Navy Association, 2020.
- [36] M McCandless, C Cooke, J Chalfant, C Chryssostomidis, A Colavitto, A Vicenzutti, A Contin, and G Sulligoi. Thermal analysis of MVDC power corridor. In 2019 IEEE Electric Ship Technologies Symposium (ESTS), pages 106–112. IEEE, 2019.
- [37] Department of Defence. MIL-STD-1472: General specification for studs, bolts, screws and nuts for applications where a high degree of reliability is required. Detail Specification, December 2000.
- [38] Department of Defence. MIL-DTL-901E: Requirements for shock tests, h.i. (high impact) shipboard machinery, equipment, and systems. Detail Specification, June 2017.
- [39] Department of Defence. MIL-STD-1472: Human factors engineering. Design Criteria Standard, September 2020.
- [40] American Bureau of Shipping. Guide for dynamic loading approach (DLA) for floating production, storage, and offloading (FPSO) installations. Standard, January 2017.
- [41] L Petersen, C Schegan, T Ericsen, D Boroyevich, R Burgos, N Hingorani, M Steurer, J Chalfant, H Ginn, C DiMarino, G Montanari, F Peng, C Chryssostomidis, CM Cooke, and I Cvetkovic. Power electronic power distribution systems (PEPDS). ESRDC Website, www.esrdc.com, 2022.
- [42] Aravamudhan Raman. Materials Selection and Applications in Mechanical Engineering. Industrial Press, 2007.

- [43] Ivan Reyes. Design and modeling of the NiPEC cooling system. Master's thesis, Massachusetts Institute of Technology, Cambridge, MA, 2022.
- [44] Robert H Thurston. A Treatise on Brasses, Bronzes, and Other Alloys, and Their Constituent Metals. John Wiley & Sons, New York, 4th edition, 1913.
- [45] S Timoshenko and S Woinowsky-Krieger. *Theory of Plates and Shells*. McGraw-Hill, New York, 2nd edition, 1962.
- [46] Aircraft Materials UK. Nickel Superalloy Waspaloy. https://www.aircraftmaterials.com/data/nickel/waspaloy.html, accessed: 03.20.2022. Brochure.
- [47] Eduard Ventsel and Theodor Krauthammer. Thin Plates and Shells: Theory, Analysis, and Applications. Marcel Dekker, Inc., New York, 2001.
- [48] W C Young and R G Budynas. *Roark's Formulas for Stress and Strain*. McGraw-Hill Education, New York, 7th edition, 2002.

## Appendix A

## Component Weights

All dimensions are in millimeters.

Table A.1: PEBB Weight

Component	Length (mm)	Width (mm)	Height (mm)	Number	Volume (m <sup>3</sup> )	Density (kg/m³)	Weight (kg)	Force (N)
PEBB Face	-	-	-	-	7.41E-04	2705	2.006	19.7
Top/Bottom	550	300	1.5	2	4.95E-04	-	-	-
Sides	550	100	1.5	2	1.65E-04	-	-	-
Front/Back	300	100	1.5	2	9.00E-05	-	-	-
Corner Overlap	950 *	1.5	1.5	4	-8.55E-06	*Effective length of corner overlap		
PEBB Key	550	4	2	2	8.80E-06	2705	0.024	0.23
PEBB Shell Total	-	-	-	-	7.50E-04	2705	2.029	19.9

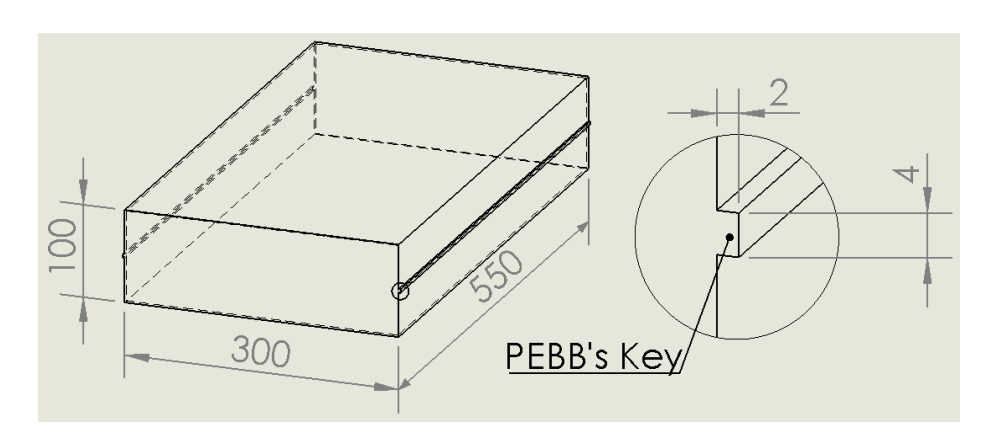


Figure A-1: PEBB Drawing and Dimensions

Table A.2: Cold Plate Weight

Component	Length (mm)	Width (mm)	Height (mm)	Number	Volume (m <sup>3</sup> )	Density (kg/m <sup>3</sup> )	Weight (kg)	Force (N)
Cold Plate	-	-	-	-	8.53E-03	2705	23.08	226.3
Side Beam	643	50.8	76.2	2	4.98E-03	-	-	-
Flow Holes	D = 25.4	A <sub>H</sub> = 506.71	640	4	-1.30E-03	*Height account	s for bends i	n piping
Front Beam	402	50.8	76.2	1	1.56E-03	-	-	-
Flow Holes	D = 25.4	A <sub>H</sub> = 506.71	380	2	-3.85E-04	*Height accounts for bends in piping		
Plate	550	300	25.4	1	4.19E-03	-	-	-
Flow Holes	D = 9.525	A <sub>H</sub> = 71.26	300	42	-8.98E-04	-	-	-
Back Collars	85.54	60	23	3	3.54E-04	4 *Length accounts for rounded edges		d edges
Hinge Hole	D = 14	A <sub>H</sub> = 153.94	60	3	-2.77E-05	-	-	-
Front Collars	50	23	24	3	8.28E-05	-	-	-
Hinge Hole	D = 14	A <sub>H</sub> = 153.94	50	3	-2.31E-05	-	-	-

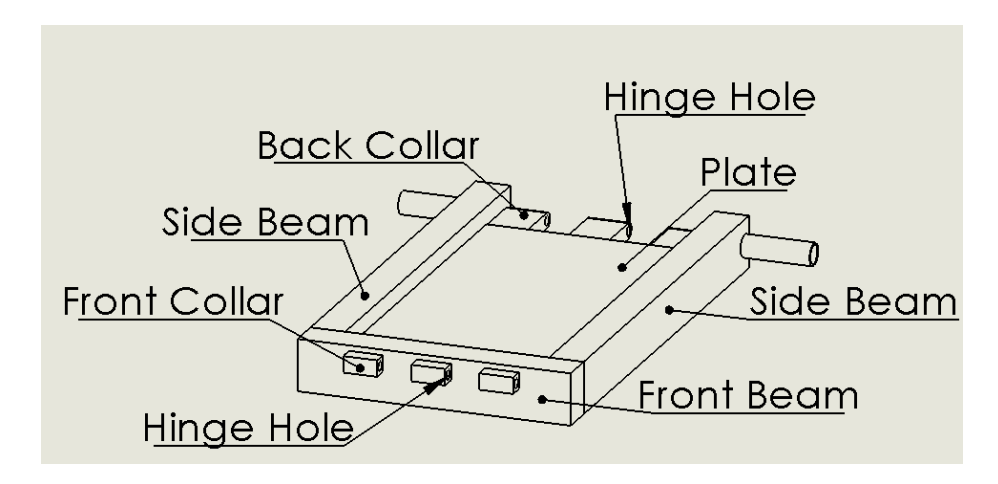


Figure A-2: Cold Plate Drawing

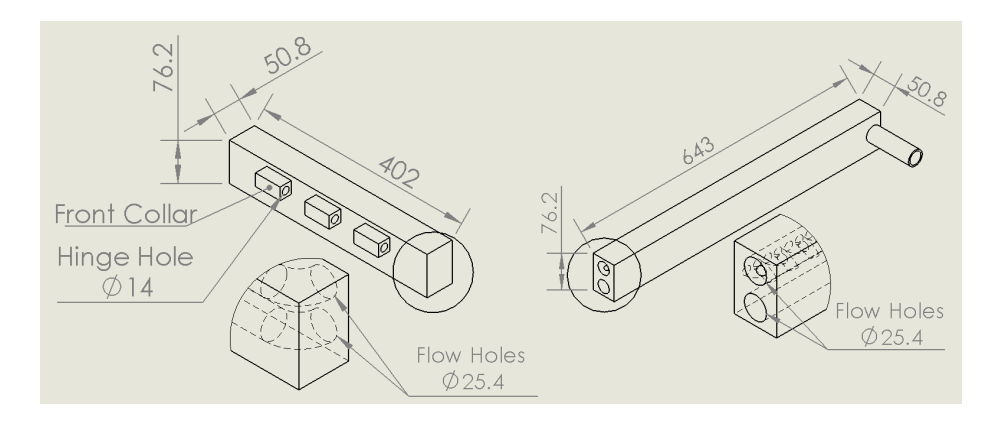


Figure A-3: Front and Side Beam Drawings and Dimensions

Table A.3: Thermal Pad Weight

Component	Length (mm)	Width (mm)	Height (mm)	Number	Volume (m³)	Density (kg/m³)	Weight (kg)	Force (N)
Thermal Pad	537.3	300	2	1	3.22E-04	3500	1.13	11.1

Table A.4: Elbow Bracket Weight

Component	Diameter (mm)	Area (mm²)	Depth (mm)	Volume (m <sup>3</sup> )	Density (kg/m³)	Weight (kg)	Force (N)
Elbow Bracket	-	-	-	1.00E-04	2705	0.27082	2.7
Side Surface Area	-	2230.2*	50	1.12E-04	*Side Surface Ar	ea	-
Bolt Hole	14	A <sub>H</sub> = 153.49	24	-3.69E-06	-	-	-
Hinge Hole	14	A <sub>H</sub> = 153.94	50	-7.70E-06	-	-	-

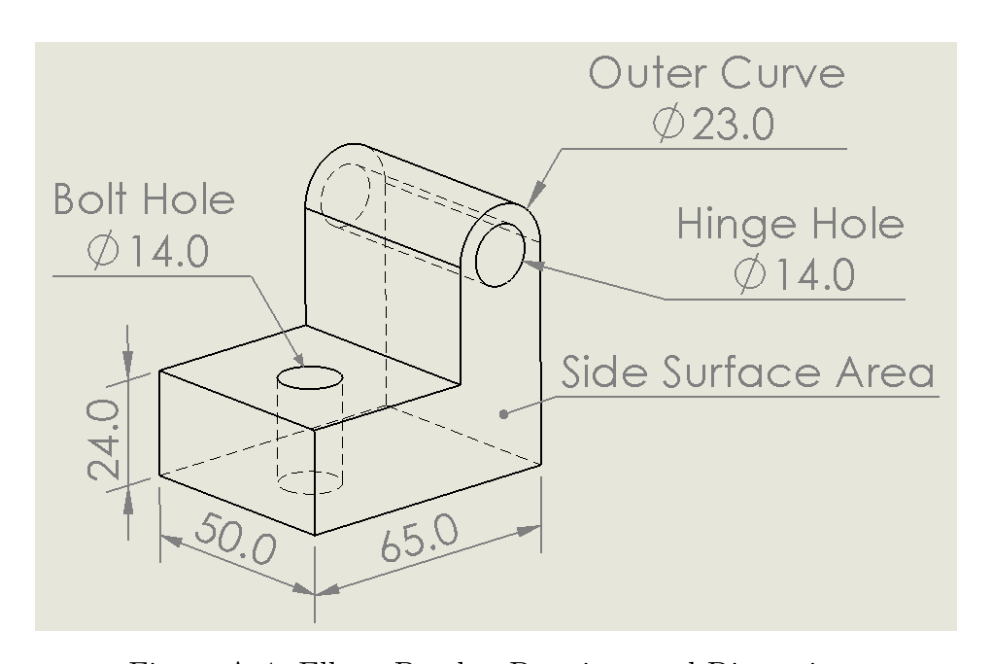


Figure A-4: Elbow Bracket Drawings and Dimensions

## Appendix B

### SolidWorks Analysis

This Appendix contains all of the SolidWorks analysis and figures. As with all computer aided analyses, the possible sources of error include human and machine factor. In this case, the large sources of error are: selecting the mesh size, simulation errors (translation occurs when no translation present), and simulation input errors (incorrect fixtures made).

#### B.1 Cold Plate

For the deflection and stress analysis of the cold plate, three method were used. for all three methods, the same material, aluminum alloy 1060, was applied to SolidWorks model.

#### B.1.1 Cold Plate - Static Loading

The first method took the 3-D cold plate and applied 10 psi to the top face. It was held in place by edges that were supported to resist only the downward pressure. This resulted in a maximum stress of  $\sigma_{CP1,max} = 9.66MPa$  and deflection of  $y_{CP1,max} = 1.902mm$ . The deflection is misleading as the plate slid horizontally in this analysis more than it deflected vertically. This doesn't make sense and seems to be an error with the way in which the analysis was performed. To correct this issue,

the edges were fixed in an additional direction such that the cold plate would only deflect vertically. This worked with the following results:  $\sigma_{CP1,max} = 8.96MPa$  and  $y_{CP1,max} = 0.05923mm$ . Fig B-1 below show this result.

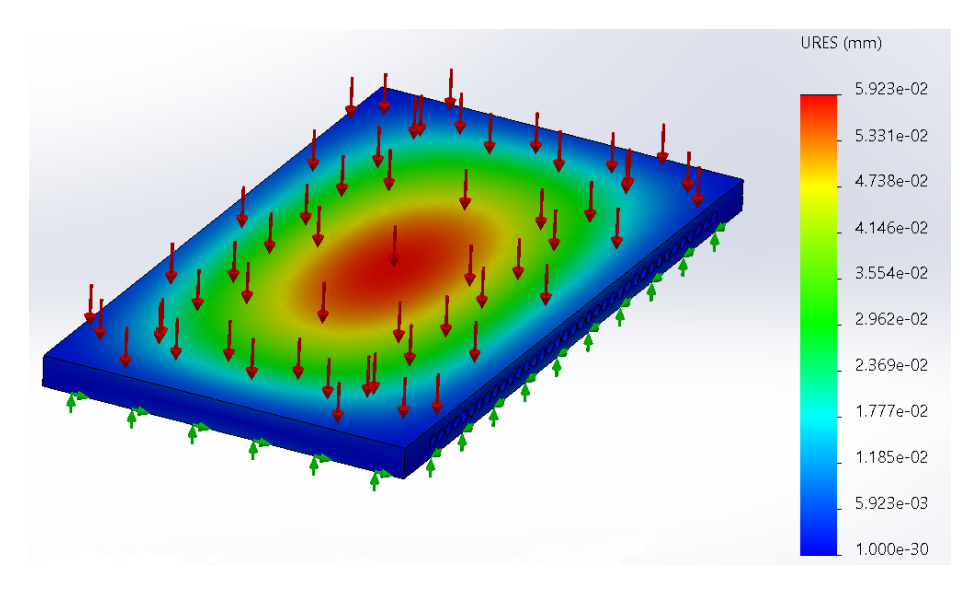


Figure B-1: SoldWorks Simulation Analysis of Cold Plate Deflection

The second method was to label the cold plate as a shell with corrected edge constraints and run the analysis. This produced  $\sigma_{CP2,max} = 8.92MPa$  and  $y_{CP2,max} = 0.060mm$ . from these two analyses, it appears that there is not a significant difference between these two methods for this loading configuration and magnitude. Additionally, the result from these analyses were both much higher than the expected values from Navier and Roark's Formulas.

SolidWorks is compliant with the International Association for the Engineering Modelling, Analysis and Simulation Community (NAFEMS) and provides verification to show that the results gathered from SolidWorks Simulation are accurate for select circumstances. The accuracy is comparing the SolidWorks studies to known analytical solutions. SolidWorks allows the user to download the model and run the simulation on their own personal machine. Thus after identifying the template that matched this cold plate analysis, the template was selected, analyzed, and modified to fit the dimension and parameters of this scenario. While modifying the template, two main difference were noticed. First, due to double symmetry, only a quarter of plate was modeled such that two of the sides were edges and the other two sides were cut

from the middle. This led to the middle edges resisting horizontal translation and moments but critically not being fixed in the vertical direction. Second, the template was shown as flat sheet but given the thickness in the shell manager section. This template file was validated for deflection against formulas from [45] and matched to 5 significant figures. The results from this test were  $\sigma_{CP3,max} = 4.842MPa$  and  $y_{CP2,max} = 0.04996mm$ . These were more inline with the results seen from Navier's Method and Roark's Formulas. Fig B-2 shows the deflection as modeled on the flat plate as a shell.

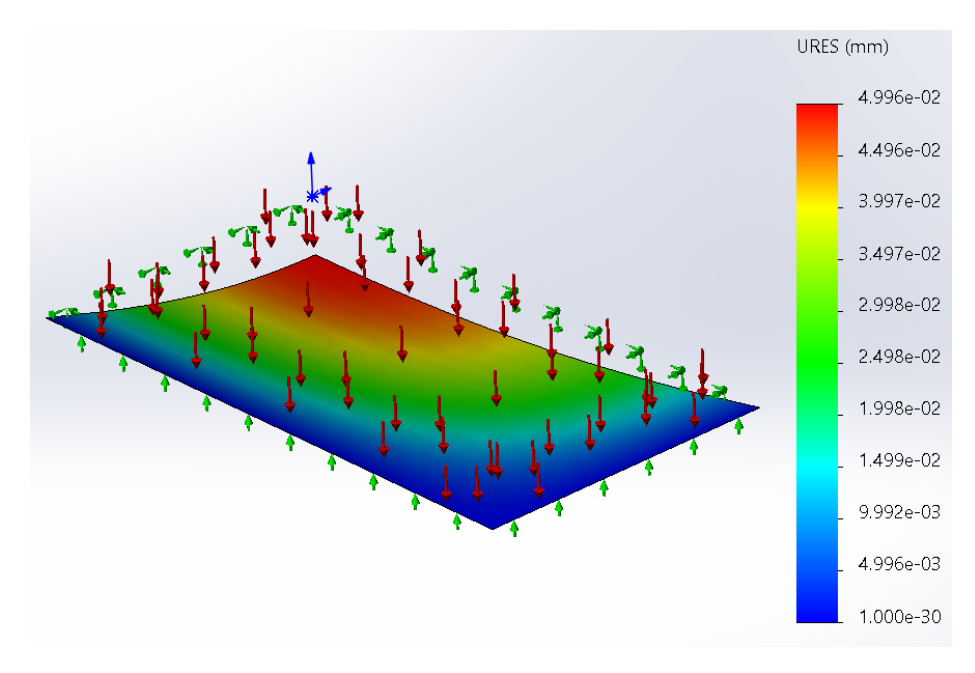


Figure B-2: SoldWorks Simulation Verification Analysis of Cold Plate Deflection for Static Loading

#### B.1.2 Cold Plate - Dynamic Loading

For the dynamic loading on the cold plate, the third method from Section B.1.1 was the only method used. It was configured in the same method as the static loading for the dimensions. The pressure was increased from the addition of the dynamic force, applied over the cold plate's top face. The total pressure was increased to 10.35 psi (71,342 Pa). The results from this test were  $\sigma_{CP,dyn,max} = 5.011MPa$  and  $y_{CP,dyn,max} = 0.05171mm$ . Fig B-3 shows the SolidWorks Simulation results for the

maximum stress.

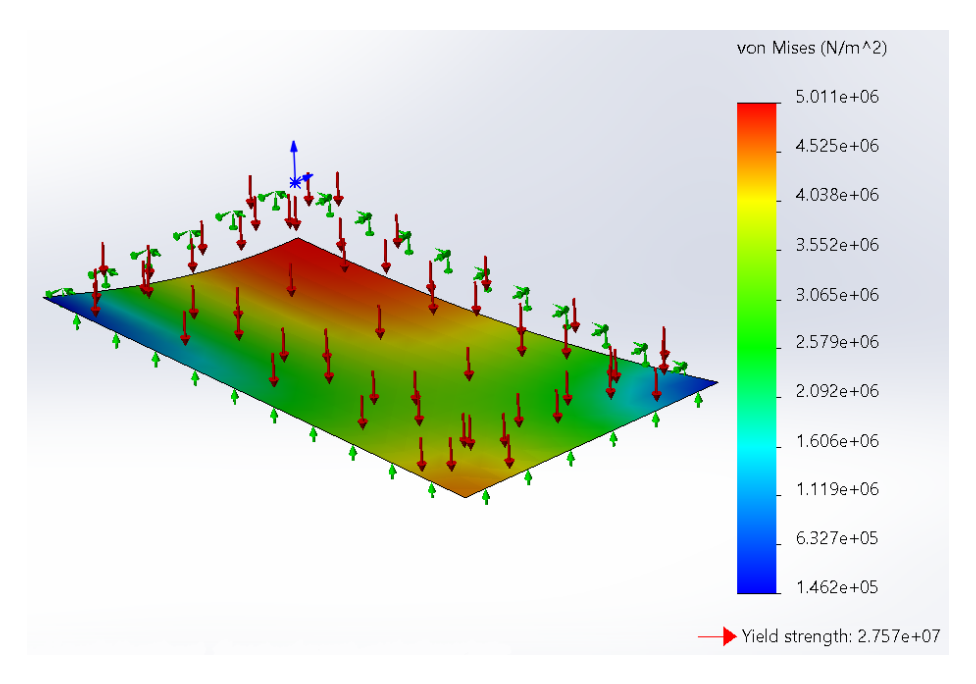


Figure B-3: SoildWorks Simulation Verification Analysis of Cold Plate Stress with Dynamic Loading

#### B.2 PEBB Shell - Side Face

In the case of side plate buckling, there was no template in the verification toolbox to use as the base for this analysis. Following the path from the cold plate analysis, the side plate was sectioned off due to symmetry. In this case since the loads were applied on the top and bottom edges, those edges remained and the plate was cut in half. Thus, the dimensions of the plate analysed was 275x100 mm. From Fig B-4, the top and bottom (where force was a applied) were simply supported. The left side (edge) was fixed. The right side (cut by symmetry) resisted translation vertically.

From the analysis performed in Section 2.4.2, the longer side plates were more susceptible to buckling that front and back plates. Expecting similar trends from the SolidWorks analysis, the front and back plates (300x100 mm) were not analysed. The results from these analyses are show below.

#### B.2.1 Side Face - Static Loading

For Static loading, the load on each of the edges was 6.870  $\frac{N}{mm}$ . As shown in Fig. B.2.1, the maximum amplitude occurs in the center as expected. The SolidWorks analysis did have the edge load along the the tip and bottom sections, which may be missed just by looking at Fig. B.2.1. The Load Factor/ $FOS_{buckling} = 4.0276$ .

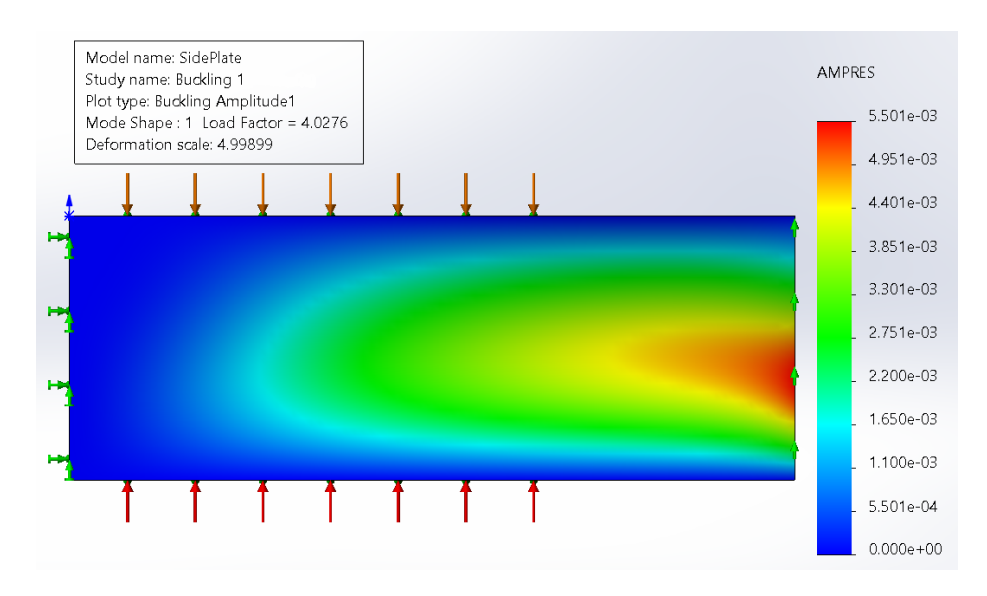


Figure B-4: SoildWorks Simulation Analysis of Side Plate Buckling with Static Loading

#### B.2.2 Side Face - Dynamic Loading

For dynamic loading, the load on each of the edges was 7.134  $\frac{N}{mm}$ . As shown in Fig. B-5, the maximum amplitude occurs in the center as expected. The Load Factor/ $FOS_{buckling} = 3.884$ .

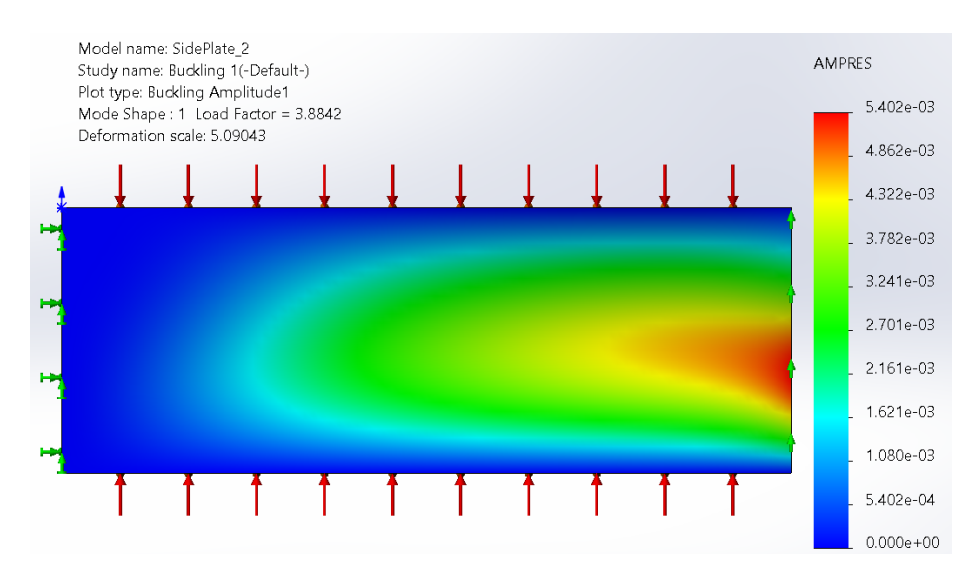


Figure B-5: SoildWorks Simulation Analysis of Side Plate Buckling with Dynamic Loading

# Appendix C

 $\eta\,$  Factor of Safety (FOS)

**p** Pitch

## List of Variables Used

$\sigma$ Nominal Normal Stress			
$\sigma_B$ Bearing Stress			
$\sigma_b$ Root Bending Stress			
$\sigma^{'}$ Von Misses Stress			
$\sigma_{1,2,or3}$ Principle Stresses			
$\sigma_{proof}$ Proof Strength			
$\sigma_{ut}$ Tensile Strength			
$\sigma_{yield}$ Yield Strength			
au Shear Stress			
$\tau_{max}$ Maximum Shear Stress			
$T_L$ Torque to Loosen			
$T_T$ Torque to Tighten/Tension			

t Thickness

v Poisson's Ratio

### Appendix D

### Calculations Performed

#### D.1 PEBB Shell - Roark's Formulas

The following calculations were performed per Roark's Formulas for Stress and Strain [48]. These formulas are the tabulated results based off of reputable analytical analysis and experimental data to serve as a quick reference for calculations and as a check for finite element analysis. These formulas are made to be simple and accurate.

#### D.1.1 Cold Plate - Stress and Deflection

The first case analyzed by Roark's Formulas is the stress and deformation of the cold plate when the compressive force is applied. Similar to the analysis performed in Section 2.4.2, all side were assumed to be simply supported, the compressive force was assumed to be uniformly distribute over the entire plate, and similar values for plate dimensions and force magnitude. From Fig D-1, a = 550 mm and b = 300 mm. The plate was loaded to 10 psi or  $0.0689 \frac{N}{mm^2}$ .

The following assumptions were made when using Roark's Formulas for plate bending:

- The plate is flat, of uniform thickness, and of homogeneous isotropic material.
- The thickness is not more than one-quarter of the least transverse dimensions and maximum deflection is not more than about one-half the thickness.

- All forces are note to the plate of the plate.
- The plate is not stressed beyond the elastic limit.
- The plate deflects and the middle surface remains unstressed.

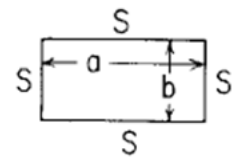


Figure D-1: Simply Supported Plate With Uniform Loading [48]

The formulas for the maximum stress and deflection are given below in Eqns D.1 and D.2. This resulted in the maximum deflection and stress in the middle of the cold plate with the associated values:

$$y_{max} = \frac{-\alpha q b^4}{Et^3} = \frac{-(0.1033)(0.0689 \frac{N}{mm^2})(300mm)^4}{(69 \frac{KN}{mm^2})(25.4mm)^4} = -0.052mm$$
 (D.1)

$$\sigma_{max} = \frac{\beta q b^2}{t^2} = \frac{(0.5757)(0.0689 \frac{N}{mm^2})(300)^2}{(25.4mm)^2} = 5.60 \frac{N}{mm^2}$$
(D.2)

The deflection is negative due to the direction, downward. The values for  $\alpha$  and  $\beta$  are shown in Table D.1. They are based on the ratio of the plate's length to width (a/b) = 1.83. Actual values, obtained by interpolation, were  $\alpha = 0.1033$  and  $\beta = 0.5757$ 

$$\begin{array}{c|cccc} a/b & 1.8 & 2 \\ \hline \beta & 0.5688 & 0.6102 \\ \alpha & 0.1017 & 0.1110 \\ \end{array}$$

Table D.1:  $\alpha$  and  $\beta$  Factors Based on  $\frac{a}{b}$  Ratio

#### D.1.2 PEBB's Shell Sidewall - Buckling

The second case analyzed by Roark's Formulas is the buckling of the side of the PEBB's Shell. This analysis provide the critical unit component stress  $\sigma'$ . Meaning

that the value of  $\sigma'$  is the smallest stress at which buckling begins. To prevent buckling, the stress on the rectangular section must be less than  $\sigma'$ .

This is similar to the analysis performed in Section 2.4.2. The variables a and b are the plate dimensions shown in Figure 2-14. This case is applied to both the front and the sides of the PEBB. This means that there are two different sized plates to analyse and in both cases, a=100mm. For the side plates  $b_{side}=550mm$  and for the front and back plates,  $b_{front}=300mm$ . The uniform loading, given by  $q_x$ , is the same as before,  $q_x=6.83\frac{N}{mm}$ .

Formula for critical stress is:

$$\sigma' = K \frac{E}{1 - v^2} \left(\frac{t}{b}\right)^2 \tag{D.3}$$

Where, the variable are defined in Appendix C

The critical stress for the side plates are:

$$\sigma'_{side} = K_{side} \frac{E}{1 - v^2} \left(\frac{t}{b_{side}}\right)^2 = (22.2) \frac{68.9 \frac{KN}{mm^2}}{1 - 0.3^2} \left(\frac{1.5mm}{550mm}\right)^2 = 12.5MPa$$
 (D.4)

Based on this critical component stresses, the Factor of Safety for buckling is  $FOS_{side} = 1.83$ .

The critical stress for the front and back plates are:

$$\sigma'_{front} = K_{front} \frac{E}{1 - v^2} \left(\frac{t}{b_{side}}\right)^2 = (22.2) \frac{68.9 \frac{KN}{mm^2}}{1 - 0.3^2} \left(\frac{1.5mm}{300mm}\right)^2 = 18.1 MPa \quad (D.5)$$

Based on this critical component stresses, the Factor of Safety for buckling is  $FOS_{front} = 2.63$ .

The values for  $K_{side}$  and  $K_{front}$  are shown in Table D.1. They are based on the ratio of the plate's length to width (a/b). For the front and back plates, the ratio  $a/b_{side} = \frac{100mm}{300mm} = 0.33$  thus the value used for constant,  $K_{front}$  was obtained by interpolation,  $K_{front} = 9.57$ . The associated factor of safety for the front and side plates is  $FOS_{buckling} = 2.63$ 

For the side plates, the ratio  $a/b_{side} = \frac{100mm}{550mm} = 0.18$  so the value used for constant,

 $K_{side} = 22.2$ . Since the actual value can not be interpolated from Table D.2, the result from this analysis cannot be trusted. There is not a correct method to conduct this analysis without performing additional experiments to bound the a/b ratio. Using the K value associated with the smallest a/b ratio, the result is a lower than actual critical unit component stress. Meaning, this is a source of error and the result is not to be trusted. Acknowledging this error and using this value ( $K_{side} = 22.2$ ), the critical unit component stress was found to be  $q_x = 12.5MPa$  and with the factor of Safety was  $FOS_{buckling} = 1.82$ .

$$\begin{array}{c|ccccc} a/b & 0.2 & 0.3 & 0.4 \\ \hline K & 22.2 & 10.9 & 6.92 \\ \end{array}$$

Table D.2: K Value Based on  $\frac{a}{b}$  Ratio [48]

#### D.2 Dynamic Loading

The following is the calculations performed to find the dynamic loading on PEBB. The characteristics of ship are given in Table 2.2. Using the notional ship characteristics and the tables in DOD-STD-1399 Sec 301, the notional ship motions were found in tables or calculated. For example, Max Roll Angle,  $\phi$ , is from Table II, Max Pitch Angle,  $\theta$ , is from Table III, and the Surge and Heave Acceleration, h and s respectively, are from Table IV [11]. The roll period,  $T_r$ , is determined from the ship's beam, B, roll constant, C, and Metacentric Height, GM.

$$T_r = \frac{C \cdot B}{GM^{1/2}} \tag{D.6}$$

Finally, the last missing link is the distances from the notional ship's center of gravity (X, Y, Z) along their respective axis. These values are approximations and based solely on the notional ship design. It was assumed that the distance from the center of gravity to the forward most power corridor would have the largest accelerations. The center of gravity was assumed to be located in the middle of ship in the x- and y-directions due to symmetry. and one deck below the water line in

Table D.3: Notional Ship Motion Characteristics

Constants	Symbol	Value	Units
Roll Period	$T_r$	16.4	sec
Max Roll Angle	φ	34	degrees
Pitch Period	$T_P$	7	sec
Max Pitch Angle	$\theta$	6	degrees
Heave Acceleration	h	0.4	g
Surge Acceleration	s	0.25	g
Gravity	g	9.807	$m/sec^2$

the z-direction. For the x-direction, half of the notional ships LBP, is 92m and it was assumed that the forward most compartment would take up 15m. Thus, the distance in the x-direction is X = 75m. In the y-direction, half of the notional ship's beam is 12m. From there an additional 1.5m is subtracted due to curvature of the hull. Thus, the distance in the y-direction is Y = 10.5m. Each level was assumed to be three meters high thus for the z-direction, it was assumed to be Z = 5m above the center of gravity.

The Equations for the loading factors are given by Eqns 2.26 - 2.27 and recreated below in Table D.4.

The loading factors are as shown in Table D.4.

Table D.4: Loading Factors in the Principle Directions

The components of the design load was determined by using Eqn 2.28. For this dynamic load analysis, the weight of the structure was assumed to be 16 kg, the weight of the PEBB. The numerical results are detailed in the table D.5.

The magnitude of the total design load is given by Eqn 2.29 and show in detail

Table D.5: Design Load in Principle Directions

$$F_{x} = \frac{W}{G} \cdot A_{x}$$

$$F_{x} = 16 \cdot 4.561 = 72.97 \text{ N}$$

$$F_{y} = \frac{W}{G} \cdot A_{y}$$

$$F_{y} = 16 \cdot 9.622 = 154.0 \text{ N}$$

$$F_{z} = \frac{W}{G} \cdot A_{z}$$

$$F_{z} = 16 \cdot 20.97 = 335.5 \text{ N}$$

below:

$$F_{tot} = ((72.97)^2 + (154.0)^2 + (335.5)^2)^{1/2} = 376.3N$$
 (D.7)

### Appendix E

### MATLAB Code

#### E.1 PEBB Shell - Top Plate - Navier Solution

```
%% Start — Top Plate
    clc %Clear all text from the Command Window.
    clear %Clear all variables from the work space.
    % Sources:
 6
    % (1) Thin Plates and Shells: Theory, Analysis, and Applications by Krauthammer and Ventsel
    % (2) Shigley's Mechanical Engineering Design by Budynas and Nisbett
    % [3] Properties of Wrought Aluminum and Aluminum Alloys from ASM Handbook,
9
    % Vol 2: Properties and Selection: Nonferrous Alloys and Special—Purpose Materials
    % Assumptions
12
    % Material: Aluminum (modulus of elasticity [3], poisson ratio [3])
    % Sides: Simply Supported
14
    % Units: cm
    % Kirchoff's assumptions are valid:
    % —Material is elastic, homogeneous, and isotropic
17
    % —Plate is initally flat
   % —Small deflection (w/h < 10)
18
    % —Vertical shear strains are negligible and normal strain may be omitted
19
20
    % —Stress normal to midplane is negligble
    \mbox{\ensuremath{\$}}\mbox{-Middle} surface is unstrained after bending
    % Thin plate (a/h = 10-80)
24
   % Constants
    a = 55; % Plate lenght in dir of x—axis (cm)
    u = 55; % Length of applied pressure area in dir of x—axis (cm)
    s = 27.5; % Distance from orgin to center of pressure area in dir of x—axis (cm)
```

```
b = 30; % Plate lenght in dir of y—axis (cm)
2.8
29
             % Length of applie pressure area in dir of y—axis (cm)
    nc = 15; % Distance from orgin to center of pressure area in dir of y—axis (cm)
30
    h = 2.54; % Thikness (cm)
    E = 69*(10^5); % Modulous of Elasticity (N/cm^2)
    nn = .333; % Poisson Ratio
    D = E*(h^3)/(12*(1 - (nn^2))); % Flexural Regidity of Plate (N-cm)
34
    m = 1; n = 1; % Set at 1 for maximum deflection
36
    po = 6.89474 ;% Force (per area; N/cm2) applied to center (10psi)
    %% Deflection
38
39
    w = zeros(a,b); %makes a x b zero matrix
40
    for y = 1:b % number of columns; y—axis. y = loop counter progresses through values 1 to b
        for x = 1:a %specifies the row; x—axis
41
            for i = 1:m
42
                for j = 1:n
44
            w(x,y) = \sin(i*pi()*s/a)*\sin(j*pi()*nc/b)*\sin(i*pi()*u/(2*a))* ...
45
                sin(j*pi()*v/(2*b))*sin(i*pi()*x/a)*sin(j*pi()*y/b)/ ...
                ((i*j)*(((i/a)^2 + (j/b)^2)^2)); %operation for ENTIRE RANGE of components
47
48
            end
49
        end
    end
    w = w .* (-16*po/(pi()^6 * D));
52
    % Plot
    surfl(w);
    %% Results
56
    % Accepttable deflection?
57
    wmax = abs(min(w, [], 'all'));
    % Small Deflection (w/h < 10)
58
59
    defl = wmax/h;
    fprintf('The maximum deflection is: %5.4f cm\n',wmax);
61
    if defl < 10
        disp("Small Deflection assumption is valid");
63
        fprintf('The deflection to thickness ratio is: %f\n',defl);
    else
65
        disp("Small Deflection assumption not met");
    end
66
```

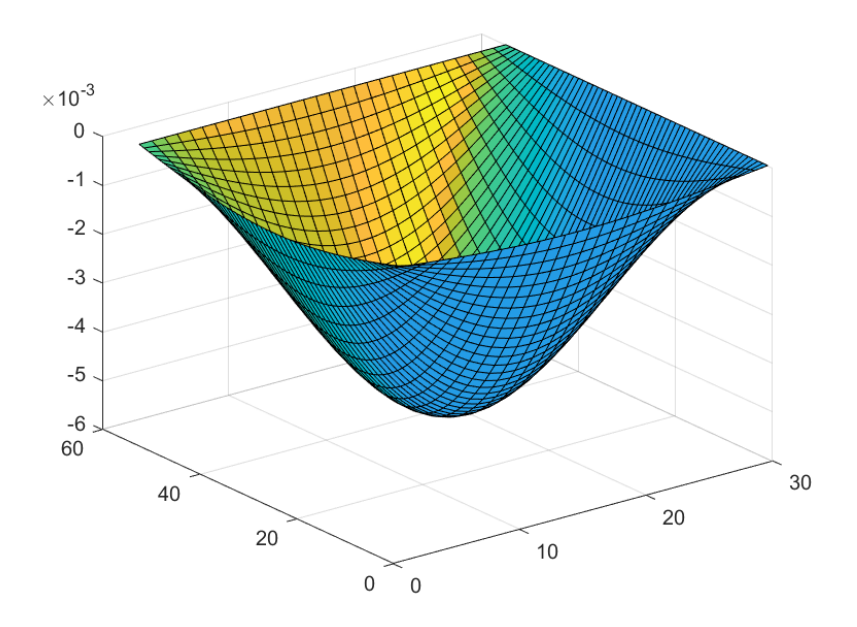


Figure E-1: MATLAB Generated Deflection for Cold Plate (in cm)

### E.2 PEBB Shell - Side Plate - Equilibrium Method

```
%% Start — Side Plates
    clc %Clear all text from the Command Window.
    clear %Clear all variables from the work space.
 5
 6
    st [1] Thin Plates and Shells: Theory, Analysis, and Applications by Krauthammer and Ventsel
    % [2] Shigley's Mechanical Engineering Design by Budynas and Nisbett
    % [3] Properties of Wrought Aluminum and Aluminum Alloys from ASM Handbook,
    % Vol 2: Properties and Selection: Nonferrous Alloys and Special—Purpose Materials
9
11
    %% Assumptions
    % Material: Aluminum 1060 (modulus of elasticity [3], poisson ratio [3])
12
    % Sides: Simply Supported
14
    % Units: mm
    % Thin plate (a/h = 10-80)
16
    % Linear Buckling
17
    \%- Plate is initially flat and loads applied at midplane
    \%- No change in plate dimensions prior to buckling
19
    \$- All loads applied are dead loads (not dynamic)
20
    \%- Kirchoff's plate bending assumptions are true
    % Equilibrium Method
    % Edge loaded uniformly
22
23
```

```
% Constants
24
25
    a = 100;
               % Plate height (mm)
              % Plate length (mm)
    b = 550;
27
    c = 300;
              % Plate width (mm)
28
    m = 1:
               % For smallest critical load
    kb = (((m*b)/a)+(a/(m*b)))^2; % Side Plate Buckling parameter
30
    kc = (((m*c)/a)+(a/(m*c)))^2; % Front and Back Plates Buckling parameter
    h = 1.5;
                 % Thickness (mm)
32
    E = 69000; % Modulus of Elasticity (N/mm2)
    nn = .333; % Poisson Ratio
    D = E*(h^3)/(12*(1 - (nn^2))); % Flexural Rigidity of Plate (N-mm)
34
    p = 0.06895; % Pressure applied for clamping (10 psi in N/mm2)
36
    area = 165000; % Applied to top of PEBB 550x300 (mm2)
    F_w = 236; % Weight of cold plate and thermal pad (N)
    F_dyn = 395; % Worst case dynamic loading (N)
38
    F_G = p*area;
40
    qx = (F_G + F_w + F_dyn)/((2*b)+(2*c)); % Assumes load uniformly applied to entire edge of top plate (N/mm
    Ny = 0; % Only loaded vertically
41
    Nxy = 0; % Only loaded vertically
42
44
    %% Buckling
45
    qxminb = kb*(pi^2)*D/(b^2*h); %Eqn 8.19 [1]
    FOS_b = qxminb/qx; % Computes Factor of Safety for buckling for Side Plate
47
48
    qxminc = kc*(pi^2)*D/(c^2*h); %Eqn 8.19 [1]
    FOS_c = qxminc/qx; % Computes Factor of Safety for buckling for Front and Back Plates
    % Results
52
    % Side Plate Results
    if qxminb > qx
        disp("Applied load will not cause bucking in the side plates");
        fprintf('The Buckling Factor of Safety is: %3.2f\n',FOS_b);
    else
56
        disp("Applied load will cause bucking in the side plates");
58
    end
    % Front and Back Plate Results
61
    if qxminc > qx
        disp("Applied load will not cause bucking in the front and back plates");
        fprintf('The Buckling Factor of Safety is: %3.2f\n',FOS_c);
    else
        disp("Applied load will cause bucking in the front and back plates");
65
    end
```

### Appendix F

### Elbow Analysis

This appendix provide in-depth calculations for the deflection and strains on the elbow bracket. The elbow bracket is shown in Fig 3-7. Similarly to Section 3.2.3, this appendix is broken up into two section based on the holed that the stress is being applied. The analysis of the bolt hole is first followed by the analysis of the front hinge hole. The force used for the analysis was a combination of the static securing force and the dynamic loading. Finding this force is detailed in Section 3.2.2.

#### F.1 Bolt Hole

When analysing the deflection and stresses from the bolt hole, the following assumptions were made:

- 1.  $\overline{JK}$  would act like a rigid wall
- 2. The distributed force from the bolt would as a point load
- 3. The space between the elbow bracket and the collars providing support will be minimal

Assumption #1 simplified the analysis to be similar to a cantilever beam. This model is shown in Fig F-1a. The length of  $\overline{HJ}=34mm$ . The bolt placed in the middle at point J ( $\overline{HI}=17mm$ ).

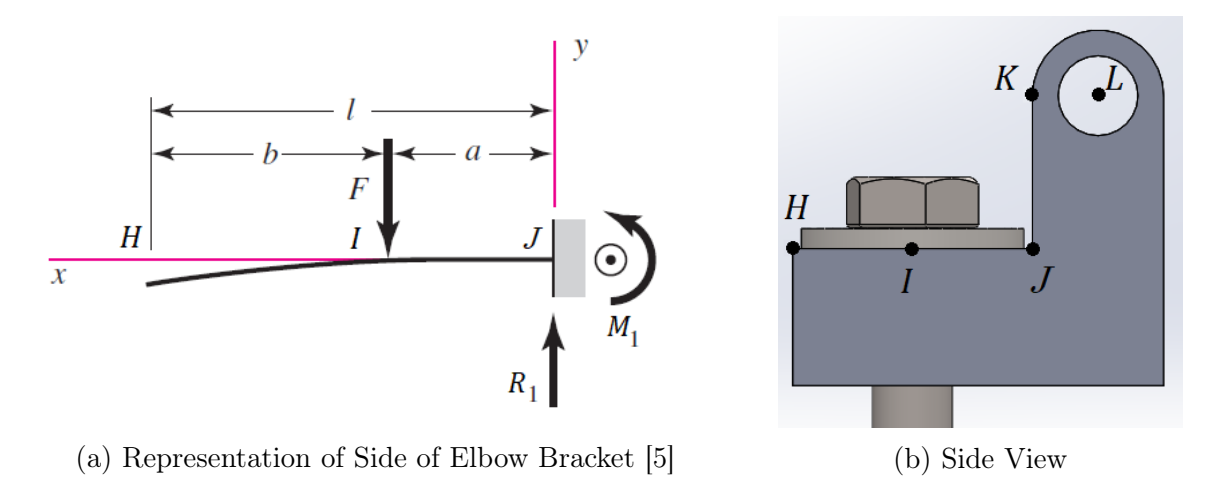


Figure F-1: Representation of Elbow for Bolt Hole Analysis

Table F.1 show the key variables and constants that were used in the elbow analysis. The depth and height are shown in Fig 3-7b. The allowable shear stress is commonly found using the formula  $\tau_{allow} = (0.67) \cdot S_{ut} = 46.23 MPa$  [5]. This was not used as the value of shear stress was found in Ref [16].

Table F.1: Key Values for Elbow Analysis

Variable	Value	Units
$\overline{HI}$	17	mm
$\overline{IJ}$	17	mm
$\overline{JK}$	34	mm
$\overline{KL}$	11.5	mm
Diameter of Front Hinge Hole, $d_{HH}$	14	mm
Depth, $b$	50	mm
Height, h	24	mm
Modulus of Elasticity, $E$	69	GPa
Tensile Strength, $S_{ut}$	69	MPa
Yield Stress $\sigma_{yield}$	28	MPa
Allowable Shear Stress, $\tau_{allow}$	48	MPa

#### F.1.1 Bolt Hole - Deflection

The deflection of a cantilever was found using the following equations from [5] The loading per side of the cold plate was found to be 6123N. From Assumption #7 in Section 3.2, there were to be two elbow brackets per side, thus the applied force from

the bolt, F, was 3062N. The second moment of area, I, was found using the following equation:

$$I = \frac{bh^3}{12} = \frac{(50mm) \cdot (24mm)^3}{12} = 57.6x(10^3)mm^4$$
 (F.1)

The deflection at point F, x = a = 17mm, at the center of the bolt was found to be:

$$y_{\overline{IJ}} = \frac{Fx^2}{6EI}(x - 3a) = \frac{(3062N)(17mm)^2}{6(69GPa)(I)}(-2 \cdot 17mm) = -1.26x(10^{-3})mm \quad (F.2)$$

The max deflection at the end of the cantilever, point H, was found to be:

$$y_{max} = \frac{Fa^2}{6EI} (a - 3l) = \frac{(3062N)(17mm)^2}{6(69GPa)(I)} (-5 \cdot 17mm) = -3.15x(10^{-3})mm \quad (F.3)$$

From these calculations, the deflection of the elbow brackets is essentially zero fort his force. This is good news at this means that the clearance on either side of the bolts will not be effected by the deflection.

#### F.1.2 Bolt Hole - Stress

The two stresses considered are bending and shear stress. It was expected that bending would be more than shear stress.

First, for bending stress, the bending moment was found in a similar manner to Eqn 2.7:

$$M_{bending} = F \cdot \overline{IJ} = (3062N) \cdot (17mm) = 52.0kN - mm \tag{F.4}$$

Plugging this into the the formula for bending stress (Eqn 2.8) where  $c = \frac{h}{2} = 12mm$ :

$$\sigma_{bending} = \frac{M_{bending} \cdot c}{I} = \frac{(52.0kN - mm)(12mm)}{57.6x(10^3)mm^4} = 10.84MPa$$
 (F.5)

From Table F.1, the yield stress is  $\sigma_{yield} = 28MPa$ . Thus the Factor of safety for

bending is:

$$\eta_{bending} = \frac{\sigma_{yield}}{\sigma_{bending}} = \frac{28MPa}{10.84MPa} = 2.58$$
(F.6)

For shear stress, the shear force, V, is the same as the force from the bolt. The area resisting the shearing force is  $A_{shear} = b \cdot h = 50mm \cdot 24mm = 1200mm^2$ . The calculation for the shear stress is as follows:

$$\tau_{shear} = \frac{ShearForce, V}{ShearArea, A_{shear}} = \frac{3062N}{1200mm^2} = 2.55MPa$$
 (F.7)

As mentioned above, the allowable shear stress is  $\tau_{allow} = 48MPa$  [16]. Thus the factor of safety for shear stress is:

$$\eta_{shear} = \frac{\tau_{allow}}{\tau_{shear}} = \frac{48MPa}{2.55MPa} = 18.8 \tag{F.8}$$

From this analysis of the bolt hole, it appears that the elbow bracket is built sufficiently to withstand the applied bending and shear stresses.

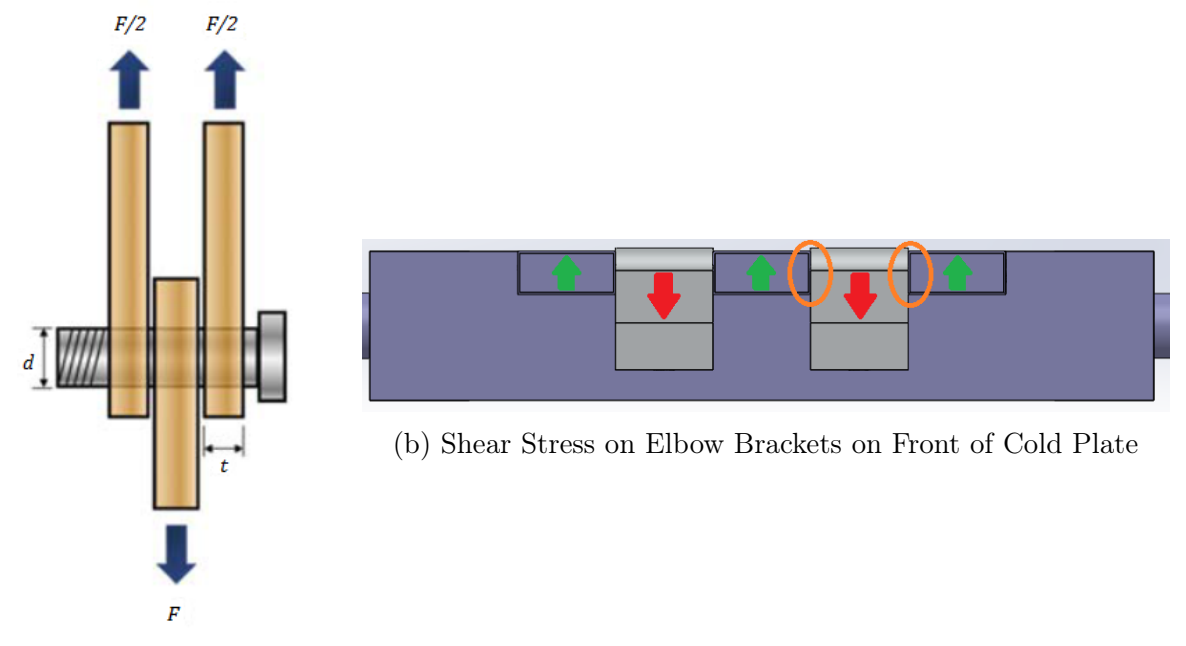
#### F.2 Front Hinge Hole

The concerns with the front hinge hole is stress from shear, tension, and bearing. For each of these stresses there will be an associated picture to reference for clarification. All equations are from Ref [32].

#### F.2.1 Front Hinge Hole - Shear Stresses

For the shear stress on the bolt, each elbow will have one supporting collar on either side. This situation resembles the double shear scenario as show in Fig F-2b. The areas of shear are highlighted in orange for the right elbow bracket.

As previously discussed the force applied but the bolt on a single elbow was  $F = 3{,}062N$ . This was used as the shear force. In a double shear application, the



(a) Double Shear of a Bolt [6]

Figure F-2: Shear Stress on Front Hinge Hole

area being sheared,  $A_s=\pi \frac{d_{HH}^2}{4}$  is doubled. The formula for the shear stress is:

$$\tau = \frac{f}{2A_s} = \frac{3,062N}{2(\pi^{\frac{14^2}{4}})} = 19.9MPa \tag{F.9}$$

The Allowable Shear Stress from Table F.1 is 48MPa. The resulting shear Factor of Safety  $\eta_{shear}$  is:

$$\eta_{shear} = \frac{48MPa}{19.9MPa} = 2.41$$
(F.10)

#### F.2.2 Front Hinge Hole - Tension Stresses

While the front hinge hole is vital, its presence does reduce the material that is able to protect again failure due to tension. The cross-section area is shown in Fig It is assumed that the tension that would be puling the elbow bracket apart is uniformly distributed on the cross-sectional area. The cross-sectional area  $A_t$  is shown below:

$$A_t = b(w - d_{HH}) = (50mm)(23mm - 14mm) = 450mm^2$$
 (F.11)

Where all of the variables are per Table F.1.

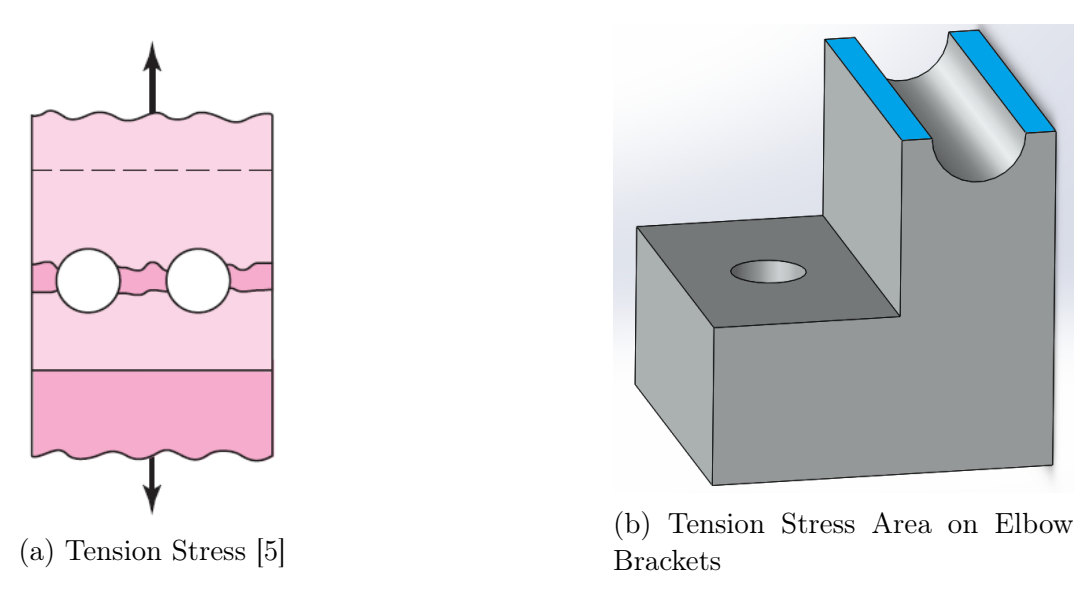


Figure F-3: Tension Stress on Elbow Bracket

This area is substituted into the tension stress formula:

$$\sigma_{tension} = \frac{F}{A_t} = \frac{3062N}{450mm^2} = 6.80MPa$$
 (F.12)

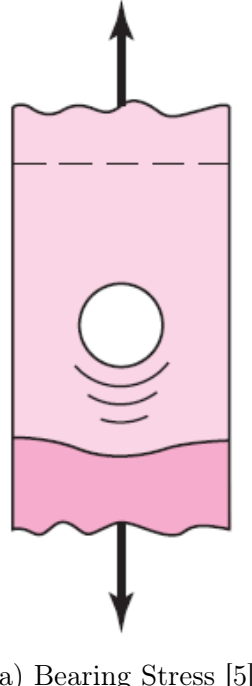
The allowable stress is the Yield Stress from Table F.1. The resulting Factor of Safety  $\eta_{tension}$  is:

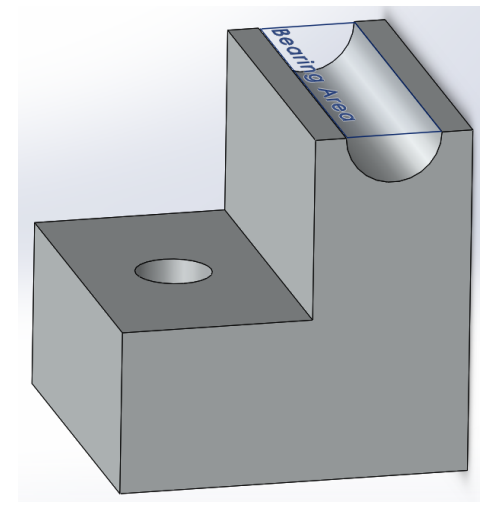
$$\eta_{tension} = \frac{48MPa}{6.80MPa} = 4.12$$
(F.13)

#### F.2.3 Front Hinge Hole - Bearing Stresses

The bearing stress is crushing of the rod or elbow. It is complicated to find the distribution of the load on the cylindrical surface. Typically, it is assumed that force is uniformly distributed on the cylindrical surface and thus the area of the bearing stress is  $A_b = d_{HH} \cdot t$ . Where the variables are per Table F.1. The resulting bearing  $(\tau_{bearing})$  stress is:

$$\sigma_{bearing} = \frac{F}{A_b} = \frac{3062N}{(17mm)(50mm)} = 4.37MPa$$
 (F.14)





(b) Bearing Stress Area on Elbow Brackets

(a) Bearing Stress [5]

Figure F-4: Bearing Stress on Elbow Bracket

The allowable stress is the Yield Stress from Table F.1. The resulting Factor of Safety  $\eta_{bearing}$  is:

$$\eta_{bearing} = \frac{28MPa}{4.37MPa} = 6.40$$
(F.15)

#### F.2.4 Front Hinge Hole - Shear Tear Out Stresses

Analysing shear tear-out stress is not typically done for structural material. Instead, it is designed out by designing space around the hole greater than or equal to 1.5 x diameter of hole. In this case, that large of spacing would have larger stress on the cold plate and increased weight of all of parts. In a effort to optimize the elbow, this analysis was performed. As show in Fig F-5, the area of shear tear-out stress  $A_{tear}$  (highlighted in blue) is the length of the material that is resisting the shear, l, multiplied by the thickness of the material, b. Typically the the material has a square edge. In this case, the elbow does not. It is assumed that it would deform in a similar manner to having a square edge with one exception, the length of l. l was found knowing the outer radius of the top of the elbow,  $\overline{KL}$  and the inner radius of the hole,  $r_{inner} = 0.5d_{HH} = 7mm$ . The equation for a circle is  $x^2 + y^2 = r^2$ . Using the inner radius as the x-value and the outer radius for the radius, the y-value, l, was calculated as shown:

$$l = \sqrt{\overline{KL}^2 - r_{inner}^2} = \sqrt{11.5^2 - 7^2} = 9.124mm$$
 (F.16)

Thus the area of shear tear-out is  $A_{tear} = l \cdot b = (9.124mm)(50mm) = 456.2mm^2$ . And since that is happening on each side of the bolt, that area is multiplied by two.

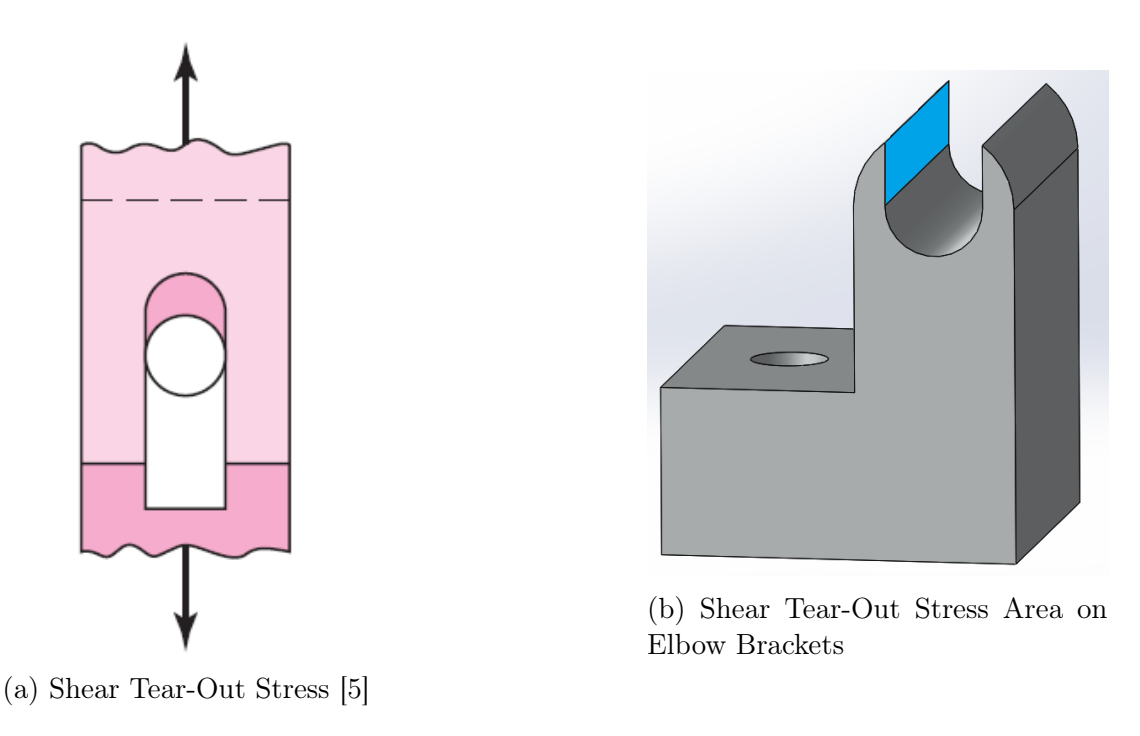


Figure F-5: Shear Tear-Out Stress on Elbow Bracket

The resulting shear tear-out stress,  $(\tau_{tear})$ , is:

$$\tau_{tear} = \frac{F}{2A_{tear}} = \frac{3062N}{2 \cdot 127.7mm^2} = 3.36MPa$$
 (F.17)

The allowable shear stress is from Table F.1. The resulting Factor of Safety,  $\eta_{tear}$ , is:

$$\eta_{tear} = \frac{48MPa}{3.36MPa} = 14.31$$
(F.18)

Thus from this analyses, the front hinge hole should not fail due to stresses anal-

ysed. Taking a closer at the Factors of Safety, not all are greater than four. For shear stress,  $\eta_{shear}$  is around 2.5. This means that while safe for this application, the elbow bracket would need to be redesigned to handled increased shear if there was going to be only one elbow bracket on the design. The other factors of safety indicated the other methods of failure will not occur under increased loading. The other way of looking at these results is that this part is over built and could be reduced in size and weight if needed.